

The Design and Implementation of GRIT-T:  
RIT's Next-generation Field-Portable Goniometer System

by

Justin D. Harms

A dissertation submitted in partial fulfillment of the  
requirements for the degree of Doctor of Philosophy  
in the Chester F. Carlson Center for Imaging Science  
College of Science  
Rochester Institute of Technology

July 28, 2016

Signature of the Author \_\_\_\_\_

Accepted by \_\_\_\_\_  
Coordinator, Ph.D. Degree Program Date

CHESTER F. CARLSON CENTER FOR IMAGING SCIENCE  
COLLEGE OF SCIENCE  
ROCHESTER INSTITUTE OF TECHNOLOGY  
ROCHESTER, NEW YORK

CERTIFICATE OF APPROVAL

---

Ph.D. DEGREE DISSERTATION

---

The Ph.D. Degree Dissertation of Justin D. Harms  
has been examined and approved by the  
dissertation committee as satisfactory for the  
dissertation required for the  
Ph.D. degree in Imaging Science

---

Dr. Charles Bachmann, Dissertation Advisor

---

Dr. Scott Franklin, External Chair

---

Dr. Carl Salvaggio

---

Dr. Sildomar Monteiro

---

Date



# The Design and Implementation of GRIT-T: RIT's Next-generation Field-Portable Goniometer System

by

Justin D. Harms

Submitted to the  
Chester F. Carlson Center for Imaging Science  
in partial fulfillment of the requirements  
for the Doctor of Philosophy Degree  
at the Rochester Institute of Technology

## Abstract

Various field portable goniometers have been designed to capture in-situ measurements of a material's bi-directional reflectance distribution function (BRDF), each with a specific scientific purpose in mind.[1, 2, 3, 4] The Rochester Institute of Technology's (RIT) Chester F. Carlson Center for Imaging Science recently created a novel instrument incorporating a wide variety of features into one compact apparatus in order to obtain very high accuracy BRDFs of short vegetation and sediments, even in undesirable conditions and austere environments. This next generation system integrates a dual-view design using two VNIR/SWIR spectroradiometers to capture target reflected radiance, as well as incoming radiance, to provide for better optical accuracy when measuring in non-ideal atmospheric conditions or when background illumination effects are non-negligible. The new, fully automated device also features a laser range finder to construct a surface roughness model of the target being measured, which enables the user to include inclination information into BRDF post-processing and further allows for roughness effects to be better studied for radiative transfer modeling. The highly portable design features automatic leveling, a precision-engineered frame, and a variable measurement plane that allow for BRDF measurements on rugged, un-level terrain while still maintaining true angular measurements with respect to the target within 0.2 degrees, all without sacrificing measurement speed. This fully automated design is capable of capturing a full hemispherical scan of 66 points, with 80 spectral samples per point, in just 34 minutes. Despite the expanded capabilities and dual sensor suite, the system weighs less than 75 kg, which allows for excellent mobility and data collection on soft, silty clay or fine sand.

# ***DISCLAIMER***

*The views expressed in this work are those of the author and do not reflect the official policy or position of the United States Air Force, Department of Defense, or the United States Government.*

## Acknowledgements

I would like to acknowledge my advisor, Dr. Charles M. Bachmann, for your support and calm demeanor through this arduous design process. Your wide-ranging knowledge and expertise were pivotal to ensuring this project's successful completion. Thank you for your guidance throughout this journey. I would also like to acknowledge the help of my committee members. Dr. Carl Salvaggio, Dr. Sildomar Monteiro, and Dr. Scott Franklin all provided very useful feedback throughout this process and ensured that the GRIT-T system was going to benefit not only the team, but the Chester F. Carlson Center for Imaging Science as a whole.

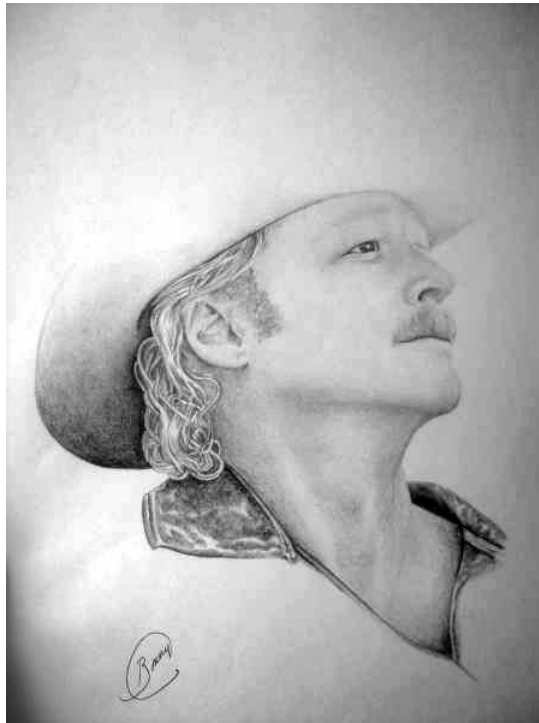
I would like to thank those that assisted me during this long design process; particularly Jason Faulring, Andres Ruiz Torres, the past and present members of the GRIT Team, my USAF brothers and sisters in arms, and the many others that were pivotal to providing support me in my studies and in the design, implementation, and testing of this new instrument. It was truly a pleasure to work with you all.

Of course, this work would never have been possible without the never-ending support of my family. To my parents and grandparents, I thank you for ensuring that I always gave my full effort in any endeavor and for instilling a strong work ethic at a young age. These traits have paid enormous dividends throughout this portion of my life and I am forever grateful for everything that you have done for me.

*It is only fitting that with so much effort put into measuring light, that I mention the person who brings light into my life. This work is dedicated to my young son, Tanner. You have brightened my world with your curiosity and given me a wonderful new perspective on life. I cherish you more than anything else, and no matter where I go you will always be my sunshine.*

*"I'm chasing that neon rainbow, living that honky tonk dream."*

*-Alan Jackson*





# Contents

<b>1</b>	<b>Introduction</b>	<b>1</b>
<b>2</b>	<b>Background</b>	<b>5</b>
2.1	Goniometer . . . . .	5
2.2	Field-Portable Goniometers: Overview . . . . .	8
2.2.1	Positioning . . . . .	9
2.2.2	Adaptability . . . . .	12
2.2.3	Survivability and Maintainability . . . . .	14
2.3	Various Field-Portable Goniometers . . . . .	16
2.3.1	FIGOS and Dual Field-of-View FIGOS . . . . .	16
2.3.2	GOPHER . . . . .	19
2.3.3	Automated Spectro-Goniometer . . . . .	22
2.3.4	GRIT . . . . .	23
2.3.5	Other notable Field-Portable Goniometers . . . . .	25
<b>3</b>	<b>Theory</b>	<b>31</b>
3.1	Light . . . . .	31
3.2	Radiometric Terms . . . . .	32
3.2.1	Material Interaction/Reflectance . . . . .	34
3.3	Methods for Describing Angular Reflectance . . . . .	38
3.3.1	BRDF . . . . .	39
3.3.2	BRF . . . . .	40
3.3.3	HDRF . . . . .	41
<b>4</b>	<b>Methodology</b>	<b>43</b>
4.1	Scientific and Operational Requirements . . . . .	44
4.1.1	Optical Requirements . . . . .	44
4.1.2	Expanded Portability . . . . .	48
4.1.3	Reduced Collection Complexity and Time . . . . .	50
4.1.4	Increased Angular Accuracy and Flexibility . . . . .	51
4.1.5	Increased Interoperability . . . . .	52
4.2	System Requirements . . . . .	54
4.2.1	Derived Optical Requirements . . . . .	54

## CONTENTS

---

4.2.2	Derived Portability Requirements . . . . .	56
4.2.3	Derived Collection Complexity and Time Requirements . . . . .	58
4.2.4	Derived Setup and Tear Down Requirements . . . . .	59
4.2.5	Derived Angular Accuracy and Flexibility Requirements . . . . .	60
4.2.6	Derived Increased Interoperability Requirements . . . . .	61
4.3	Methods for Meeting System Requirements . . . . .	62
4.3.1	Frame Subsystem . . . . .	62
4.3.2	Carriage Subsystem . . . . .	73
4.3.3	Scientific Payload Subsystem . . . . .	77
4.3.4	Software Design . . . . .	78
4.4	Methodology for System Characterization . . . . .	79
4.4.1	Mechanical Testing . . . . .	79
4.4.2	Optical Testing . . . . .	81
4.5	Method for Creating Background-Compensated BRDF . . . . .	82
4.5.1	Background-Compensation Technique Characterization . . . . .	84
<b>5</b>	<b>Results</b>	<b>85</b>
5.1	System Implementation . . . . .	85
5.2	System Characterization . . . . .	89
5.2.1	Mechanical Testing Results . . . . .	89
5.2.2	Optical Testing Results . . . . .	95
5.2.3	Software Implementation and Testing . . . . .	97
5.3	BRDF Retrieval Results . . . . .	100
5.4	Nevada Field Experiment . . . . .	100
<b>6</b>	<b>Summary</b>	<b>117</b>



# List of Figures

2.1	CLabSpeG goniometer showing angular source and sensor.[5]	7
2.2	LAGOS goniometer from the University of Zürich.[6]	8
2.3	Lab goniometer created out of a robotic arm.[7]	8
2.4	Early researchers performing field measurements.[8]	9
2.5	Plot showing possible errors present if cross-calibration is not performed.[9]	11
2.6	Illustration of parallax error that is possible with many goniometers.	13
2.7	ULGS 2 system. Notice that the top portion can be raised or lowered to accommodate tall vegetation.[10]	14
2.8	Photo of the GRIT system shortly after completing a scan. Notice the soft mud on which the goniometer was required to operate.	15
2.9	Assembly of FIGOS goniometer. In this photo, the large 2 meter diameter rings are clearly illustrated.[11]	17
2.10	Photo of the Dual Field-of-View FIGOS goniometer. Note the eccentric ring and foreoptic setup on the right that helped mitigate self-shading.[8]	18
2.11	Various views of the GOPHER instrument.[12]	20
2.12	GOPHER overall GIFOV example for an entire scan plotted on one figure. Note the movement of the measured spot depending on the current azimuth and zenith position.[12]	21
2.13	Automated Spectro-Goniometer deployed on snow.[4]	22
2.14	GRIT device with leveling jacks attached.	24
2.15	Locations of key components on the GRIT system.	25
2.16	FIGIFIGO system illustrating arm configuration and case.	26
2.17	Unique FIGIFIGO optical design that allows for steering the measurement spot.	26
2.18	University of Twente goniometer system measuring vegetation.	27
2.19	Ultra-portable ULGS device.[13]	27
2.20	Larger variant of ULGS 1 constructed out of aluminum.[14]	28
2.21	ManTIS goniometer system measuring vegetation.[15]	29
3.1	Illustration of absorption features in the Earth's atmosphere.[16]	35
3.2	Illustration of the types of reflections.	36
3.3	An illustration of a Lambertian reflector. Note that the radiance from a Lambertian reflector is the same from all view angles since the decrease in radiance (due to being off nadir), is exactly offset by the increase in the FOV's projected area on the material.	37

## LIST OF FIGURES

---

3.4	Illustrations of the types of reflectance quantities.[8]	39
4.1	Angular diffuse fractions for clear and cloudy atmospheres as collected by Dual Field-of-View FIGOS.[2]	46
4.2	Both the sensor head itself and the frame of the goniometer can cast shadows into the scene in most designs. An example of this is shown for a design similar to that found in FIGOS[1].	48
4.3	Especially in remote areas, the GRIT device was often moved via trailer behind an ATV.	49
4.4	The automated light source utilized in the laboratory setting; the original GRIT is positioned underneath the rotating truss that moves the light sources to simulate direct solar illumination.	53
4.5	An illustration of the first GRIT-T design provided by Dr. Bachmann to the author before the project began.	57
4.7	The fully assembled GRIT-T system in the laboratory.	62
4.6	Diagram showing the device connections for the three GRIT-T subsystems.	63
4.8	The top ring piece.	65
4.9	The cross-section of the top ring showing the double edge used to guide the carriage.	66
4.10	The middle ring piece. Note that the external gear is not shown in this rendering.	66
4.11	The cross-section of the middle ring.	67
4.12	The bottom ring piece showing the custom designed tabs that hold the leveling actuators.	67
4.13	The cross-section of the bottom ring. This view also illustrates the actuator mount point in detail.	68
4.14	The entire frame structure including the mounting bracket for the spectrometers and other support equipment.	68
4.15	The cross-section of entire assembled frame.	69
4.16	A visualization of the modeling results for frame rigidity. Note that the units are in millimeters and the scale of the deformation has been greatly magnified to allow the reader to better understand the deflection that would take place.	70
4.17	Frame design with Exlar actuators attached.	71
4.18	The GRIT-T carriage drive motor and gearbox.	74
4.19	The GRIT-T arm mount attaching the arm to the rotary stage.	75
4.20	A photo of the GRIT-T head motor casing and the attached pointing head.	76
4.21	A photo of the GRIT-T pointing head with both fore optics and fiber optic cables attached.	77
4.22	An example of a pointing error plot. This plot is for the Dual Field-of-View FIGOS system.[2]	80
5.1	A photo of the bottom and middle ring layers after water jet cutting.	86
5.2	A photo of the top layer before the guide rails were machined.	86
5.3	A photo of the middle layer after being water jet cut, surface ground, and gear cut.	87

5.4	A photo of the bottom layer, showing the large computerized numerical control (CNC) mill machining the mounting points for the leveling actuators. . . . .	87
5.5	GRIT-T after final assembly in the GRIT Lab, note that the spectrometers are not attached in this photo. . . . .	88
5.6	Figure showing the alignment test setup, including small optical alignment laser. . .	90
5.7	Alignment test results from 632 mm distance. All error measurements and distances are provided in millimeters. . . . .	90
5.8	Alignment test results from 732 mm distance. All error measurements and distances are provided in millimeters. . . . .	91
5.9	Plot indicating the results of the 632 mm distance alignment test. . . . .	91
5.10	Plot indicating the results of the 732 mm distance alignment test. . . . .	92
5.11	Alignment test results from the DEM alignment test performed at 740 mm distance. All error measurements and distances are provided in millimeters. . . . .	93
5.12	Plot indicating the results of the DEM alignment test performed at 740 mm distance.	94
5.13	Leveling Test Results. Note that the test was completed for 15 different roll/pitch scenarios and that the final roll and pitch achieved was then used as an offset for the Rieker inclinometer. Thus allowing the system to achieve true level within 0.1 degrees.	95
5.14	Figure showing the signal-to-noise ratio for typical laboratory conditions with ASD S/N: 18205. This SNR was determined for radiance leaving an Algodones Dunes sediment sample collected with a 5 degree fore optic. The broadband source used for laboratory experiments is a 70 watt ASD Illuminator. . . . .	96
5.15	Figure showing the relative signal throughput of a 2 meter fiber optic cable versus a 1.5 meter fiber optic cable on an ASD Field-Spec 4 spectroradiometer. . . . .	97
5.16	GRIT-T Control Software Startup page. . . . .	101
5.17	GRIT-T Control Software Leveling page. . . . .	102
5.18	GRIT-T Control Software Spectrometer Control page. . . . .	103
5.19	GRIT-T Control Software Scan Setup page. . . . .	104
5.20	GRIT-T Control Software DEM Scan Setup page. . . . .	105
5.21	GRIT-T Control Software Field View page. . . . .	106
5.22	GRIT-T Control Software DEM View page. . . . .	107
5.23	GRIT-T Control Software Manual Movement page. . . . .	108
5.24	GRIT-T Control Software System Control page. . . . .	109
5.25	GRIT-T Control Software Status View page. . . . .	110
5.26	GRIT-T capturing BRDF in a powdery salt flat area. This surface has a soft, flaky crust that would break away under pressure. . . . .	111
5.27	GRIT-T capturing BRDF in a very soft, silty area. In areas such as these, multiple people aided in carrying the instrument due to the extremely soft conditions. . . .	111
5.28	GRIT-T capturing BRDF in a completely saturated clay environment. Much like the silty areas, approximately 4 people were used to move the system to ensure that the instrument was safe at all times. . . . .	112

## **LIST OF FIGURES**

---

5.29	Photo of GRIT-T capturing a true 70 degree zenith angle with respect to the target. Notice that the head has been counter-rotated to ensure that the same portion of ground is captured at each view angle. . . . .	113
5.30	GRIT-T capturing sediment reflectance while leveled on the side of a large sand dune. Note that the system is still tracking the same spot on the target sediment but that the maximum zenith angle is reduced due to the distance to the target. . .	114
5.31	GRIT-T capturing spectra from a white reference panel at a very muddy target location. . . . .	114
5.32	GRIT-T artificially lifted with the actuators to show the extension rods and attached feet. . . . .	115
5.33	GRIT-T capturing BRDF while leveled on a hard clay hillside. . . . .	115
5.34	A preliminary result of a Nevada test site without the inclusion of background illumination compensation or temporal compensation. . . . .	116
6.1	The author collecting a white reference plaque after a BRDF scan using the GRIT-T.	119
6.2	GRIT-T measuring reflectance on the side of a sand dune while the author monitors the GRIT-T Control Software. . . . .	120
6.3	BRF of a sediment performed in the laboratory with 10 degree intervals in azimuth and zenith. This BRF was the first performed by the goniometer in the lab. . . . .	121

# Chapter 1

## Introduction

Early in life, every human will realize that objects look different based on how they are oriented. Whether it is the reflection off of a lake, the dull looking concrete, the sand on a beach, or a perfect mirror, objects look very different based on how you look at them. This difference can be caused by a variety of things including the material of which the object is composed, the temperature of the object, how smooth or rough the surface of the object is, whether the object is painted, or whether the object is covered in dust. These are just a few of the things that can change how objects appear to the observer. Scientifically, we study the way that objects look by trying to quantify the amount of reflected light off of these objects. While an object may look different at varying observation angles, or when the light hits it just right, ultimately, it is still the same object and the reflected light coming off of that object can be described very well if one knows the angle from which it is viewed and where the source (light bulb, sun, etc.) is that is illuminating it.

In order to help frame the scientific purpose of this work for any reader, consider the imagery collected off of an airborne or spaceborne platform. These devices capture tremendous amounts of information in the images that they collect. And, these images can be used for a large number of purposes, for example, helping with disaster relief after a natural disaster, gauging the effects of climate change, or aiding in precision agriculture. In each of these applications, it is often necessary to classify the objects seen by the imaging system. This classification is typically automated by a computer that uses the image to make a decision about what the camera is seeing. However, since objects can look much different based how you view them, it can be difficult to get an accurate classification without the extra information that describes how objects look from various angles. In addition, overhead imagery also suffers from the same issues that casual observers may have, i.e. the reflected light off of an object can change dramatically if that object is even slightly altered by rain, dust, or just typical weathering of the coatings. For these reasons, it is even more important for the light being reflected off of an object to be well characterized.

Similar to the classification problem is that of target detection. However, instead of trying to place every pixel into a specific bin based on the type of material, the system is trying to find one or more pixels that indicate that an object of interest has been found. One specific example of this type of detection is when one nation tries to detect if another nation has used chemical weapons. If the nation understood how light reflects off of specific gases or powders, then it may be possible to determine whether certain substances were used, even on small areas, based on the overhead imagery.

For many years, devices have been created to measure how objects reflect light based on various view and illumination angles. In the remote sensing community, these devices are referred to as goniometers. Most goniometers resemble robots that undergo various movements to point a sensor at a target at all angles. Depending on the purpose of the goniometer, it may employ a variety of different types of sensors to measure light. These may include standard cameras capturing only a few bands (red, green, and blue), or very high-end spectrometers that measure light in thousands of bands. These goniometers can be engineered to provide the specific information necessary to help solve the image classification and target detection applications outlined above. They can also be used to help calibrate the sensors and cameras on airborne and spaceborne platforms by providing what is known as ground truth. Ground truth is information obtained from an object or material at the ground-level that can be used to compare with overhead imagery of the same object or material. This comparison can be used to make sure that various sensor settings are properly determined, and that there is not a malfunction. In addition, goniometers can be used to perform spectroscopy of a particular material or set of materials. Spectroscopy refers to the science of interaction of electromagnetic radiation with matter, particularly with respect to the wavelength dependence of observable features.[17] For this paper, we limit this definition to only include light visible to a spectrometer, and therefore spectroscopy can be defined as determining the mineral or material makeup of a material by viewing it with a spectrometer that measures the reflected light. The data from the spectrometer can then be analyzed to determine specific absorption features that are present, and thus, identify the type of material remotely, without ever actually interacting or touching the material.

As can be imagined, these devices are typically used in both laboratory and field environments, the latter of which can be extremely challenging. As with all machinery operated in outdoor conditions, there are a variety of considerations that must be accounted for to ensure proper operation. These considerations are even more stringent when the machinery is a scientific robot that is meant to measure with the utmost accuracy even in unfavorable conditions. Field goniometer designs must take into account the typical material that they will measure, the accuracy required for that material or scenario, the environment in which they must operate, the amount of people

---

that will be involved in the operation, the expected reliability, and many other aspects. As one might expect, the design and engineering of a purpose-built field goniometer can be challenging at best.

In this paper, the design and engineering of the next-generation field-portable goniometer for the Rochester Institute of Technology's (RIT) Digital Imaging and Remote Sensing Laboratory will be discussed. In order to provide the necessary background for the reader, many notable field goniometers will be outlined and described in detail. The description of these devices includes their intended purpose, the scientific payloads utilized to perform the reflectance measurement, the basic mechanical and electrical design, and a list of their biggest strengths, as determined by the author. These goniometers include both of the FIGOS systems from Switzerland, the ULGS and GOPHER systems designed in Canada, the ASG device built in California, the original RIT field goniometer, GRIT, created in New York, and others from around the world. Each of these designs provided great influence in how the next-generation field-portable goniometer, known as the Goniometer at the Rochester Institute of Technology version Two (GRIT-T) was designed and engineered.

In order to prepare for the technical discussion to follow, a short synopsis of the theory utilized in this project will also be provided. This chapter begins with definitions for various wavelengths of light and culminates by providing detailed descriptions of the various types of reflectance functions that are commonly used in the remote sensing community. This theory chapter provides the necessary foundation for the thoughtful discussions about system use that will occur later in the paper. In chapter 4, various methods will be described that afford the reader insight into how the detailed design decisions were accomplished. While the device is intended to be very flexible and able to handle a variety of tasks, certain requirements were set based on the research for which it will typically be used. The GRIT-T will largely be put to use studying various sediments, and at times low lying vegetation, both in remote locations and in the laboratory. Ultimately, the research group hopes to be able to extract various geotechnical parameters from the reflectance information gleaned from GRIT-T as described in various proceedings, journal papers, and books.[18, 19, 20, 21, 22, 23, 24, 25, 26, 27, 28] Understanding how the reflected light is tied to sediment density, grain size distribution, moisture content, and other parameters requires a very accurate measurement device, both in an optical and mechanical sense. To achieve this accuracy, various methods are discussed to handle precise sensor pointing, multiple illumination sources, system reliability, and other necessary topics.

This begins with an overview of each of the high-level, scientific and operational requirements that the goniometer system must fulfill, and follows with an intricate discussion of how these requirements must be met. The derived system requirements section breaks each of these overarching goals down into more fundamental design choices that creates a system-level tradespace which can

then be solved with an engineering approach. Once the set of derived requirements has been established, the author then methodically addresses each of the requirements, and proposes a solution that ensures a balanced design that will allow for the scientific goals to be achieved without interfering with other requirements. Once the system-level decisions have been discussed, the methods for handling the output data are then thoroughly described, and the testing methods are outlined. Finally, the results of the various testing methods and the status of the final system are discussed.



## Chapter 2

# Background

In remote sensing, collection of the Bidirectional Reflectance Distribution Function (BRDF) is often necessary to classify objects in airborne or satellite hyperspectral imagery based on their spectral reflection. The spectra of objects found in remote sensing imagery can vary drastically depending on whether they are of natural or artificial origin, however most display non-Lambertian characteristics.[29][1] This non-Lambertian behavior is best captured by collecting the BRDF of an object, which allows the user to understand how the material will reflect light spectrally while taking into account the incident and reflected angles. [30] Collecting the BRDF of a target can be done in a variety of ways in either a laboratory or field environment, depending on the phenomenology being studied. While some phenomenologies can be studied in a controlled lab setting as in the field, others require the study of objects that might change if removed from their original environment, such as vegetation or soils.[3][20] Another example of when in-situ measurements are required is in the calibration of airborne or satellite instrumentation over the earth.[31] These type of calibrations typically have a large field of view (FOV) and dictate that measurements be taken on the ground at the same moment in time as the overhead collection happens. This ensures that the target of interest has not changed in between the measurements. Collecting the BRDF of objects in-situ can be extremely challenging due to naturally changing illumination conditions and rugged terrain.

### 2.1 Goniometer

The word goniometer can be used to describe a variety of different devices, depending on the context in which it is used. The word originates from two greek words, gonia and metron, which when combined mean to measure angles. Goniometers are used widely in the medical, engineering, and scientific communities. In the remote sensing community, a goniometer is described as a device that measures reflected light at precise angles. [32] Many goniometers are created for specific

purposes depending on the types of materials to be measured, but the general idea remains the same. That is, adjust a target or a sensor so that the reflected light is measured at precise angles with respect to the target and light source. Therefore, it is possible to use a goniometer to create a hemispherical scan pattern that one can use to determine the BRDF of a target. The sensor attached to the goniometer can vary and depends only on the scientific requirements, form factor, and weight that the goniometer apparatus can support. Depending on the main purpose of the research being conducted, certain sensor types may be more conducive to goniometer design than others. For devices primarily being used to study vegetation, a silicon-detector-based spectrometer may fulfill all of the scientific requirements since certain indices for studying vegetation only require information below 1000 nanometers.[17] Due to spot size considerations, it may also be necessary to utilize an imaging spectrometer so that the sensor FOV is small enough to distinguish between various features of the target itself. If this analysis can be done in the visible or near-infrared (VNIR) portion of the spectrum, silicon-based detectors are a likely solution since they typically do not need to be cooled to operate with a respectable signal-to-noise ratio (SNR). This lack of cooling also ensures that the spectrometer will be much smaller and lighter than others, and cost less. This all equates to reduced complexity of the goniometer apparatus itself since aiming lighter, smaller sensors is much easier to perform. Scientific requirements such as those found when working with soils and sediments would require the use of the short-wave infrared (SWIR), in addition to the VNIR, to adequately characterize the mineral absorption features present. Since measuring the SWIR is best done with sensors that are cooled, the mechanical requirements to aim such a sensor can become very challenging to meet due to the increased size and weight of the support equipment attached to the sensor. Failing to properly engineer the mechanical structure can have a large impact on the overall accuracy of the measurement, and ultimately the BRDF.

Measurement accuracy can also be determined by a broad range of factors besides mechanical stresses. However, many of the factors have little to do with the goniometer apparatus itself, but instead with the spectral accuracy of the instrument, the stability of the light source, the likelihood that the target will change over the course of the scan, and any background effects, such as stray light, adjacent objects, etc. that may be present in the scene. Each of these secondary causes of error can be handled quite well if the collection is performed in a laboratory setting with calibrated equipment in a room outfitted with light baffles to create an optically dark space. Removing excess equipment and using a calibrated light source can also aid measurement accuracy. The integrity of the scan also depends greatly on the precision of the movements that the goniometer performs. Laboratory goniometers have been made with various parts found in optical laboratories, and are often very simple if the scientific use only requires measurement over one or two azimuth directions of the hemisphere. These typically do not need to be automated due to the simplicity of the scan

and could be created to mount virtually any sensor package. As the scan complexity increases, particularly with the addition of many azimuth directions, so does the complexity of the hardware required to perform the movements accurately. This is then compounded if the sensor package being used to measure the reflected light is large or heavy, possibly due to sensor cooling devices. As the pointing requirements become more arduous and the sensor suite grows, it is more difficult to achieve viable results using standard optical laboratory hardware and this often forces scientists to create a custom design that fits their specific goals. As can be seen in figures 2.1, 2.2, and 2.3, the hardware to perform these scans quickly becomes so complex that automation is required if the experiment is to be performed in any reasonable time frame.



Figure 2.1: CLabSpeG goniometer showing angular source and sensor.[5]

While adding automation can be time consuming and costly at first, its benefits can pay dividends when dense scan patterns are repeated many times to observe phenomenological effects in materials. Through automation, it is possible to tie the entire system operation together to control not only the movements of the system, but also the sensor suite. Many goniometers have been automated to reduce operator input and decrease collection time. These systems typically ask the user to provide scan parameters, such as azimuth step size and zenith step size, or a specific pattern that is then executed autonomously. This level of automation is particularly desirable for goniometers that operate in the lab as well as in a field-portable configuration.



Figure 2.2: LAGOS goniometer from the University of Zürich.[6]

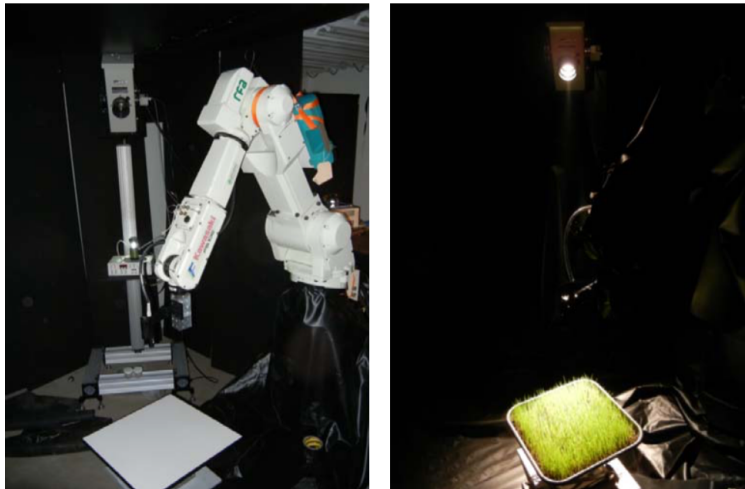


Figure 2.3: Lab goniometer created out of a robotic arm.[7]

## 2.2 Field-Portable Goniometers: Overview

While engineering and design can get quite complicated for goniometers that take measurements in a laboratory, devices that see frequent field use are typically far more difficult to design and create. This added difficulty arises from a new set of requirements, in addition to those already discussed for the lab-based devices, that are specific to equipment that is intended for use in long

field campaigns that typically occur in austere environments without the support and stability of a well-equipped lab. The most basic of these new requirements pertains to where the system is with respect to the target and other measurement devices. Since these devices allow for very repeatable angular movements, they also reduce the possibility of human error influencing the measurement that may occur without the use of a properly designed field goniometer. As you can see in figure 2.4, various techniques were utilized in field environments to capture information about objects in-situ.



Figure 2.4: Early researchers performing field measurements.[8]

### 2.2.1 Positioning

As previously discussed, one of the main reasons to perform field BRDF measurements is to calibrate sensors, either on an aircraft or on a spacecraft. In order to do this, one has to know precisely where these users are in the world while taking the measurement. This is necessary to ensure that the ground truth BRDF captured during the overflight can be tied back to an individual pixel in a hyperspectral image from the sensor being flown. The size of a pixel's ground-instantaneous field of view (GIFOV) depends on a variety of other considerations such as the altitude of the sensor, the type of sensor, and the resolution of the sensor. Because of this, the standard GPS accuracy of 2 meters is not always sufficient to ensure that the point collected on the ground can be tied back to a specific pixel in the image. Existing systems accomplish this by typically using survey-grade

GPS units and post-processing the collected data with the available GPS ephemeris data to achieve accuracy on the order of a few centimeters. This level of accuracy is near the current technological limit of affordable positioning equipment and is generally sufficient for the purposes discussed here. This equipment can either be integrated into the goniometer itself or it can be utilized as a stand alone system separate from the instrument.[33] In addition to the spatial accuracy that a high-end GPS unit can provide, it is also necessary to achieve a certain level of temporal uniformity across the various instruments in use on any given collect. Many systems also utilize GPS for this temporal information since the current GPS time is encoded in the signal passed down from the orbiting satellites. In order to ensure that the data being collected is accurately timestamped and can be tied to other datasets that might be present, the instruments themselves are often used with a GPS receiver that is directly connected. This ensures that the current worldwide GPS time is added to the metadata of each file with a minimal amount of latency between the receiver and the sensor collecting the spectra.

Another issue with positioning the field goniometer apparatus is understanding the location of the sun. In laboratory measurements, the source is often well-defined and positioned exactly as needed, thus reducing the complexity of determining the BRDF. However, in a field environment, where the sun is the main source, one must ensure that the movement of the sun is taken into account when determining incidence angles since, depending on the time of day, the sun can move a non-negligible amount in the time it takes to capture the entire BRDF. Understanding the sun's position and movement can be handled quite easily given accurate information about the current latitude, longitude, time of day, and apparatus heading. The first three of these required pieces of information have already been discussed and can be handled with standard survey-grade GPS equipment; however, capturing accurate heading information is easily as important and can be more challenging to obtain. In order to capture heading information, many goniometers utilize digital compasses which are typically only accurate to a couple degrees in ideal conditions and are subject to magnetic interference from nearby motors, power electronics, and other ferrous objects. Any error in the goniometer heading information directly impacts the accuracy of the BRDF as this is used to determine source location with respect to the angular measurements taken.

In field goniometer measurements, the sun is considered the main source as it provides approximately 85 percent of the downwelled light, depending on atmospheric conditions, while the atmosphere itself provides the remainder.[2] However, it is important to note that the direct solar radiance may not be stable over the course of the measurement due to the changing atmosphere and the possibility of passing clouds. The presence of even very thin cirrus clouds, that are not visible to the naked eye, can have dramatic effects on the spectral accuracy of the BRDF if not accounted for.[34] Many researchers have developed methods to compensate for these atmospheric

effects. Most people using goniometers for in-situ measurements utilize a sun photometer to gather information about the irradiance of the sun at the particular field site in question.[35, 36] This technique provides valuable information about the overall intensity of the sun, but only does so over a very specific number of bands. While this technique is widely used and accepted for the purpose of understanding the solar downwelling radiance on a target, there are inherent limitations in measuring in fewer spectral bands than the main sensor looking at the target. As described in Bachmann et al.[9] and Hueni et al.[37], utilizing a sensor with less spectral bands to measure incoming radiance can result in dramatic spectral artifacts in the post-processed data that are not present in the dataset. The magnitude of these effects will vary depending on the alignment of the wavelength grid between the two sensors, the climate, the weather, and general location, but they are often prevalent near coastal remote sensing sites since the maritime atmosphere can change rapidly.[9] In order to prevent these types of artifacts, it is necessary to measure the downwelling radiance with at least a similar number of spectral bands and preferably with the same model of instrument, in an effort to limit the magnitude of the difference in wavelength grid.[37, 9] This will ensure that any changes in radiance that might affect just a narrow window of the spectrum will be accounted for, ensuring that the true reflectance spectra from the target is properly captured. It is also necessary to carefully calibrate the instruments used in the entire collection to eliminate effects from differences in the wavelength grid and shifts in wavelength accuracy. If this cross-calibration is not performed, spectral artifacts may occur as seen in figure 2.5.[9]

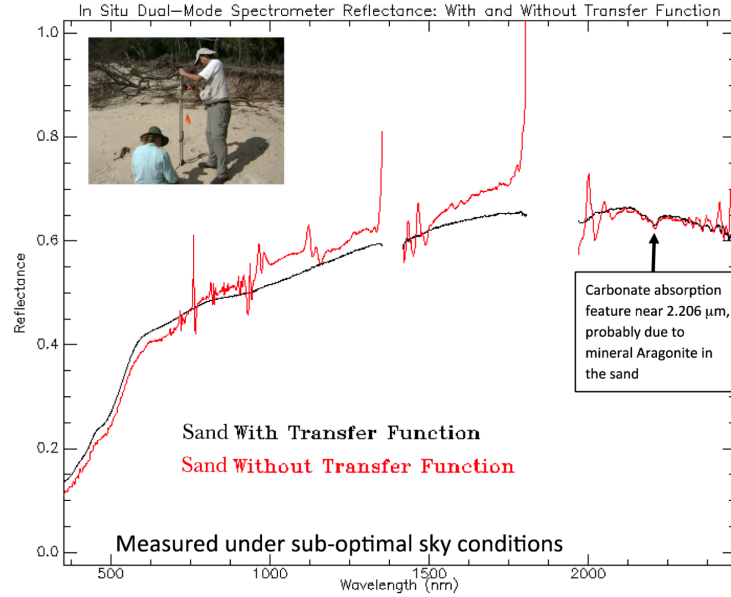


Figure 2.5: Plot showing possible errors present if cross-calibration is not performed.[9]



### **2.2.2 Adaptability**

Other challenges that are unique to field-portable goniometers are those that affect the apparatus design itself. Since these devices are often meant to be used in some of the most remote environments on earth, the designer must carefully analyze the potential environments and balance the requirements of the operating location with the scientific requirements to ensure both are being met. Neglecting either set of requirements during the design of a system can prove very problematic and result in bad data at best, and no data at worst. Climate, the types of targets being measured, collection length, site topography, and distance between collects can all have a large influence on how a goniometer must be designed. Depending on the scientific use, devices may have to contend with climates ranging from extreme cold with snow cover to the hottest deserts with blowing sand. In order to ensure that the system will be able to adapt, the designer must ensure that the components chosen to perform, control, and power movements are rated for such temperature ranges. Ensuring that operating temperature and environmental ratings are properly chosen for each part will allow a goniometer to continue operating even in some of the worst conditions. Additionally, it may be necessary for a field goniometer to take spectra of a wide variety of targets from sand to tall vegetation and while sensor requirements have already been briefly discussed, varying targets can provide a unique set of criteria when it comes to structure design that supports sensor movement. If a system must accommodate measuring flat ground, slopes and the possibility of tall grass accurately, careful consideration must be afforded to how stable and rigid the frame of the goniometer is, since flexing or settling during the measurement would ultimately affect the integrity of the scan being performed and result in erroneous or unrealistic data. Building a strong frame into a field goniometer can mitigate many causes of movement error and allows a system to adequately handle being raised to measure tall grass or unlevel field sites that might otherwise not be ideal for BRDF collection.

At times the requirements to ensure accuracy and portability are at odds with each other; for example, a large stiff frame that is able to measure most targets is then also typically too heavy and unwieldy for a remote sensing team to move from site to site quickly, especially in harsh areas. Another aspect of accommodating various outdoor targets is understanding how the movements will position the sensor with respect to the target. Since the surface geometry of an in-situ target is not controlled or adjustable, as it might be in a laboratory setting, how a field goniometer positions the sensor above the target must be carefully considered in the design phase. Typically, goniometers have a fixed measurement plane that is determined by the structure, and the surface being measured must be placed in this plane in order to ensure that parallax errors do not occur.

As seen in figure 2.6, if parallax errors are present, the measurements being taken are effectively from a combination of various spots on the surface rather than of a particular spot that the user



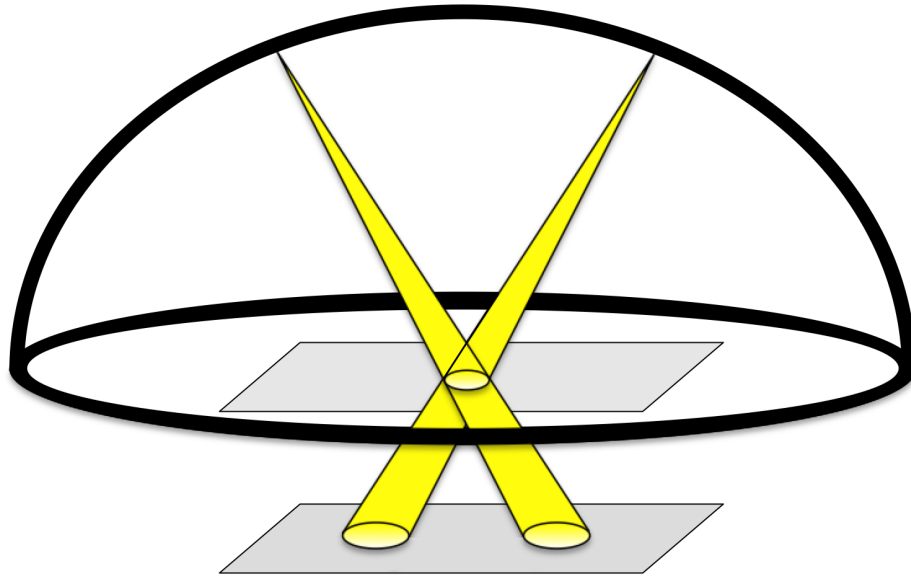


Figure 2.6: Illustration of parallax error that is possible with many goniometers.

has chosen. This can have dramatic effects on the data since the goniometer is effectively taking measurements of multiple objects at specific angles and stitching them together to create one BRDF. The errors present in the BRDF due to this parallax error are dependent on the severity of the parallax and the overall uniformity of the surface within the parallax region. In certain situations, such spatial variation may even be caused by wildlife, and the field plan for measurement with the goniometer system must ensure that the target area is of adequate size based on the overall combined GIFOV, including parallax effects, to ensure accuracy.[38] In order to combat this, some goniometers incorporate a method of raising or lowering the hemisphere over which the scan is performed. However, these devices can be prone to error as they rely on the user to appropriately set the height, and they are still limited in their ability to accommodate unlevel terrain since many would collide with the ground in order to complete a full BRDF scan. Others ensure that the goniometer system is carefully placed over the target of interest to be certain that it falls within the single measurement plane available. Both of these mitigating techniques can be effective, but they still result in reduced flexibility to handle a wide variety of targets, and lengthen the setup time of the system. Ultimately, reducing or eliminating parallax error is a common issue with field goniometers and it presents a series of challenges to an aspiring designer wanting to be able to measure a large target set with minimal setup time.



Figure 2.7: ULGS 2 system. Notice that the top portion can be raised or lowered to accommodate tall vegetation.[10]

### 2.2.3 Survivability and Maintainability

As many who operate field goniometers already know, remote experiments to collect BRDF of in-situ targets are often relatively long campaigns that can last weeks in order to adequately capture the relevant information about a scene or set of scenes. As previously mentioned, the operating conditions encountered are typically not forgiving to the machinery or the sensors. It can include temperatures above 100 degrees Fahrenheit or below freezing, strong winds with blowing sand, deep mud or snow, the unexpected rise in tide, or torrential downpour. Figure 2.8 provides an example of the type of terrain that is sometimes encountered. These events are often difficult to predict; and it is all but inevitable that a well-traveled goniometer will experience one or more of them in its lifetime. Handling these situations in stride while ensuring that the instrument can continue with future collections is an arduous task at best, as adverse conditions can quickly damage electronics or completely destroy a drivetrain system needed to perform the BRDF scan. It is therefore imperative that these situations be carefully planned for when designing a goniometer intended for field use. Not only must a goniometer survive these type of events, it must also be able



Figure 2.8: Photo of the GRIT system shortly after completing a scan. Notice the soft mud on which the goniometer was required to operate.

to quickly return to duty with the same precision and accuracy as experienced before, otherwise it may result in potential degradation in the data which will lead to erroneous BRDFs.

Utilizing electronic and motion components designed for harsh use outdoors can pay dividends when it comes to recovering from an unexpected event, especially since field campaigns can cost easily in the tens of thousands of dollars per trip. Industrial computers and movement components are typically rated for extreme temperatures and have environmental protection from dust and water. This allows the system designer to be sure that the worst situations are accounted for and that wear and tear due to these events will be greatly reduced. This will in turn provide confidence that the movements being performed are still accurate while reducing downtime for repairs. Another issue confronted in coastal remote sensing is salt spray and therefore the need for corrosion resistance in the instrument design. Even short exposure to salt spray can have devastating effects on a robotic system if its materials are not corrosion resistant, resulting in inaccurate or possibly incomplete movements due to rust that then create a lack of integrity within the measured BRDF. Due to this, it may be necessary to utilize non-corrosive materials when creating the structure or mechanical components of a field goniometer.[12]

As mentioned, since remote sensing field campaigns can take place virtually anywhere on earth, and last for weeks at a time, they are often extremely expensive. This places a premium on creating

an easily maintainable system that can be fixed quickly in the event of failure to reduce downtime and wasted expense. Despite the best design and highest quality components, it is inevitable that something will fail. In these instances, having a system designed for maintainability will allow a user to replace any failed part with a new one quickly without leaving the field.

## **2.3 Various Field-Portable Goniometers**

Since the first publication of the effects and necessity to consider the angular response of reflections, the remote sensing community has been creating various goniometers to capture the BRDF of materials. Many of these goniometers have been field-portable to provide for such collection in outdoor locations within a natural scene, in order to better capture accurate information about materials in-situ. Each portable design that has been created was carefully engineered with specific target, environmental, and sensor requirements as discussed in 2.2. In order to better understand the background of field-goniometers, a brief overview of some of the more historically significant devices is provided below.

### **2.3.1 FIGOS and Dual Field-of-View FIGOS**

One of the most widely recognized field-portable goniometers is the Field Goniometer System (FIGOS) created by the Remote Sensing Laboratories in the Department of Geography at the University of Zürich in Zürich, Switzerland. This system was first described by Sandmeier and Itten, and it was first operational in 1996.[1] The device features a large azimuth ring that is approximately 4 meters in diameter, and a half ring with a 2 meter radius and a motorized carriage that is used for zenith positioning. The movement of the motorized carriage allows for zenith angle selection, and the ability to spin the zenith ring entirely allows for azimuth angle selection. The target set for this design includes small, dense vegetation canopies, man-made surfaces, and soils, hence, the large movement rings.

The FIGOS system originally incorporated a Spectra Vista Corporation (SVC) GER-3700 spectroradiometer that has 704 bands from 300 nm to 2450 nm. This sensor provided sampling at 1.5 nm bands from 300-1050 nm and 8.4 nm bands from 1050-2450 nm and was paired with a 3 degree foreoptic. This foreoptic choice, combined with the height of the sensor above the target, provided a 10.5 cm spot diameter at a nadir viewing location, and was stretched to approximately 10.5 cm by 41 cm at the maximum achievable zenith angle of 75 degrees. Due to the careful design and engineering of the goniometer, the authors reported the ability to position the sensor within 0.2 degrees of the requested angle, based on the geometry of the frame, but did not report specifically how the system as a whole was geolocated.



In order to obtain accurate heading information, they reported that the initial orientation to geographical north was performed by aligning a reference point on the ring with a compass. Another great achievement of FIGOS was the quality of the rings themselves which can be seen in figure 2.9. This is evident in the laser tracking that was performed with the instrument after creation. The team tracked the laser, which was attached near the sensor, over various zenith and azimuth movements. They found that the laser spot wandered from center a maximum of 3.5 cm. In an effort



Figure 2.9: Assembly of FIGOS goniometer. In this photo, the large 2 meter diameter rings are clearly illustrated.[11]

to minimize the weight of the system, despite its large size, the creators opted for an all-aluminum design that tipped the scales at roughly 230 kg. Even though it was relatively lightweight for its size, the system had to be disassembled and hauled on a custom built trailer to and from field sites. Once a field site had been chosen, the system could be assembled in 90 minutes with a two-person team. For a typical collect, the system used 15 degree zenith steps and 30 degree azimuth steps. This resulted in a collection time of approximately 18 minutes. A Spectralon reference panel was measured at each nadir position to capture the downwelling radiance. Typically the system was used with a sunphotometer to track the atmospheric conditions.[1] The FIGOS system also had a unique mechanical design that was intended to allow for very low phase angles between the sun and the sensor. This was achieved by mounting the zenith arc eccentrically with respect to the

azimuth arc. This in turn then allowed the shadow from the zenith arc to be out of the target area, and therefore, reduced the self-shading effect in the solar plane to just the shadow cast by the foreoptic itself. This system quickly became very popular, and a similar version known as the Sandmeier Field Goniometer was created for NASA's Ames Research Center.[39] Figures 2.9 and 2.10 give an illustration of the system and showcase the eccentric zenith ring that greatly reduced shadowing. More recently, the FIGOS system underwent a serious upgrade that greatly enhanced



Figure 2.10: Photo of the Dual Field-of-View FIGOS goniometer. Note the eccentric ring and foreoptic setup on the right that helped mitigate self-shading.[8]

its capability of providing spectrally accurate BRDFs. This upgrade consisted of adding an upward looking spectrometer that is used to capture the incoming illumination profile angularly during the collection. This spectrometer's foreoptic was placed in line with the downward-looking foreoptic but aimed away from the target to capture the spatial variability in the diffuse illumination incident on the target. The system was also upgraded from the SVC GER-3700 spectroradiometer to a pair of Analytical Spectral Devices (ASD) FieldSpec 3 spectroradiometers with sampling intervals at 1.4 nm from 350-1050 nm and 2 nm from 1000-2500 nm. Both of these devices were connected to 3 degree foreoptics and rode along on a carriage that traversed the zenith arc, in order to minimize fiber optic length and ensure that the SNR was acceptable. The new Dual Field-of-View FIGOS, as it was known, still utilized a 2 meter zenith arc radius and the unique off-center design that reduced the possibility of self-shading near the hot spot location, as seen in figure 2.10. The

upgraded system also had very similar characteristics with respect to pointing accuracy. When tested with the same laser method as the original FIGOS, the spot moved a maximum of 4 cm at the most extreme zenith angles that it can achieve, 75 degrees. Much like other goniometers, the current FIGOS made use of a sunphotometer to track the temporal changes of the sun's radiance over the course of a scan cycle. Overall, the addition of a second spectrometer did not greatly affect the scan time which has been published as 25 minutes. [40] The Dual Field-of-View FIGOS goniometer represented a large step forward in handling many of the issues encountered in field remote sensing. The diffuse illumination profile approach helped to compensate for semi-stable atmospheric issues and problems associated with background illumination effects due to nearby objects that scattered light into a scene.

### **2.3.2 GOPHER**

The Goniometer for Outdoor Portable Hyperspectral Earth Reflectance (GOPHER) is a system purchased by the Naval Research Laboratory's (NRL) Remote Sensing Division in Washington, D.C.[12] This system was created, under contract to SpectraVista Corporation, by the University of Lethbridge and the University of Saskatchewan in 2010 to meet various scientific requirements. As discussed in Bachmann et. al.[12], the system must be very portable and able to take BRDF's quickly in the VNIR and SWIR regions with minimal self-shading due to structure. The overall system design was based on the ULGS 2.0 goniometer[41] created at the University of Lethbridge but was greatly modified to compensate for the added weight of the larger VNIR and SWIR spectrometer. The addition of the SWIR region to the goniometer allowed for better inspection of the mineral absorption features found in soils and sediments, a key target for GOPHER as this device was primarily used in coastal or littoral areas. The sensor utilized by GOPHER was a SVC HR-1024 spectrometer that measured from 350-2500 nm with 1024 spectral channels that measure with bandwidths of 1.5 nm from 350-1000 nm, 3.5 nm from 1000-1850 nm, and 2.4 nm from 1850-2500 nm. Much like the FIGOS systems, the spectrometer rode on a carriage along a zenith arc. However, unlike the FIGOS device, this zenith arc was suspended from a large transom that could be raised or lowered to allow for various object heights. [3] This suspended design was able to scan only half of an azimuth slice at any given position since the carriage only moved over the quarter arc shown in figure 2.11. This reduced the shadow caused by the supporting structure but required twice the amount of azimuth movements per hemisphere scanned, when compared to the FIGOS system. This large suspended truss design allowed for just a single point of contact to steer and stabilize the sensor, but was therefore more susceptible to wind and other stresses than other field goniometers. The azimuth rotations were performed by a single stepper motor located on the end of the boom at the top of the lifting mast. The zenith positioning was performed by





Figure 2.11: Various views of the GOPHER instrument.[12]

another stepper motor that was connected to a drive train that moved the carriage containing the spectrometer. The system employed a 1.6 meter radius arc that was approximately 20 percent smaller than FIGOS or ULGS 2.0. As previously stated, goniometers with truss systems that raise and lower to accommodate a certain target plane are useful but can still exhibit parallax errors. Figure 2.12 provides the reader with a look at what effect this can have on the overall GIFOV with a system as large as GOPHER. Since a main goal of the GOPHER system was portability, the entire goniometer could fold down into a transport configuration that allows for the device to be



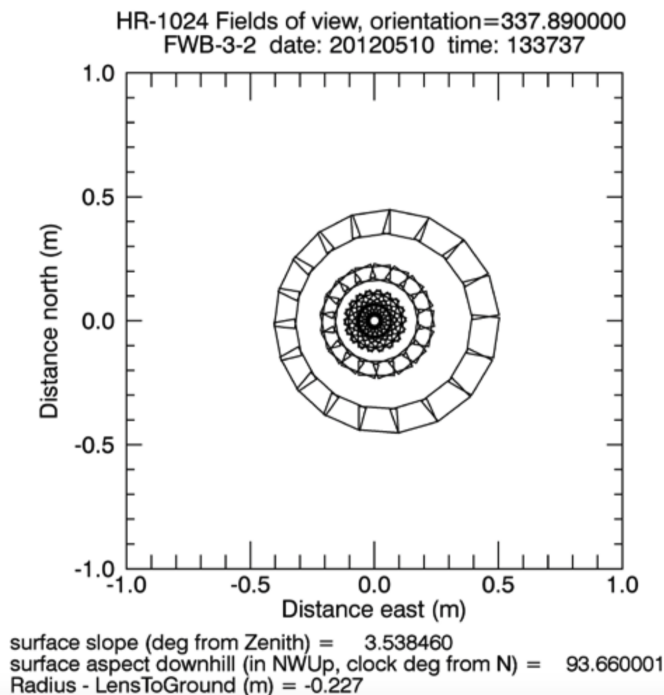


Figure 2.12: GOPHER overall GIFOV example for an entire scan plotted on one figure. Note the movement of the measured spot depending on the current azimuth and zenith position.[12]

trailed behind a truck or all-terrain vehicle as seen in figure 2.11. While in the folded position, GOPHER could be towed at reasonable speeds for the terrain encountered. The authors stated that the system had large flotation tires that allowed travel through muddy areas and aided in fording shallow waterways of less than 0.6 meters depth, if necessary. If the terrain was smooth enough, the system could also be towed in its erected state to reduce setup time between BRDF measurements, which could be substantial for a large goniometer. Based on the size and the complexity of the 450 pound GOPHER instrument, it was estimated that the system would require at least 90 minutes to transition from folded to unfolded and ready to take data. Much like other instruments, this system must be manually leveled using two electric jacks to ensure the consistency of the mechanical movements and to provide reference angles with respect to other airborne or spaceborne sensors. Overall, the GOPHER system created for NRL is a very adaptable system that displays many of the benefits of the original FIGOS and ULGS 2.0 systems, but had been specifically adjusted to suite the needs of the owner. The key differences are noted as the ability to adjust target height, manually accommodate greater slopes, and to be rugged and mobile enough to reach soft tidal locations.[12]

### 2.3.3 Automated Spectro-Goniometer

The Automated Spectro-Goniometer (ASG) is a system created by environmental scientists at the University of California at Santa Barbara. This system was designed to enable the study of snowmelt by better understanding the hemispherical-directional reflectance function (HDRF) of different types of snow. Much like with sediments, the attributes of the snow reflectance are dependent on grain size and other physical parameters. This necessitates an instrument that can be taken to the field to measure the samples in-situ. The ASG system was the first automated field goniometer that was specifically created for use in measurements of snow. Due to this, the system was designed with mobility and accuracy as key performance parameters, and was substantially smaller than most automated devices. The apparatus provides a 0.65 meter distance to target over the entire hemisphere and had a stationary target plane located at the center of the base circle. Much like ULGS 2.0 and GOPHER, the ASG had a rotating structure supported from above that positioned the sensor-head at a specific azimuth and elevation for collection. This design aided in the reduction of self-shading, and it ensured that the motors and gearing are located as far from the snow as feasible, further increasing the system's reliability. These features can be seen in figure 2.13. The ASG utilized an ASD-FR field portable spectrometer that collected radiance information

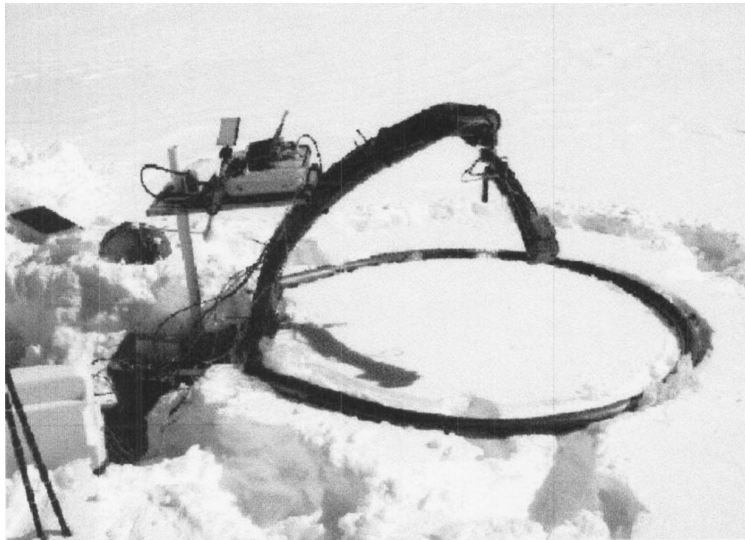


Figure 2.13: Automated Spectro-Goniometer deployed on snow.[4]

from 350 nm to 2500 nm. The spectral resolution was 3 nm from 350 to 1000 nm, and 10 nm from 1000 to 2500 nm. This spectrometer was attached to fore optics of varying FOV including 1 degree, 4 degrees, and 8 degrees. Given the viewing geometry, the 4 degree fore optic provided a 4.5 cm diameter GIFOV at nadir. The motions of the ASG were completed using two brushless servo

motors with built-in encoders affixed to pre-loaded worm gears. This method of facilitating motion worked well for small systems as the worm gears will eliminate much of the backlash associated with direct gearing, therefore reducing the movement error in the system. This helped the system meet its goal of 2 degree accuracy motions in both azimuth and zenith directions with respect to the frame of the device itself; understanding geolocation and heading with respect to earth were not expressly discussed. The maximum achievable zenith look angle with respect to the target was given as 80 degrees. Electrically, the system operated on 120 volt AC power, in contrast to most portable devices, which utilize DC power that can be easily extracted from batteries. One of the main attributes of the ASG system overall was its rapid sampling. The mechanical motions were designed around the capabilities of the spectrometer itself and it can therefore could obtain an entire hemispherical scan in 15 degree azimuth and zenith steps in less than 6 minutes. This was substantially faster than other portable goniometer systems and ensured that the natural motion of the sun during the course of a scan is almost negligible. This rapid scanning combined with the total weight of 49 kg makes this goniometer one of the most mobile, fully automated designs created to date.[4]

### **2.3.4 GRIT**

The Goniometer at the Rochester Institute of Technology, or GRIT[18], was a system designed and built in the Chester F. Carlson Center for Imaging Science. This device was created in 2013 by Bachmann et al.[18] to study various sediments in laboratory and field environments. Due to the need for SWIR measurements to study mineral content, GRIT employed an ASD FieldSpec-4 spectroradiometer that provided sampling from 350-2500 nm with a spectral bandwidth of 1.4 nm from 350-1000 nm and 1.1 nm from 1001-2500 nm. In order to achieve an adequate GIFOV on the target, this spectrometer was usually coupled to a 5 degree fore optic, providing for a 4.36 cm diameter spot at nadir. The device utilized a 1 meter ring and 0.5 meter arc to allow for full hemisphere scanning. As seen in figure 2.14, the device operated similarly to the ULGS and GOPHER systems in that it captured half of a given azimuth plane at a time, then combined this with azimuth rotations to gather the entire hemisphere. Due to the short timeline for the design and construction of GRIT, it was largely created out of commercial off-the-shelf (COTS) items. This limited the choices for frame and structural design to what could be quickly obtained. Due to this, the main ring for the GRIT device was a two-piece design where the bottom ring was stationary and the top ring would spin to provide azimuth motion. The arc that provided for zenith motion was also created out of similar ring material and utilized a carriage that aimed the sensor by driving up and down the zenith arc with the use of a belt drive. This arc allowed for a maximum zenith angle of 65 degrees. For both motions, standard stepper motors with spur gearboxes would

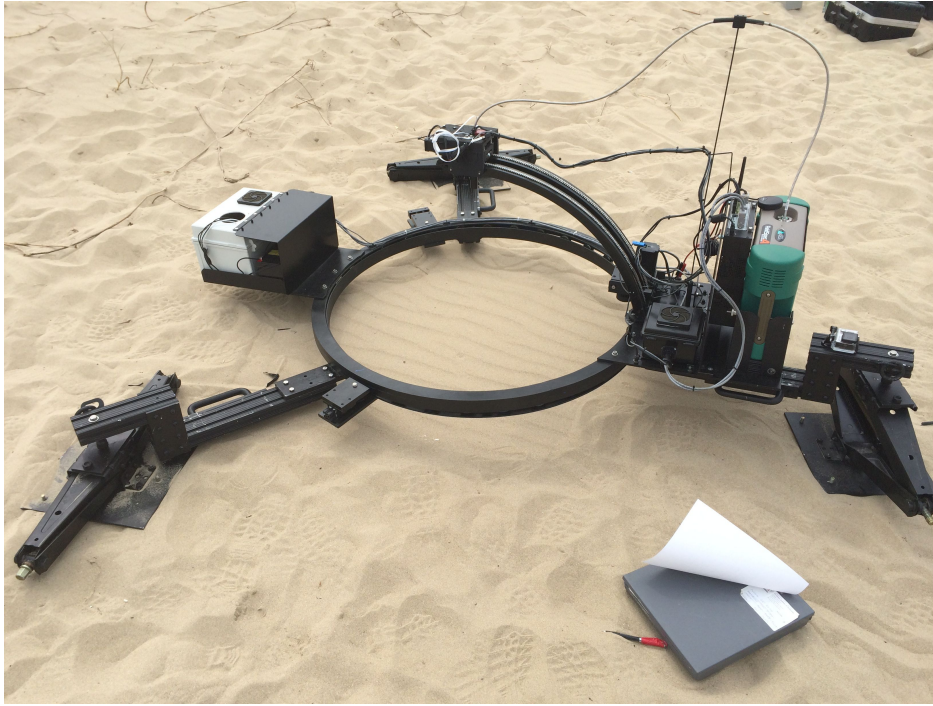


Figure 2.14: GRIT device with leveling jacks attached.

drive the azimuth ring and zenith carriage using a timing belt drive pulley. In order to capture the current position of the azimuth ring and zenith carriage, two VectorNav inertial measurement units (IMUs) were used. To monitor sensor pointing, a VN-100 compact IMU rode atop the zenith carriage and provided angular information about the fore optic's current position. GRIT then used a second IMU, a VN-300 with differential GPS heading, to monitor the overall heading of the frame and to provide GPS timing and position information. These devices, along with the motors and ASD spectrometer, were coordinated using a wireless connection through a Linux-based computer that ran GRIT in a partial automation mode. This mode allowed for the programming of scan patterns, spectrometer parameters, and movement speeds, but still required the user to request the spectral retrieval and then prompt the system to begin the next motion. Given that the system was mostly created out of steel components, the GRIT system weighs approximately 230 pounds with spectrometer and leveling jacks attached. Since the device was still relatively lightweight, and exhibited a compact form factor, the portability was considered to be quite decent and had allowed for the measurement of HRDF atop large sand dunes and in soft, muddy areas. In addition, setup and tear down time was approximately 30 minutes with just one researcher, and the system could be stowed entirely inside one 5 foot by 5 foot by 2 foot transport container.

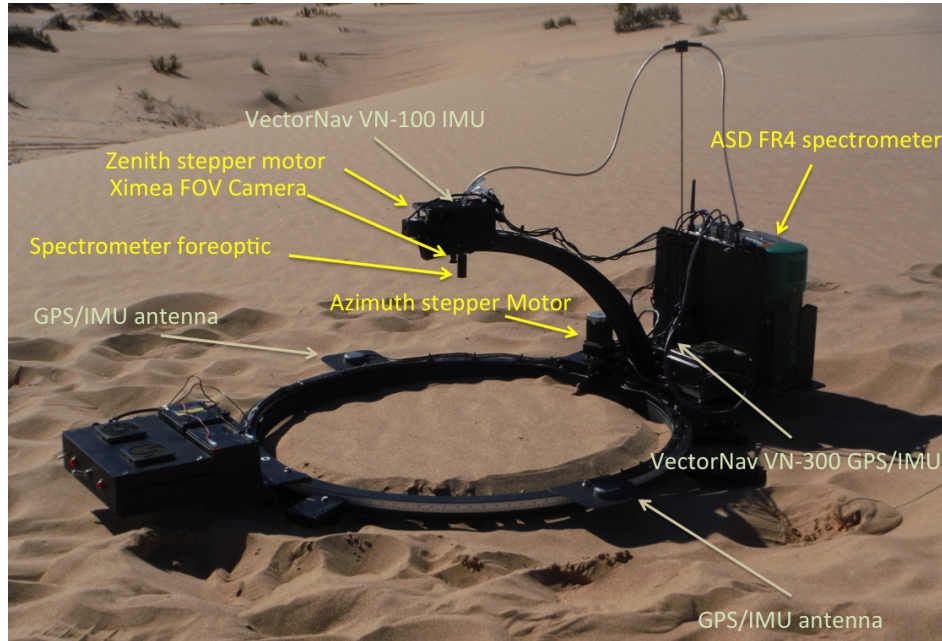


Figure 2.15: Locations of key components on the GRIT system.

### 2.3.5 Other notable Field-Portable Goniometers

In addition to the devices outlined in detail above, there are also many other goniometer systems that have been put to use in field environments. This section is meant to briefly introduce just a few of these other systems that have been created around the world. While the GRIT-T system did not heavily leverage any of these devices, each has attributes that may be highly desirable in other applications.

The first of these is the FIGIFIGO system designed at the Finnish Geodetic Institute in Finland. This device only featured a single azimuth plane but could be manually moved if a more dense scan is desired. Primarily contained in a single case, the design was very portable and had been hardened for use in remote locations. In addition, the goniometer featured a very unique optical design that could be used to greatly reduce the effects of parallax involving a steerable mirror with laser guidance. Figure 2.16 shows the device and figure 2.17 illustrates the novel optical design.[36, 42]

The next system physically resembles the final GRIT-T system in overall design, and involved a carriage and open ring approach to capture BRDF of vegetation. This goniometer, designed at the University of Twente in the Netherlands, was originally fully manual but has since been updated to allow for computer-controlled movements. Specifically designed for vegetation, the device featured a zenith arm that can be raised to move the target plane to an adequate height for measuring tall





Figure 2.16: FIGIFIGO system illustrating arm configuration and case.

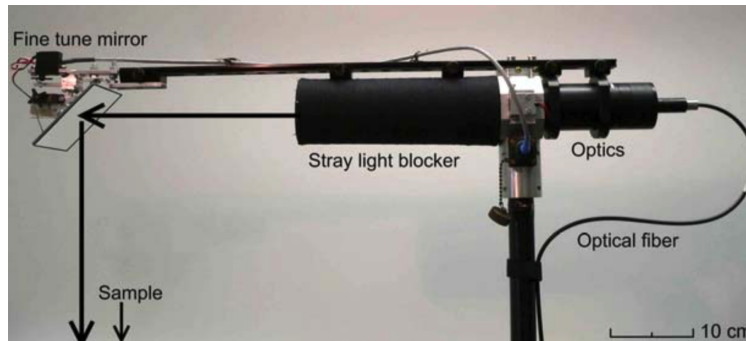


Figure 2.17: Unique FIGIFIGO optical design that allows for steering the measurement spot.

grass. This device typically used spectrometers, but has also been outfitted with thermal imaging sensors. This device can be seen in figure 2.18. [43]

Among the most ultra-portable goniometers is the fully manual ULGS 1 device created at the University of Lethbridge in Canada.[13] Consisting of an apparatus that resembles a scaled-down FIGOS, the goniometer provided the user with a lightweight method to accurately steer a spectrometer through fully manual means. See figure 2.19 and figure 2.20 below.[14, 13]

Another lightweight device that allows for more automation is the ManTIS device created by the Alfred Wegener Institute, Center for Polar and Marine Research in Germany. This tripod-



Figure 2.18: University of Twente goniometer system measuring vegetation.



Figure 2.19: Ultra-portable ULGS device.[13]



Figure 2.20: Larger variant of ULGS 1 constructed out of aluminum.[14]

based approach allowed for measurement of medium sized vegetation and was precision-machined out of aluminum. Therefore it weighed only 27 kg without the spectrometer. Designed to be very portable, the device disassembled to fit in a small case yet still provided some level of automation. However, due to the concessions made in order to achieve such a lightweight design, the overall angular accuracy of the view angles provided by the device may be less than those required for many scientific applications. The device is shown in figure 2.21.[15]



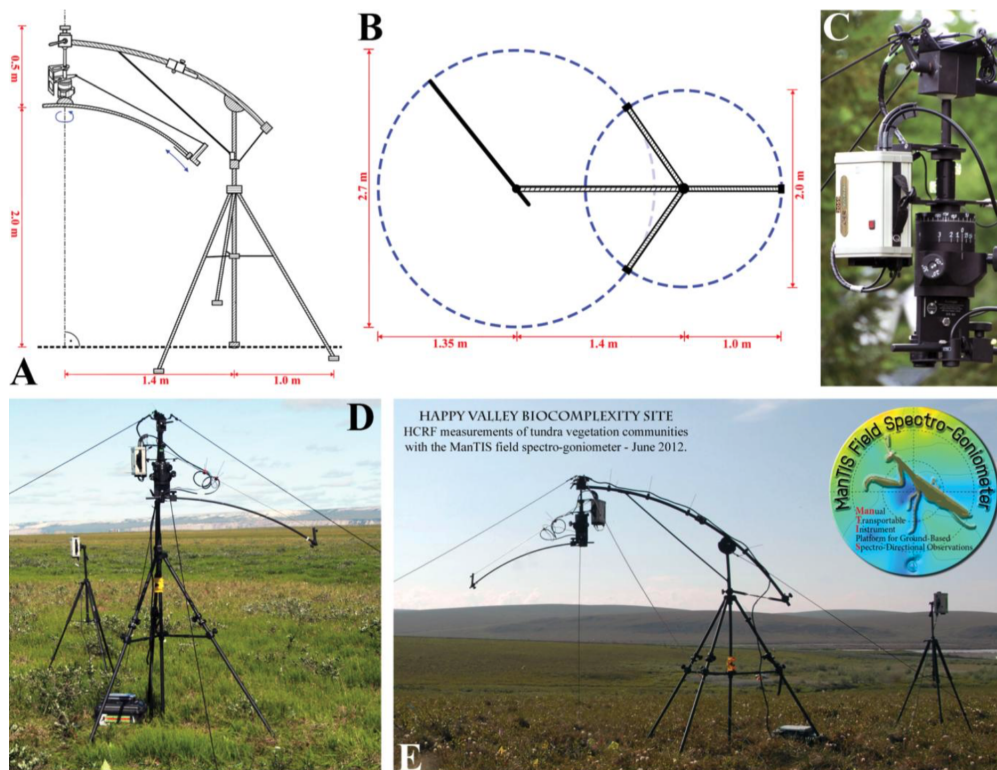


Figure 2.21: ManTIS goniometer system measuring vegetation.[15]



## Chapter 3

# Theory

Ultimately, the purpose of a goniometer is to measure the light leaving various objects. In order to provide the reader with a small foundation for the discussion later in this paper, the main concepts of radiometry are discussed in this section. These concepts include definitions for radiometric terms used in the paper, and a short background of the methods for describing the reflecting properties of materials. This section also identifies the main functions used to describe directional reflectance including bidirectional reflectance distribution function (BRDF), bidirectional reflectance factor (BRF), and hemispherical-directional reflectance function (HDRF).

### 3.1 Light

While it is assumed that the reader has some background in the study of light propagation, it is worthwhile to outline the terms used and their definitions as utilized by the author. In this document, as with all remote sensing discussions, various terms will be used to describe the regions of the electromagnetic (EM) spectrum with wavelengths from 10 nm to 14000 nm. These regions are defined as bands and are listed in table 3.1.

<b>Name</b>	<b>Abbreviation</b>	<b>Wavelength (nm)</b>
Ultraviolet	UV	10 - 400
Visible	VIS	400 - 700
Near Infrared	NIR	700 - 1100
Shortwave Infrared	SWIR	1100 - 3000
Midwave Infrared	MWIR	3000 - 5000
Longwave Infrared	LWIR	5000 - 20000

Table 3.1: Definitions for pertinent regions of the EM spectrum.[44]

Depending on the region of the light, the source of this could be a variety of objects. For the remote sensing purposes discussed in this paper, the primary regions of operation for a field goniometer would include the ultraviolet (UV) through the shortwave infrared (SWIR). While many objects could emit light of this wavelength if brought to the appropriate temperature, as defined by the Planck blackbody curve, the average observer does not come into contact with objects that hot very often. For this reason, we assume that any light that is captured in these regions has originally emanated from the sun, even if it has been reflected off of nearby objects. Beyond these regions, including the mid-wave infrared (MWIR) and long-wave infrared (LWIR), the origin of the light is more difficult to determine as the temperatures required to emit such light are far more common in everyday life.

## 3.2 Radiometric Terms

In order to prepare for discussion throughout the paper, certain radiometric terms will be described to ensure that the nomenclature is clear to all readers. These terms are consistent with the internationally recognized standard for discussing light. [45].

### Radiant Energy

In order to discuss light energy, it is necessary to define the energy contained in a photon. This energy,  $q$ , is calculated using equation 3.1 where Planck's constant is  $h = 6.626 \times 10^{-34}$  [joules  $\cdot$  sec].[44]

$$q = h\nu = \frac{hc}{\lambda} \text{ [joules]} \quad (3.1)$$

From here you can notice that shorter wavelength photons carry more energy than longer wavelength photons. It is then possible to determine the total energy in a ray of light over all wavelengths, as shown in equation 3.2.

$$Q = \sum_i \frac{n_i hc}{\lambda_i} \text{ [joules]} \quad (3.2)$$

This can then be broken down into spectral energy density using equation 3.3.

$$Q_\lambda = \frac{dQ}{d\lambda} \text{ [joules} \cdot \text{nm}^{-1}] \quad (3.3)$$

### Radiant Flux

Typically, the rate at which energy is deposited is more useful than the overall amount of energy deposited over some time period as a whole. To describe this, we use the term radiant flux, or power. This power is defined by dividing the total energy by change in time as shown in equation 3.4.[44]

$$\Phi = \frac{dQ}{dt} [W] \quad (3.4)$$

To calculate the amount of flux by wavelength, we use equation 3.5.

$$\Phi_\lambda = \frac{d\Phi}{d\lambda} [W \cdot nm^{-1}] \quad (3.5)$$

### Irradiance

Now that we have quickly discussed the idea of flux and how energy is deposited over time, it is possible to define the concept of irradiance. This is similar to flux in that it describes the energy deposit temporally, but it also incorporates a spatial factor. This allows for inspection of how much energy (light) is hitting an object per second per unit area, as given in 3.6.[44]

$$E = \frac{d\Phi}{dA} [W \cdot m^{-2}] \quad (3.6)$$

Depending on the scene geometry, it may be necessary to modify the irradiance equation if the source is not at nadir with respect to the object. In this case, the projected area of the object must be accounted for. The observed area from the source is represented by equation 3.7 where  $dA_\theta$  is the projected area. It is then possible to combine 3.6 and 3.7 to produce the corrected irradiance,  $E_\theta$ , found in equation 3.8.

$$\cos \theta = \frac{dA_\theta}{dA} \quad (3.7)$$

$$E_\theta = \frac{d\Phi_\theta}{dA_\theta} = \frac{d\Phi}{\frac{dA}{\cos \theta}} = E \cos \theta [W \cdot m^{-2}] \quad (3.8)$$

### **Radiant Intensity**

Another method to describe the light interacting with a surface is by the use of radiant intensity. Unlike irradiance, intensity does not provide a spatial description but rather an angular description of the amount of light in a cone. In order to describe the size of this cone, we use the term solid angle or  $d\Omega$ . The quantity used to define the solid angle is referred to as a steradian (sr) and the amount of steradians in a particular solid angle is given by  $d\Omega = dA/r^2$  [sr]. It is then possible to define intensity,  $I$ , as the total power in a solid angle. This is given in equation 3.9.[44]

$$I = \frac{d\Phi}{d\Omega} [W \cdot sr^{-1}] \quad (3.9)$$

### **Radiance**

A more complex way to describe a quantity of light is with the term radiance,  $L$ , which has attributes of both irradiance and intensity. Simply put, radiance describes the amount light in a spatial sense and in a angular sense simultaneously. While this term may be more difficult to understand initially, it is very useful and commonly heard when discussing cameras and other sensors that measure light, including spectrometers. The popularity of using radiance for light propagation stems from the fact that it is constant over distance assuming no transmission losses. The mathematical expression for radiance is given in equation 3.10.[44]

$$L = \frac{d^2\Phi}{dA \cos \theta d\Omega} [W \cdot m^{-2} \cdot sr^{-1}] \quad (3.10)$$

It is also possible to describe radiance in terms of irradiance or intensity, as found in equations 3.11 and 3.12, respectively.

$$L = \frac{dE}{d\Omega \cos \theta} [W \cdot m^{-2} \cdot sr^{-1}] \quad (3.11)$$

$$L = \frac{dI}{dA \cos \theta} [W \cdot m^{-2} \cdot sr^{-1}] \quad (3.12)$$

#### **3.2.1 Material Interaction/Reflectance**

When light comes into contact with an object it is either reflected back away from the object, transmitted through the object, or absorbed by the object. While there are many interesting effects observed for light that has passed through or been absorbed by an object, for the purpose of

this document the focus will be on light that has been reflected. Based on the material interaction and the wavelength of the incoming light, the reflected light will exhibit properties that indicate something about the surface. Typically, this reflected light indicates the type of materials in the reflecting object by absorbing more of a certain wavelength than others, due to absorption features. Furthermore, the depth of these absorption features is typically indicative of the relative amounts of the various materials present as given by figure 3.1 showing the absorption features of earth's atmosphere. Specifically, we speak of reflectance in terms the ratio of the irradiance leaving a scene,

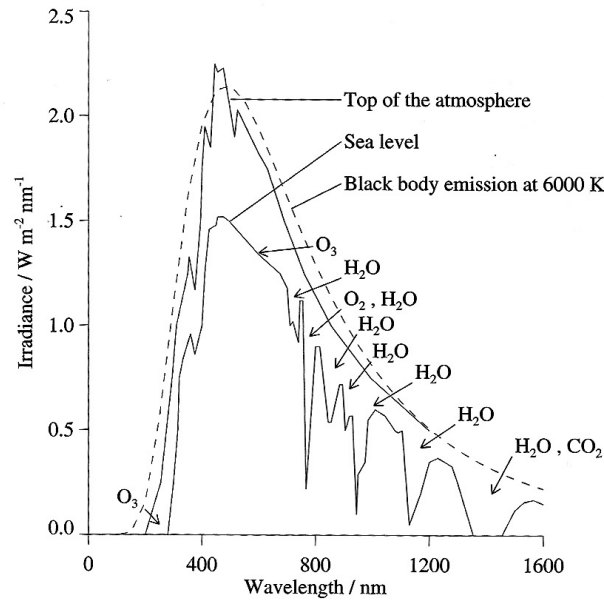


Figure 3.1: Illustration of absorption features in the Earth's atmosphere.[16]

known as exitance, divided by the amount of irradiance arriving at a scene, based on wavelength, which is given in equation 3.13.[44, 17]

$$\rho(\lambda) = \frac{M(\lambda)}{E(\lambda)} \frac{[W \cdot m^{-2}]}{[W \cdot m^{-2}]} \quad (3.13)$$

Describing how light reflects off of an object requires the reader to understand the various terms used to characterize the reflections that can occur. These terms describe the direction of the reflected light once it has interacted with an object. They are specular reflections, diffuse reflections, and a mixture of the two, known as directional diffuse reflections. Surfaces that are very smooth will typically exhibit specular reflections, such as a mirror. Rough surfaces that have many facets

typically reflect light diffusely, such as unpolished concrete. Since many surfaces are neither perfectly smooth or very rough, their reflections fall in the middle and are referred to as directionally diffuse. These types are further described below and are depicted in figure 3.2.

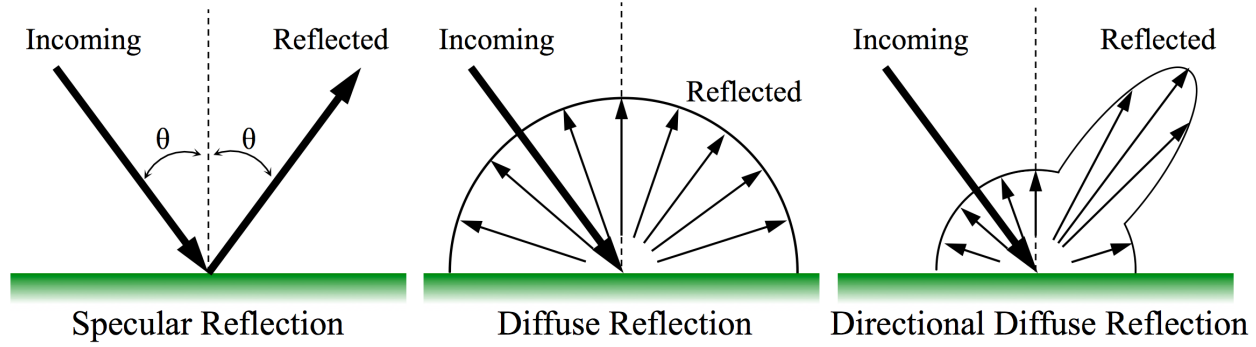


Figure 3.2: Illustration of the types of reflections.

### Specular Reflections

Specular reflections are commonly found in everyday life when a person looks into a mirror or at the hood of a new car and sees a perfect reflection. In this situation, the light is being reflected at the same angle off of an object as when it hit the object. That is, the angle of incidence is equal to the angle of reflection as described by the law of reflection, equation 3.14. From a remote sensing perspective, this interaction is less interesting since the majority of objects of interest do not exhibit this type of reflection.[34]

$$\theta_i = \theta_r \quad (3.14)$$

### Diffuse Reflections

Diffuse reflections are those that scatter light equally in all directions. This is typically found on rough surfaces and is caused by the facets of the surface randomly scattering light in all directions, independent of the incident direction. These objects are referred to as being Lambertian. To put this in radiometric terms, this means that the outgoing intensity of the light falls off equally with view angle, with respect to the surface normal. This angular falloff is described by equation 3.15, where  $I(\theta)$  is the intensity of light at an angle,  $\theta$ , off of surface normal.[44]

$$dI(\theta) = dI_0 \cos \theta \text{ [W} \cdot \text{sr}^{-1}] \quad (3.15)$$



From this equation, it is possible to substitute the definition of radiance in terms of intensity, 3.12, to determine the radiance leaving the object, as seen in 3.16.

$$L(\theta) = \frac{dI(\theta)}{dA \cos \theta} = \frac{dI_0 \cos \theta}{dA \cos \theta} = \frac{dI_0}{dA} = L_0 \text{ [W} \cdot \text{m}^{-2} \cdot \text{sr}^{-1}] \quad (3.16)$$

This equation shows that for a perfectly Lambertian surface, the reflected radiance is the same regardless of direction. This is because the decrease in intensity seen as the observation angle increases away from nadir is exactly offset by the increase in projected area. This phenomenon is depicted in figure 3.3. In addition to discussing radiance off of a Lambertian surface in terms of intensity, it is also useful to observe how radiance and irradiance are related for these surfaces. Equation 3.17 provides the groundwork to discuss this relationship, where  $E_\theta$  is the irradiance onto the diffuse surface from a given angle relative to the surface normal.

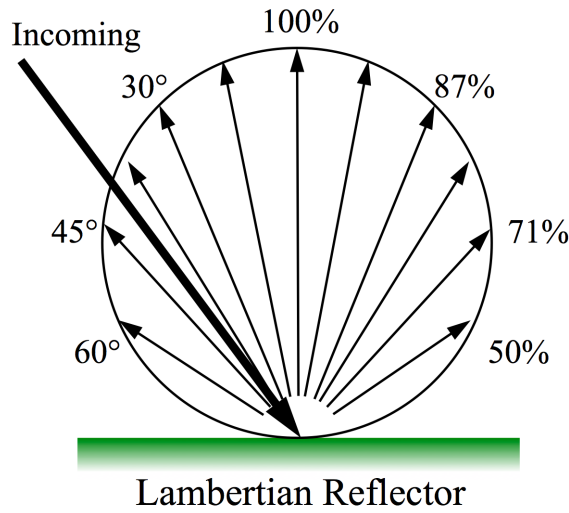


Figure 3.3: An illustration of a Lambertian reflector. Note that the radiance from a Lambertian reflector is the same from all view angles since the decrease in radiance (due to being off nadir), is exactly offset by the increase in the FOV's projected area on the material.

$$E_\theta = E_0 \cos \theta \text{ [W} \cdot \text{m}^{-2}] \quad (3.17)$$

The reflected exitance can then be found using 3.13 to create 3.18.

$$M = E_{\theta} \rho \text{ [W} \cdot \text{m}^{-2}] \quad (3.18)$$

Finally, it is possible to relate this concept back to radiance by substituting equation 3.11 and reducing to ultimately achieve 3.19.

$$L = \frac{M}{\pi} \text{ [W} \cdot \text{m}^{-2} \cdot \text{sr}^{-1}] \quad (3.19)$$

While the average person may not encounter a Lambertian surface, in the remote sensing community, imaging devices are typically referenced to panels that are mostly Lambertian. These panels are often created with Spectralon reflectance material, which is NIST trace-able and advertised as being over 99% reflective for most wavelengths in the VNIR through SWIR spectral range.[8]

### **Directional Diffuse Reflections**

The vast majority of surfaces exhibit reflectance characteristics that would not be described as either specular or diffuse. In this paper, we refer to these less-idealized surfaces as directional diffuse. This means that the reflection is some combination of specular and diffuse as seen in figure 3.2. Since the direction of the reflected energy, especially when resolved spectrally, can be thought of as a material's fingerprint, these reflections are often measured by goniometric methods such as those described in this paper. Describing the magnitude of the reflected light is typically done via a bidirectional reflectance distribution function, or BRDF, which is discussed at length in the next section.

## **3.3 Methods for Describing Angular Reflectance**

Describing angular reflectance can be done in a variety of ways. The illumination of the scene and the method for capturing the reflected light dictate which method should be utilized. As originally described by Nicodemus[30] and as seen in figure 3.4, there are nine cases in which to describe reflectance quantities. For the purpose of this paper, two of these will be the focus, as they are typically the ones measured by goniometers. Those two are the BRDF, which is a case of directional light and directional reflectance, and the HDRF, which is a case of hemispherical light and directional reflectance. [30]

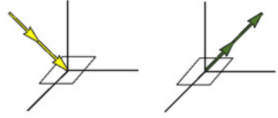
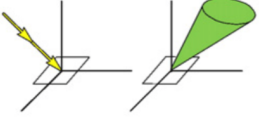

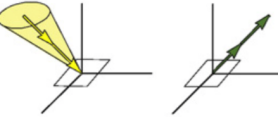
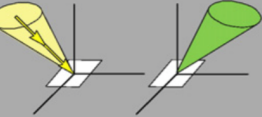
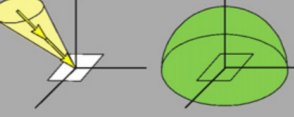
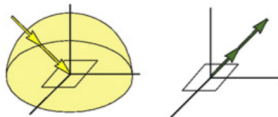
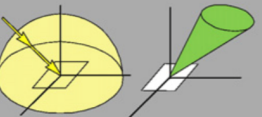

<i>Incoming/Reflected</i>	<b>Directional</b>	<b>Conical</b>	<b>Hemispherical</b>
<i>Directional</i>	<b>Bidirectional</b> <b>Case 1</b> 	<b>Directional-conical</b> <b>Case 2</b> 	<b>Directional-hemispherical</b> <b>Case 3</b> 
<i>Conical</i>	<b>Conical-directional</b> <b>Case 4</b> 	<b>Biconical</b> <b>Case 5</b> 	<b>Conical-hemispherical</b> <b>Case 6</b> 
<i>Hemispherical</i>	<b>Hemispherical-directional</b> <b>Case 7</b> 	<b>Hemispherical-conical</b> <b>Case 8</b> 	<b>Bi-hemispherical</b> <b>Case 9</b> 

Figure 3.4: Illustrations of the types of reflectance quantities.[8]

### 3.3.1 BRDF

The BRDF, shown as case 1 in figure 3.4, of a surface is used to describe how incident light will be scattered into various directions away from the surface. Based on the definition from Nicodemus[30], this is calculated using the incoming irradiance, given in 3.21, from a particular illumination direction and the reflected radiance as observed from a particular view direction, as seen in equation 3.20. [30, 46]

$$\rho_{BRDF}(\theta_i, \phi_i; \theta_r, \phi_r) = \frac{dL_r(\theta_i, \phi_i; \theta_r, \phi_r)}{dE_i(\theta_i, \phi_i)} [sr^{-1}] \quad (3.20)$$

$$dE(\theta_i, \phi_i) = \cos \theta_i \sin \theta_i L_i(\theta_i, \phi_i) d\theta_i d\phi_i = d\Phi_i(\theta_i, \phi_i) / dS \quad (3.21)$$

In 3.20,  $\theta_i, \phi_i$  represent the zenith and illumination angles of the direction of illuminating irradiance and  $\theta_r, \phi_r$  represent the reflection angles of the direction of leaving radiance. It is worth noting that many in the remote sensing community refer to the azimuth that describes the source's position to

be the azimuth of the principle plane. This plane therefore represents a slice of both the forward scatter and backward scatter lobes of the BRDF. While the equation provided above discusses BRDF monochromatically, this is typically extended to allow for a BRDF for each wavelength of interest. Due to the fact that every source and sensor have a finite size, and that the BRDF equation represents illuminating and reflected light in terms of differential solid angles, it is not theoretically possible to measure the BRDF of an object. However, in practice, this definition is loosened to allow for collimated light and a reasonable sensor size with the understanding that this has effects on the accuracy of the BRDF. Therefore, it is prudent for those attempting to measure BRDF to use as small of a source and detector as possible to achieve the best accuracy. For certain objects or when there is a lack of data, the BRDF is considered to be azimuthally symmetric. While this assumption may be adequate for certain applications, it may be wildly inaccurate for objects that have spatial organization, such as a field of crops. [46]

### 3.3.2 BRF

Very similar to BRDF, the bidirectional reflectance factor (BRF) is another method used to describe how reflectance is dispersed from a surface. The BRF, still relies on having directional illumination and directional reflectance, but is normalized to that of a perfect Lambertian reflector. The definition of BRF is given as the ratio of reflected flux from a surface in a particular direction to the reflected flux from a perfectly Lambertian surface in the same direction, when under similar illumination. The mathematical expression for BRF is given below in equation 3.22.[46]

$$\rho_{BRF}(\theta_i, \phi_i; \theta_r, \phi_r) = \frac{d\Phi_r(\theta_i, \phi_i; \theta_r, \phi_r)}{d\Phi_r^{Lam}(\theta_i, \phi_i)} \quad (3.22)$$

It is then possible, with substitution from 3.21 and reduction, to relate BRF to BRDF mathematically. This reduction utilizes the fact that the BRDF of an ideal Lambertian surface is equal to  $1/\pi$ . The final result is that BRF is related to BRDF through only a factor of  $\pi$ , as shown below in 3.23.

$$\rho_{BRF}(\theta_i, \phi_i; \theta_r, \phi_r) = \pi \cdot \rho_{BRDF}(\theta_i, \phi_i; \theta_r, \phi_r) \quad (3.23)$$

It is also useful to note that BRF is a unitless quantity, unlike BRDF, since it is normalized to a Lambertian reflector.

### 3.3.3 HDRF

The hemispherical-directional reflectance factor (HDRF) is another method of describing the angular reflectance off of an object, as shown in case 7 of figure 3.4. With the HDRF method, the illumination on an object is provided by the entire hemisphere above it, while the observed reflectance is still angularly resolved. This type of reflectance is very useful when measuring the reflectance of objects outside, where both the sun and the diffuse skylight are illuminating the surface. The expression for HDRF is given in equation 3.24, including a substitution and reduction with 3.21 to allow for equating radiance measurements.[46]

$$\rho_{HDRF}(\theta_r, \phi_r) = \frac{d\Phi_r(\theta_r, \phi_r)}{d\Phi_r^{Lam}} = \frac{L_r(\theta_r, \phi_r)}{L_r^{Lam}} \quad (3.24)$$

Since this type of reflectance is conducive to outdoor measurements, it is often used with field experiments to provide a reasonable angular reflectance function under typical sky conditions. It is important to note, however, that the HDRF measured under outdoor conditions is not universal to all situations, but specific to the spatially dependent diffuse illumination at the time it was gathered. This is due to the fact that no angular illumination information is required to determine HDRF. That being said, it is possible to retrieve BRDF but only assuming that knowledge exists for the surrounding diffuse illumination, which could be either gathered directly or modeled in an atmospheric compensation software. If this is achieved with atmospheric compensation software, it is important to note that the multiple scattering effects between the surface and atmosphere are being neglected. Otherwise, retrieval of BRDF from HDRF can be accomplished using equation 3.25.[46]

$$\rho_{HDRF}(\theta_r, \phi_r) = \frac{\int_0^{2\pi} \rho_{BRDF}(\theta_i, \phi_i; \theta_r, \phi_r) \cos \theta_i \sin \theta_i L_i(\theta_i, \phi_i) d\theta_i d\phi_i}{(1/\pi) \int_0^{2\pi} \cos \theta_i \sin \theta_i L_i(\theta_i, \phi_i) d\theta_i d\phi_i} \quad (3.25)$$



## Chapter 4

# Methodology

When designing a new remote sensing system, such as a goniometer, the design process must always begin with a set of well-defined requirements that the system is intended to meet, based on its intended use. These requirements will include specifications and intended modes of operation that will shape each design decision made as the system is engineered. These requirements can then be broken down into derived requirements that will further specify how each aspect of the system must behave in order to effectively achieve the final scientific goals. This basic systems engineering approach was utilized for this effort to effectively manage competing requirements and to ensure that each systems-level design decision was being made with a focus towards producing the most accurate BRDF feasible, given financial constraints and time constraints. By combining these requirements along with knowledge of how the system would be operated, and the other equipment that it would interact with, it was possible to ensure that various subsystems would compliment each other and achieve a synergy that would ultimately reduce the complexity of the concept of operations for both laboratory and field environments. Once the system had been created and finalized, methods were developed that were intended to quickly and accurately post-process the resulting data into a more compact format that would be easier for the observer to comprehend, therefore increasing the ability to discern meaningful trends. In order to understand and characterize how well the system performed, a comprehensive test method will be described in section 4.4. Methods are proposed to test the system from both a mechanical and optical standpoint, providing consumers of the output data with a greater level of confidence. Finally, methods are proposed to determine the effectiveness of the background illumination compensation technique.

## **4.1 Scientific and Operational Requirements**

The scientific requirements for the GRIT-T were largely derived from the unique targets and often austere environments visited by the research group in support of radiative transfer modeling, i.e. extracting sediment density, grain size distribution, and moisture content, and satellite calibration and validation. The main targets of interest for the GRIT-T effort are various types of sediments and low vegetation, often measured in situ and in the laboratory. As previously mentioned, these targets are typically in remote deserts or coastal areas that are very difficult to reach by automobile, and these targets can range in temperature from below freezing to over 100 degrees Fahrenheit. This wide temperature range, combined with occasional gusts of blowing dust or sand, muddy clay, and at times unpredictable weather conditions can cause havoc for the operation of a robotic instrument, such as a field goniometer. In addition to fundamental environmental and scientific requirements, certain features were added to decrease operator fatigue, decrease the overall time to complete a scan, and increase mechanical and optical accuracy. These features were determined based on the experiences from past field and laboratory experiments with the current GRIT system, as well as from other well-known goniometer systems, such as Dual Field-of-View FIGOS and GOPHER.

### **4.1.1 Optical Requirements**

At the heart of the scientific requirements are the optical requirements of the system. The first optical requirements consist of obtaining an adequate GIFOV and performing spectroscopy at relevant wavelengths, both of which were completely target dependent. The extent of spatial averaging can have a significant impact on the BRDF when collecting in areas that have fast spatial changes in material composition or surface roughness. While this large scale averaging may be desirable for certain satellite calibration techniques, it is not necessarily desirable when collecting data for radiative transfer modeling. Due to this, a nominal GIFOV was chosen of reasonable diameter (5 cm at nadir) to allow for adequate spatial averaging to get a characteristic spectra of the mixed sediments while remaining small enough to ensure that only the desired target area was measured. The requirements also dictated that this GIFOV be adjustable, within reason, to allow for larger or smaller FOVs depending on the objectives of the collection campaign. Since the studies conducted by the research group often included collecting spectra at large zenith angles, it was also decided that this next generation device be able to achieve zenith view angles of at least 70 degrees from nadir.

Another optical constraint that goes hand-in-hand with spatial averaging is the reduction of parallax error found in the inflexible target planes of most field goniometers, illustrated in 2.6. As seen in various systems discussed in chapter 2, this undesirable effect can further complicate under-



standing the optical accuracy of a goniometer system and ultimately misrepresent the reflectance spectra of a target at certain look angles, depending on the surrounding areas, since that area may not be of the same composition as the target area. The severity of this parallax is tied to the distance between the instrument's target plane and the actual distance to the ground, which varies due to sloped terrain when measuring in the field environment. For the GRIT-T system, eliminating the effects of parallax became a hard requirement due to the nature of the design, as discussed later in this document, and the fact that the GRIT-T system must be able to conduct measurements on sloped areas. However, unlike other gantry-type systems, where adjusting the target plane is a manual process completed by a user, it was decided that this system must be able to automatically adjust the target plane elevation due to the frequency of measuring in-situ targets on sloped terrain. The effects of compensating for this parallax on angular accuracy, as well as pointing consistency, are discussed further in 4.1.4 and 4.3.

Much like the GOPHER and the GRIT systems discussed in sections 2.3.2 and 2.3.4, respectively, the GRIT-T system was designed to measure sediments and vegetation. While much information can be gleaned from measuring each of these types of targets in the VNIR regime, capturing the relevant material absorption features of sediments requires the use of a spectrometer with SWIR capabilities. Specifically, the wavelength requirement for the device included capturing reflectance data from approximately 350 nm to 2500 nm in at least 1000 bands under varying illumination conditions, as might be found on a very sunny day in the field or in the relatively lower light conditions that occur in the laboratory setting. Also, the spectral resolution must allow for the observation of various absorption features throughout the VNIR and the SWIR. In addition to the wavelength requirements, the spectrometer chosen must exhibit adequate SNR (especially in the SWIR) as judged by the noise-equivalent change in radiance ( $NE\Delta L$ ). This SNR requirement must be kept in mind also when considering overall system design, since some mechanical designs require a spectrometer's fiber optic cable to be lengthened. This lengthening can further increase the  $NE\Delta L$  and reduce the SNR.

Due to the variety of terrains encountered, the effects of background illumination from light reflected off of nearby objects were a valid concern in designing the GRIT-T system. Tall trees and vegetation, or large hills and sand dunes, can introduce unwanted effects into the collected spectra and, therefore, allow for misrepresentation of the actual target's reflectance. Even in clear sky conditions, without nearby vegetation, diffuse illumination from the sky alone can have a non-negligible effect on the target's reflectance. Studies have found that this effect can impact the signal from 15% to 40% for a clear sky, depending on solar zenith angle, or more than 40% in less-than-ideal atmospheric conditions. Therefore, the effects of this spatially varying illumination profile should not be ignored.[2, 47] The spatial effect of this diffuse skylight is illustrated in figure

4.1. These effects are often at certain wavelengths, depending on the material properties of the nearby object and atmospheric conditions, and may affect the target in varying magnitudes depending on illumination and sensor geometry which introduces errors in the understanding of the illuminating light interacting with the target. With standard goniometers, these errors are then embedded in the radiance data collected from the spectrometer, and it becomes impossible to remove or compensate for them if the background illumination that caused them is spatially dependent. As mentioned in 2.3.1, methods have been developed to help compensate for this background illumination error, but those require adding another spectrometer to the system that is outward-looking in order to map the spatial variation in the illumination surrounding the target. Despite the extra cost of this option, it was decided early on in the requirements development phase that since the GRIT-T system would frequently encounter situations where background illumination should not be ignored, a method for compensating must be included.

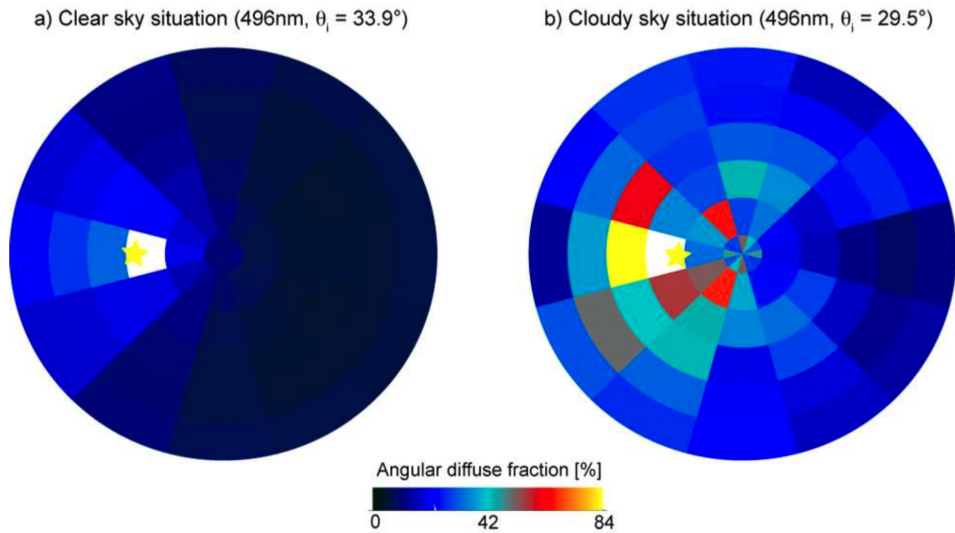


Figure 4.1: Angular diffuse fractions for clear and cloudy atmospheres as collected by Dual Field-of-View FIGOS.[2]

Equally important as the effects of background illumination are the temporal effects of illumination change during a scan. Since a BRDF scan is built up over the course of tens of minutes, the spectral data captured by the spectrometer is subject to the possibility that the sky may dim slightly with a thin passing cloud or other atmospheric effects, many of which are very common in the coastal environments in which the GRIT-T system will operate.[9] This may occur even without the user being aware, as some atmospheric effects, such as cirrus clouds, may not effect the visible

portion of the spectrum as much as the near infrared.[17] This can cause a significant error in calculated reflectance if the downwelling skylight is not monitored and temporally compensated for. For this reason, the GRIT-T system must be able to integrate with the illumination compensation methods described in Bachmann, et al.[9] This method utilizes a spectrometer that is dedicated to monitoring the overall downwelling light on a Spectralon panel with very high spectral resolution, and then uses this data to temporally compensate for decreases or increases in illumination per wavelength. This "base station" can also be utilized to provide direct solar illumination by blocking the sun and measuring the overall diffuse illumination, which provides direct illumination via subtraction. This approach is more accurate than typical methods of monitoring skylight since it is capturing illumination information in the same bands as the spectrometer that is sampling the target, thereby reducing the risk of artificial spikes in reflectance due to detector calibration mismatch. These artificial spikes are hereby referred to as spectral artifacts, since they are often very narrow and do not represent an attribute of the target.

In addition to those optical requirements listed above, the reduction of self-shading is also a very important requirement. As seen in the figures in chapter 2, many goniometer designs struggle with the effects of self-shading depending on the overall design, time of day, day of year, and latitude of the collection site. The effects of this self-shading can have a dramatic influence on the BRDF gathered, and virtually force the user to eliminate points impacted by self-shading since the radiance or reflectance data collected is based on unobstructed illumination conditions. This results in erroneously low calculated reflectance that is not representative of the target's actual reflectance at those angles. While many systems have found creative ways of trying to obtain a full BRDF while reducing self-shading, many are still large, heavy systems that would not satisfy other requirements established for the GRIT-T project. Other systems discussed in 2.3, such as FIGIFIGO, are able to reduce the self-shading and retain adequate size and weight parameters, but often lack the features of a fully-automated goniometer system. Due to this, the self shading requirements for the GRIT-T system meant minimizing the overhead footprint as much as possible. Since the width of the head that aims the fore optics is ultimately what dictates the angular amount of the obscuration as seen in figure 4.2, the requirement became a head that was as small as feasible while still achieving the other system requirements. Therefore, the designer eliminated the idea of a gantry-style design similar to that found on ULGS and GOPHER. Another source of self-shading when imaging on sloped terrain is that of the frame of the system itself. The supporting structure of a ring-based goniometer can also cast shadows into the measurement area, with most issues occurring when the sun is low in the sky. To combat this, the overhead footprint requirement was made more restrictive to further ensure that any obscuration, including the frame or any other support structure, was kept at a minimum.

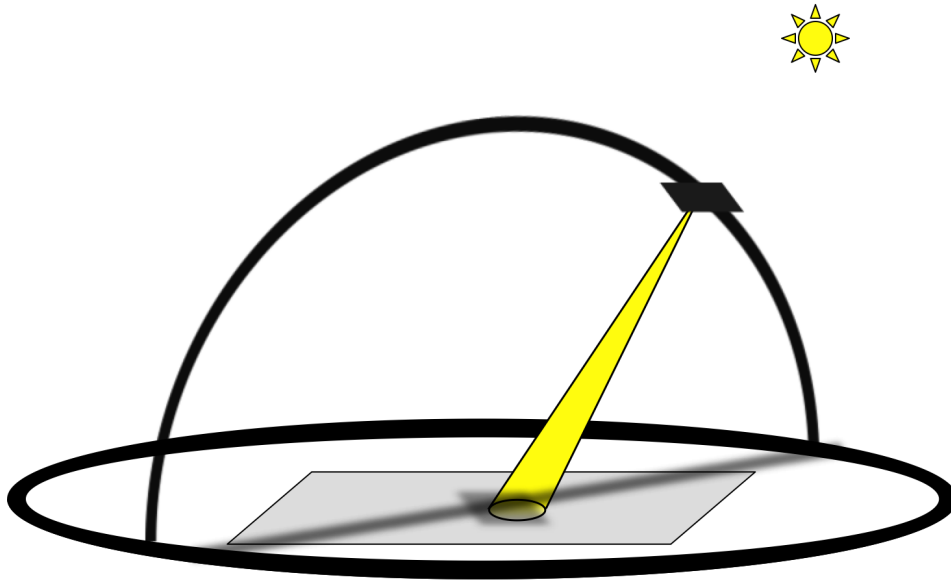


Figure 4.2: Both the sensor head itself and the frame of the goniometer can cast shadows into the scene in most designs. An example of this is shown for a design similar to that found in FIGOS[1].

#### 4.1.2 Expanded Portability

Unlike field-portable goniometers that remain stationary throughout the day, the GRIT-T system must be able to quickly reach multiple remote test sites. This is done in order to adequately map the natural variability in the landscape, and to capture as much information about the various types of sediments or vegetation as possible during the often short collection window. This generic requirement was then broken into more fundamental requirements that better describe what makes a system portable in terms of the terrain that would be encountered by this system. That is, the system must be lightweight, movable while fully assembled, adaptable to accommodate rugged terrain, and compact.

When considering the weight requirement of the instrument, various factors must be included in the discussion. The main factor is that of team size. When venturing out to remote test sites, it is often difficult financially and logistically to travel with a team of over six people. This fundamentally limits the number of individuals who can be dedicated to operating and moving the goniometer from site to site, given that the research team at RIT typically operates other optical and geotechnical instruments concurrently with the goniometer. Due to the nominal team size and the operation of other equipment, there are often only two or three researchers that can support the goniometer's needs at any given time, to include operation and movement. This means that the system must be

sufficiently lightweight to be lifted by only two researchers. Note, it could then be hand carried to the next collection site or placed on a small garden trailer for transport behind an all-terrain vehicle (ATV), as GRIT has been moved in the past. Figure 4.3 shows GRIT transport during the NASA Algodones Dunes Experiment in March of 2015. In addition to the weight requirement, another key



Figure 4.3: Especially in remote areas, the GRIT device was often moved via trailer behind an ATV.

to system portability was the ability to move the GRIT-T while fully assembled. Unlike many larger field-portable goniometers, the next-generation RIT goniometer must be of a size and weight that it can be moved from site to site without removing any hardware, batteries, leveling components, or scientific instruments, or shutting down the system; thus allowing for rapid movement, minimal downtime between collections, and an overall more efficient field data collection. This requirement proved to be a serious challenge since it meant that the maximum system weight must include the weight of both spectrometers used onboard the device. Another outcome of this requirement was that the mechanical stability of the system in movement situations, when solid footing might be difficult to come by, must be adequate enough to allow for only four points of contact from two people without causing lasting harm to the system itself or damaging the expensive spectrometers.

As mentioned above, the GRIT-T system might be put into use anywhere around the world. Because of this, the system was purposefully designed to be shipped via standard methods. Similar to the other larger goniometers, the GRIT-T system is expected to be dismantled into a compact form factor that allows for storage and travel. As seen with the original GRIT system, at times, it is necessary to ship goniometer systems across country or overseas in order to complete a field

data collection. Due to this expectation, the overall system design had to support being reduced to something that would fit inside a large shipping case no bigger than 5 feet by 5 feet by 2 feet. But, a focus was put on making this reduced size as small as possible, while ensuring that all other requirements of accuracy and assembly time were still met.

#### **4.1.3 Reduced Collection Complexity and Time**

As previously mentioned, the GRIT-T system must be extremely efficient both in the field setting and the laboratory setting. This increases the scientific value of expensive field experiments that the team conducts around world by essentially gleaning more information per field day than other goniometers would be capable of. At the heart of this efficiency is reducing the collection complexity of each BRDF scan, and therefore, reducing overall collection time and operator fatigue. The original GRIT system lacked a few features that dramatically slowed down the collection process. These desirable features, combined with others from various systems, were added as requirements before beginning the engineering and design phase of the GRIT-T system. The most important of these being a fully automated collection sequence. Even though the original GRIT system was partially automated, as discussed in 2.3.4, the time lost due to the necessary operator inputs over the course of the collection would cost valuable minutes and put strain on the individual running the control laptop. Collection with this device was very tedious, and it required the full attention of two operators to verify the mechanical motions and the integrity of the optical data. For the next generation GRIT-T device, a requirement was added to ensure that only one researcher would be needed to operate the GRIT-T system from the point it is set to the point it is moved, assuming a field environment. Given the harsh environments that the system will often operate in, this requirement placed a limit on the human interaction needed for the goniometer to perform a BRDF scan, in an effort to reduce operator fatigue and human error. This limit on human interaction would require that the operator monitor the system's status and collection from a tablet or laptop, but it would not require the operator to issue commands during a BRDF scan.

In addition to improving the user experience, it was also necessary to perform the movements and spectral collections as quickly as possible once the scan started. Since the time to collect each spectra with the spectrometer is mostly predetermined, with the exception of determining the number of samples and subsamples, this meant that the system must be able to aim the foreoptics quickly while maintaining the pointing accuracy requirements. Once the site has been chosen, to further the time savings, setup time must be kept at a minimum. As discussed in 2.3, most goniometer systems must be placed over the target and then carefully leveled. This leveling process allows the angles referenced by the system to match up with any overhead imagery that is being taken without further processing. While this could be achieved in a post processing scheme,

leveling also aids mechanical precision since the loads on the system are better distributed. Since the leveling process is very tedious, especially on soft sediments, and prone to operator error, automated system leveling was added to the list of requirements on the new GRIT-T system. This requirement dictated that users only need to place the system on the ground and issue a leveling command before beginning the data collection. The system would then need to automatically level itself to within 0.5 degrees of level, both in the X and Y directions, thus saving minutes of time per site. Likewise, once a scan has been completed, the system will automatically return to its resting state in preparation for movement to the next field site.

Another massive cost of time for many of the systems discussed in this paper, is the intricate building and tearing down of the instrument between field days. Since many of the field sites of interest to the research group are not fully secured overnight, it is necessary to completely erect the system every morning and then pack it away every night. This may also be necessary throughout the day, depending on the ruggedness of the terrain that the system must traverse when traveling from site to site. Depending on the complexity of the system, this results in an hour or more of each day that is spent only preparing for or recovering from a day in the field. The GRIT-T system requirement was that this time be kept to an absolute minimum, with a maximum budget of 20 minutes for setting up or packing away the system. The addition of this requirement further shaved unnecessary time from the day, and thus, it could easily result in at least one more BRDF scan per field day.

#### **4.1.4 Increased Angular Accuracy and Flexibility**

As with all goniometer systems, angular accuracy is of the utmost importance with the GRIT-T system. This refers to all aspects of the system required to produce a BRDF, including sensor position with respect to the target throughout the scan and source position with respect to the target. The various methods that have been used to understand these angles on other goniometer systems are discussed in chapter 2. For the next-generation RIT goniometer, a very strict requirement was set that the instrument precisely hold sensor view angles within 0.2 degrees of the commanded angle in both azimuth and zenith, with respect to the target itself. This requirement contrasts with the operation of most goniometers where the angles are held with respect to the system. Also, this requirement added a substantial level of complexity since the system was also required to accommodate measuring targets on sloped terrain. Furthermore, in an effort to compensate for movement errors and mechanical stresses experienced in a field environment, the system must be able to report the actual angle that was achieved by each movement and store that value for later integration into the dataset.

The second portion of the angular accuracy requirement dictated that the source's position

be understood within less than 0.5 degrees of error in azimuth or zenith. While this may be handled in stride when the system operates in a lab setting, obtaining this accuracy in remote locations can be very challenging. By definition, this required knowledge of the system's exact location on Earth, the exact time of collection, and the exact heading of the system. As previously mentioned, obtaining the latitude, longitude, and time of day is done using standard, survey-grade GPS equipment, however, obtaining accurate heading is a very difficult task on a robotic system that operates in a dynamic field environment. Often times the electronics and motors operating on the system will ensure that any magnetometer reading is inaccurate, frequently by five or more degrees based on real-world experience with other systems. Nonetheless, since any error in solar positioning corresponds directly to error in the understanding of angular reflectance, this must be reduced as much as possible using robust techniques.

Another requirement that was added is that of system flexibility. This can be split into two main sub-requirements: flexibility to measure the necessary target sets and flexibility to accommodate future imaging devices. As previously discussed, the GRIT-T system is expected to measure both sediments and low vegetation accurately. In order to achieve this, it is necessary for the system to be placed above the surface or vegetation being measured in order to perform the scan, which could be over half a meter above ground level. Thus, a method must be designed to allow the system the flexibility to measure sediments at ground level and vegetation at tall heights. Due to the large investment being made by the research group into a new and very accurate pointing device that could be taken virtually anywhere in the world, it was quickly realized that it must be built such that other types of sensors could be attached with minimal change to the overall design. This included the possibility of swapping the spectrometers for various framing cameras, polarimetric imaging devices, and possibly long-wave infrared imaging sensors. Essentially, this constraint added a requirement that the mounting and pointing capabilities of the device must be universal enough to allow for these types of devices to be incorporated in the future.

#### **4.1.5 Increased Interoperability**

When remote sensing research groups conduct field experiments, there are typically many imaging modalities being utilized simultaneously. They may include satellite imagery, aerial imagery, other goniometers, or illumination characterization devices. With this in mind, it was necessary for the research group to determine a common method for these devices to be cued and store data. This approach would then be incorporated into GRIT-T to allow for better integration of instrumentation during future field data collections. In particular, a robust method must be designed to allow for the GRIT-T system to communicate and coordinate sampling with the systems that monitor downwelling illumination. This includes cuing of the systems that monitor spatial illumination



changes to help compensate for background illumination, and temporal illumination changes to ensure that minimal interpolation is needed to allow for these measurements to be post-processed with the target reflectance information. Reducing this need for interpolation further increases the accuracy of the final BRDF product output by the post-processing techniques.

This interoperability requirement also had implications for the laboratory setting in which the device also will operate. The GRIT lab at RIT includes a broadband light source attached to a large, computer-controlled, rotating truss, that allows for simulated solar movement, and provides the capability to automate multiple source angles without user input. The new goniometer system must provide for the possibility of integrating this control directly into the laboratory goniometer software, thereby providing a fully-automated laboratory suite that could complete unusual sensor and source interactions that allow for further interrogation of materials for radiative transfer modeling. The figure below, 4.4 shows the broadband source attached to the rotating truss structure.

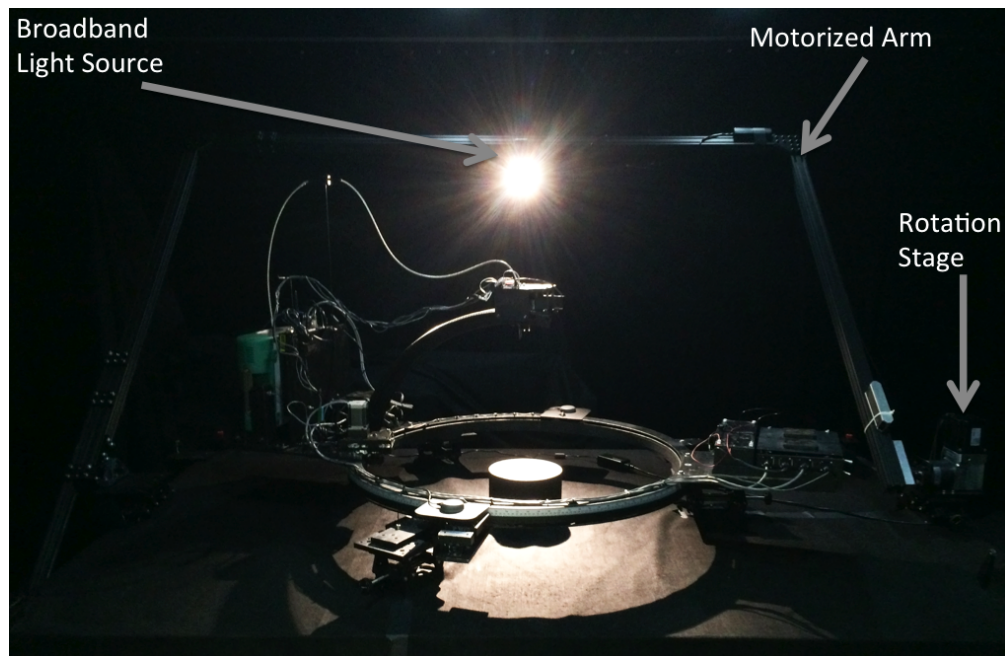


Figure 4.4: The automated light source utilized in the laboratory setting; the original GRIT is positioned underneath the rotating truss that moves the light sources to simulate direct solar illumination.

## **4.2 System Requirements**

In order to adequately understand the effect of the scientific requirements on the overall design of the GRIT-T goniometer, it is necessary to further break down these requirements into something that more directly translates to mechanical, electrical, and software design. This section describes how each of these high-level requirements shaped the system design, and it lays the foundation for discussions of the decisions made at the lower levels of the design and engineering processes.

### **4.2.1 Derived Optical Requirements**

As can be expected, achieving the optical requirements of the GRIT-T system dramatically shaped the final design. As mentioned in section 4.1.1, the FOV of the system was extremely important, and it would largely drive the overall size of the device once a nominal FOV size was chosen. Based on the information gleaned from past field experiments, it was decided that the GRIT-T system should have a typical FOV of approximately 5 cm in diameter at nadir with a moderately sized fore optic of 5 degrees. The goniometer's FOV could be adjusted by just swapping in larger or smaller FOV fore optics. Since 1 degree, 3 degree, 5 degree, and 8 degree fore optics were available from the spectrometer manufacturer as standard inventory, choosing a 5 degree fore optic allowed for a relatively painless adjustment up or down. This fore optic choice, along with the desired FOV size, resulted in a typical radius of 0.6 meters for the distance from sensor to target.

Unlike most goniometer designs, the GRIT-T design required that parallax be minimized as much as possible. Since the system is also designed to handle sloped terrain and the distance to target is subject to change, this scientific requirement translated into an extra motion requirement that would allow the sensor to be re-aimed at the target during situations where parallax would be present, in addition to the standard azimuth and zenith ranges of motion. This requirement also meant that the distance to target from the sensor would need to be captured for each scene before beginning the scan, in order to allow for motions to be translated into actual motor movements. This extra motion and distance information could then be combined to allow for coordinated motion between the zenith movement and the parallax reduction movement thus ensuring that the GIFOV maintained a constant location on the target. With the addition of an accurate distance measurement from head to target, it would also be possible to add the capability to produce a digital elevation model (DEM) of the target area, for further compensation of sloped terrain in post-processing and for incorporation of surface roughness into radiative transfer models. Due to the strong desire for this feature, it became a requirement that this capability be added to the goniometer.

As mentioned in the section 4.1.1, the GRIT-T system is meant to measure both sediment

and vegetation targets. This requires a spectrometer than can measure from the UV through the VNIR and into the SWIR to obtain the necessary information about the various absorption bands present. Based on the spectrometer systems available that are engineered for a field environment, this limited the choices to just two companies: Analytical Spectral Devices (ASD), Inc. and SpectraVista Corporation. For the GRIT-T system, the ASD FieldSpec-4 High-Res spectrometer was chosen due to the wide spectral range (350-2500 nm), the variety of fore optic choices, the narrow spectral bandwidth (1.4 nm from 350-1000 nm and 1.1 nm from 1000-2500 nm), the ethernet/WiFi connection, and the permanently attached fiber optic cable.[48] This choice was also made partly due to the fact that the research group already owned one of these instruments, which would help reduce additional costs to the system and to ensure the reduction of spectral artifacts when comparing radiance data between the systems. This spectrometer also exhibited acceptable SNR and had the option of custom fiber optic lengths that would help achieve other system requirements.

The system requirement for background illumination compensation added another large complication to the overall design. In order to handle background illumination, the GRIT-T system must provide a spatial illumination profile of the incoming light, which will be incorporated with the direct solar illumination profile to increase BRDF accuracy. Achieving this spatial illumination profile with similar spectral resolution and range, to reduce the effect of spectral artifacts, required the use of a second full-range ASD FieldSpec-4 High Res spectrometer that would be pointed away from the target to capture incoming light. This technique is similar to that discussed in the Dual Field-of-View FIGOS system in section 2.3.1. However, implementation of this technique on a much smaller, more portable goniometer required significant planning and unique mechanical movements to ensure proper calibration. Further complicating this requirement, the GRIT-T system must be able to automatically calibrate the second spectrometer before the scan, preferably with the same Spectralon panel used to calibrate the downward-looking spectrometer. This required the goniometer to be able to calibrate the downward-looking spectrometer, then rotate the pointing head 180 degrees to allow the upward-looking spectrometer to calibrate from the same Spectralon panel placed near the ground, and then rotate back in order to begin the scan.

The temporal compensation requirement further shaped how the goniometer must interact with the spectrometers. Since the system was expected to use the dual spectrometer technique described by Bachmann et al.[9], this meant that the goniometer would need to accurately cue three separate spectrometers to ensure that the temporal changes in the scene were being adequately handled. Of course, this cuing is also dependent on the state of the motions of the goniometer itself since spectrometer readings should only take place once the system is stable and not in motion. This required the GRIT-T system to send commands to each of the spectrometers, one of which is not attached to the goniometer, to ensure that each spectral measurement was taken within a

reasonable amount of time with respect to the others. This time was determined to be nominally 500 milliseconds. Since the skylight monitoring spectrometer, known as the base station, is typically stationary throughout the field day, and since the GRIT-T system moves frequently throughout the field day, a wireless method of communicating with this device must be designed that is robust enough to handle the data transfer from each spectrometer, and is fast enough to ensure proper cuing.

In addition to the system requirements described above, the scientific requirement for the reduction of self-shading dramatically shaped the overall design of the next-generation goniometer. To ensure that self-shading is kept to an absolute minimum, it was necessary to remove any stationary overhead structure that could possibly induce shadow into the target area, including any structural supports for the system frame. This requirement further influenced the frame design by dictating that no part of the frame or leveling system be able to introduce shadow into the target area, regardless of the slope that the system would operate on. In order to accommodate this necessity, the frame of the system had to be open on one side (C-shaped), to allow for the direct solar illumination to fall on the scene unobstructed. This derived requirement, that can be seen in the original depiction (see figure 4.5 provided to the author before this project began, quickly shaped the type of design that could be used while still achieving a full hemispherical scan. This required that the sensor head be aimed with an arm that could move through the entire zenith motion (from -70 to +70 degrees) since only 180 degrees of azimuth travel would be possible. In addition to the frame, this requirement also influenced the method for pointing the sensor fore optics, since this apparatus would inevitably introduce shadow into the scene when the goniometer attempted to measure the target at very small phase angles, i.e. when the sensor angle is very small with respect to the solar angle. It was then necessary to minimize the size and the amount of devices located at the sensor head to a minimum, while still achieving the overall scientific goals of the system. Also, since it was not only shadows that could cause errors, but also skylight obscuration, an effort must be made to ensure that the system components and spectrometers themselves kept a low profile. While the adjacency compensation technique would ultimately account for this type of obscuration, it was still not desirable as it was a departure from a perfectly natural scene.

#### **4.2.2 Derived Portability Requirements**

Since the GRIT-T system was required to be light enough for only two people to lift, every device on the system had to not only be accurate, but relatively lightweight. A system requirement was then defined based on the U.S. military lift standards outlined in MIL-STD-1472G. This standard defined that the maximum weight to be lifted and carried up to 10 meters (33 feet) by males is 82 lbs. each, when in a team of two lifters. Given that the research group could only count on two

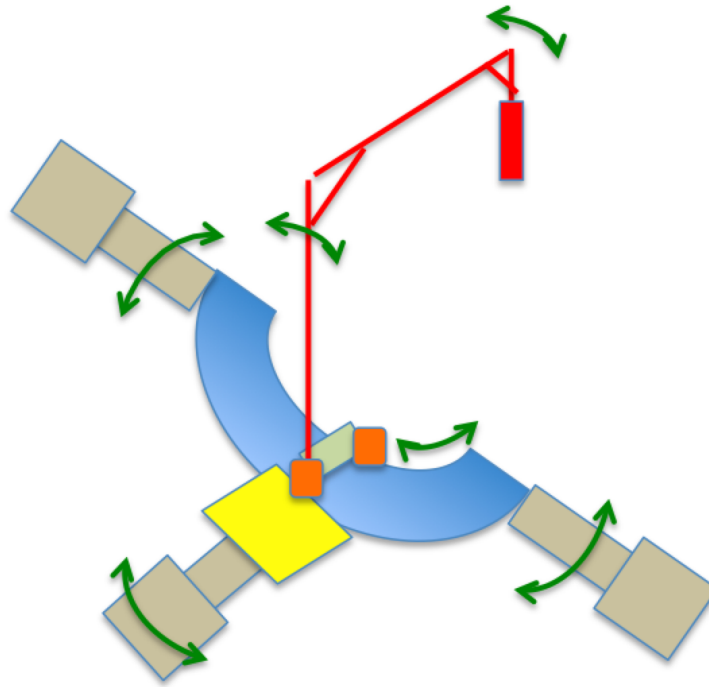


Figure 4.5: An illustration of the first GRIT-T design provided by Dr. Bachmann to the author before the project began.

individuals at any given time, this standard set a hard limit on the overall weight of the system to be 164 lbs. Alternatively, according to the same standard, if the object were to be only lifted and placed on a surface no greater than 91 cm (3 feet) from the floor, the maximum weight to be lifted is increased to 87 lbs. each, for a total of 174 lbs.[49] This second requirement would only pertain to the situation where a small trailer is used to move GRIT-T, and the team only needed to get the system on to this small trailer. These strict weight limits, which included the weight of both on-board spectrometers, forced the system design to emphasize weight reduction. This meant that many parts would have to be custom designed for efficiency, and fabricated out of lightweight, but very strong materials for robustness.

In order to allow the system to be moved from site to site without removing any hardware or shutting down the device, the frame of the system must be very strong and rigid, even when subjected to the mechanical stresses of being lifted and possibly hauled on a trailer. This also meant that the system must be reasonably balanced, to allow for adequate lifting. Also, the moving components must be able to be put in a travel configuration and locked into place to reduce the risk of damage during the short movements from site to site.

Overall, system portability also depended on creating a goniometer that was compact when disassembled to allow for shipment via standard methods. In order to ensure that GRIT-T could travel in a reasonably sized shipping container, a modular approach had to be implemented that would allow the system to be disassembled and packed into as small a space as possible without violating structural integrity. This translated to careful thought about how the various components would interact and where a logical break could be made to allow for disassembly and packing, without disturbing the carefully aligned sensor positioning apparatus.

### **4.2.3 Derived Collection Complexity and Time Requirements**

The scientific requirement of reduced collection complexity and time on a system as intricate as the GRIT-T system resulted in many derived requirements. To achieve full automation, the main control computer on GRIT-T must have the ability to determine and issue motor commands, cue other scientific instruments, and store the resulting data in a format that allows for straightforward post-processing. This level of automation also requires a very comprehensive graphical user interface (GUI) which allows the users to initialize the device, program scan patterns, control any scientific hardware manually, perform manual movements with motors, perform system maintenance, and monitor the status of any on-going scan or movement. This requirement also dictated that only one person be required to operate the system once placed above a target site. In order to accomplish this, the GUI must incorporate a comprehensive status screen that is capable of providing system warnings, real-time view of the spectra being captured by each spectrometer, real-time status of the scan progress, and subsystem status indicators that quickly provide the user with health information for each subsystem.

Along with automation and user fatigue issues, it is also necessary to ensure that the mechanical motions and scientific collections are completed as quickly as possible, without sacrificing accuracy. In order to complete each scientific collection quickly, while maintaining adequate SNR, it is necessary to carefully select the averaging scheme used on each spectrometer. Particularly with ASD spectrometers, the time required to complete a single spectral measurement is dependent on the number of samples and subsamples being collected at each point on the hemisphere. Optimizing these parameters to be in line with the desired SNR will allow for the fastest spectral collection. To achieve quick mechanical motions, the system must be designed to allow for fast acceleration and deceleration without slipping or losing positioning accuracy. While there are many ways to accomplish this, it was decided that the GRIT-T system would employ direct-drive techniques on each motion combined with spring tensioners, where necessary, to reduce mechanical backlash. This, combined with carefully chosen gearing and motor speeds, would allow for the fastest possible movements without sacrificing angular positioning accuracy. Simultaneously issuing motor move-

ment commands further reduced the time between spectral collections, and resulted in the fastest BRDF possible.

Another aspect of reducing collection time involved the implementation of an automatic leveling system that eliminated the tedious process of users adjusting jacks manually. The derived system requirements for this included the addition of an industrial inclinometer to determine the frame's current roll and pitch, and motor driven actuators of appropriate travel. This leveling apparatus must be lightweight enough to meet weight requirements while still being powerful enough to lift the entire goniometer system. The chosen actuators must also exhibit fine movement resolution and excellent lateral stability properties to ensure a precise and solid footing when GRIT-T is operated on sloped terrain. Since this process must also be computer controlled, both the inclinometer and motors must be able to communicate with the control hardware and software. As per the scientific requirements, the inclinometer used for providing the leveling solution must be able to consistently provide roll and pitch information accurately enough to ensure GRIT-T comes within 0.5 degrees of perfect level in both axes.

#### **4.2.4 Derived Setup and Tear Down Requirements**

In order to create a system that can be quickly setup and torn down each day, a multifaceted approach must be utilized to ensure that each step would take no longer than 20 minutes. This meant that the system must be designed to be as complete as possible immediately upon removing it from the shipping container. Minimizing the number of components to be attached at the field site is key to a rapid setup. With the GRIT-T system, this meant that only support equipment should be required to be removed in order to pack the system, i.e. no component that ensures pointing accuracy should be removed. Components that point the fore optics must stay attached during transport. Enforcing this eliminated the tedious process of alignment, sped up the set up and tear down process, and further increased the accuracy of the pointing. In addition, any equipment that is to be removed for tear down must utilize quick disconnecting interfaces for all electrical connections, and must be mechanically attached with standardized hardware. For GRIT-T, standardized hardware refers to ensuring that each bolt that attaches to the typically removed components must be of a standard size, thereby, reducing the need to have a variety of tools to accomplish setup and tear down. While these requirements may seem mundane, they can ensure a timely setup of the system even if assembly is being completed by researchers who are unfamiliar with GRIT-T.

#### **4.2.5 Derived Angular Accuracy and Flexibility Requirements**

Since the GRIT-T system was required to provide sensor movement angles with respect to the target itself, versus with respect to the instrument as is the case with many other goniometers, the requirements for performing this positioning had to be rethought from what had been done for the original GRIT system. In order to achieve this, the distance from the target to the sensor pointing head must be carefully understood, and the system must employ a precision engineered arm with precisely known distances. Theoretically, this provides the basic information necessary to calculate the motor motions that will accommodate any sensor viewing angle, with respect to the target, that the system can mechanically provide. Since the system already had the requirements of understanding the distance to target and having an extra axis of motion to reduce parallax effects, these capabilities could be leveraged with adjustments in software to give true pointing, while maintaining pointing at the same target area. From a mechanical perspective, this scientific requirement also further increased the need to have absolute encoders that could be used to understand where the system was pointed with excellent precision. This also meant that each sensor pointing motion must employ very fine resolution gearing and zero-backlash methods since the necessary motor movement angles would be changing from site to site, and since no standard movement would meet the pointing requirements.

In addition to the pointing requirements of the system, this scientific requirement had implications for how the system's position was understood with respect to the earth. The requirement to understand the source's position within 0.5 degrees in azimuth and zenith forced the device to employ more accurate techniques than most goniometers use to understand their position. This meant derived requirements for how level the system was at any given time, how well the system's heading was understood, and how well the latitude and longitude of the system were known. Since GRIT-T already employed a precision leveling subsystem, that same inclinometer information could be leveraged to fulfill a portion of this derived requirement. Obtaining accurate heading, however, is a far more difficult task since magnetometers are not robust enough, given the high density of electronics and motors on the system, and the possibility of GRIT-T being used in ferrous target sites. This then forced the goniometer design to adopt a GPS solution of obtaining heading by using differential GPS antennas that were accurate to 0.5 degrees or better, which would meet the scientific requirements despite the electrical and magnetic interference found on or near the system. In addition to heading, this GPS solution could provide latitude and longitude within 0.6 meters. If better positioning accuracy were required, the system could be augmented with a survey-grade GPS solution (Trimble Pro 6H) that could be post-processed to obtain accuracy within 10 centimeters. While this high accuracy GPS performed better than needed for understanding solar position, it also allowed for excellent calibration information of overhead sensors since it could precisely de-



termine which pixel the GRIT-T system would have been placed in during an overflight. All of these devices combined, would allow the GRIT-T system to meet the overall scientific goals for positioning.

In order to adequately ensure that the flexibility requirements for GRIT-T were being met, the system had to adhere to the derived requirements listed below. The next-gen goniometer would be expected to measure not only sediments, but also low vegetation. This meant that the leveling actuators must have very high lateral loading capabilities, since the GRIT-T device would likely be placed on stilts or another frame to achieve effective positioning over the vegetation. This requirement also placed optical requirements on the method utilized to determine overall system height above a target of interest, since vegetation and sediments have very different optical properties. The distance measurement unit must be capable of measuring diffuse targets that could be either very bright (high reflectance) or very dark (low reflectance) without recalibration, and while minimizing the overall error in the measurement. This flexibility requirement also allowed for the addition of future sensors that may be of different weight and size. To accommodate this, the derived requirements dictated that the system must be engineered mechanically and electrically to handle the possibility of a 3 pound sensor with moderate power consumption (35 watts).

#### **4.2.6 Derived Increased Interoperability Requirements**

As previously mentioned, the GRIT-T system must allow for extensive interoperability with various instruments. To accomplish this from a system's perspective, the device must utilize a standard communications protocol that can be expanded to include other computers and imaging devices, and to possibly control hardware for laboratory light sources. This also required that the device have a robust cuing capability to ensure that temporal compensation would be possible without unnecessary interpolation, even in remote areas. Since GRIT-T already had accurate GPS information on-board the instrument, it was decided that GPS timing would be utilized to allow for precise cuing that would meet the scientific requirement of 500 milliseconds or less between various instruments. To achieve a standard communications protocol that could be easily extended to devices that resided off of the system itself, a local ethernet network was chosen that could allow for other devices to connect via ethernet cable or WiFi network and receive cuing signals from the main GRIT-T computer. Based on these requirements, the software residing on GRIT-T must also be easily upgraded to allow for future connections.

### 4.3 Methods for Meeting System Requirements

As was seen in section 4.2, many of the requirements necessary to meet the overall scientific goals of the system have significant overlap. Due to this overlap, the methods for meeting the requirements will be broken down into a more logical framework based on the main subsystems that make up the GRIT-T system. These subsystems are the scientific payload subsystem, the frame subsystem, and the carriage subsystem. In this section, each subsystem will be broken down to discuss the mechanical and electrical considerations that ultimately led to fulfilling the derived requirements, and therefore, the overarching scientific goals. Figures 4.6 and 4.7 give an illustration of the various subsystems both from a block diagram perspective and how they exist on the system itself, respectively.

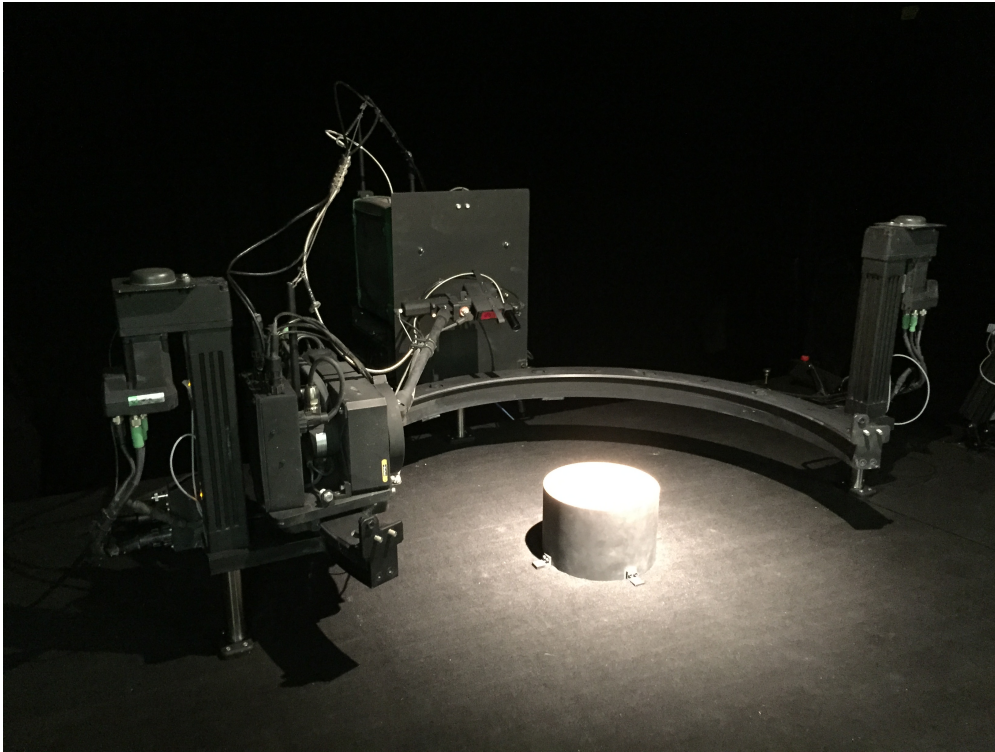


Figure 4.7: The fully assembled GRIT-T system in the laboratory.

#### 4.3.1 Frame Subsystem

The Frame subsystem consists of a few main components and provides the foundation of the goniometer. These main components are the frame railing, the automatic leveling system, and the electrical enclosure which houses various other components as described below.

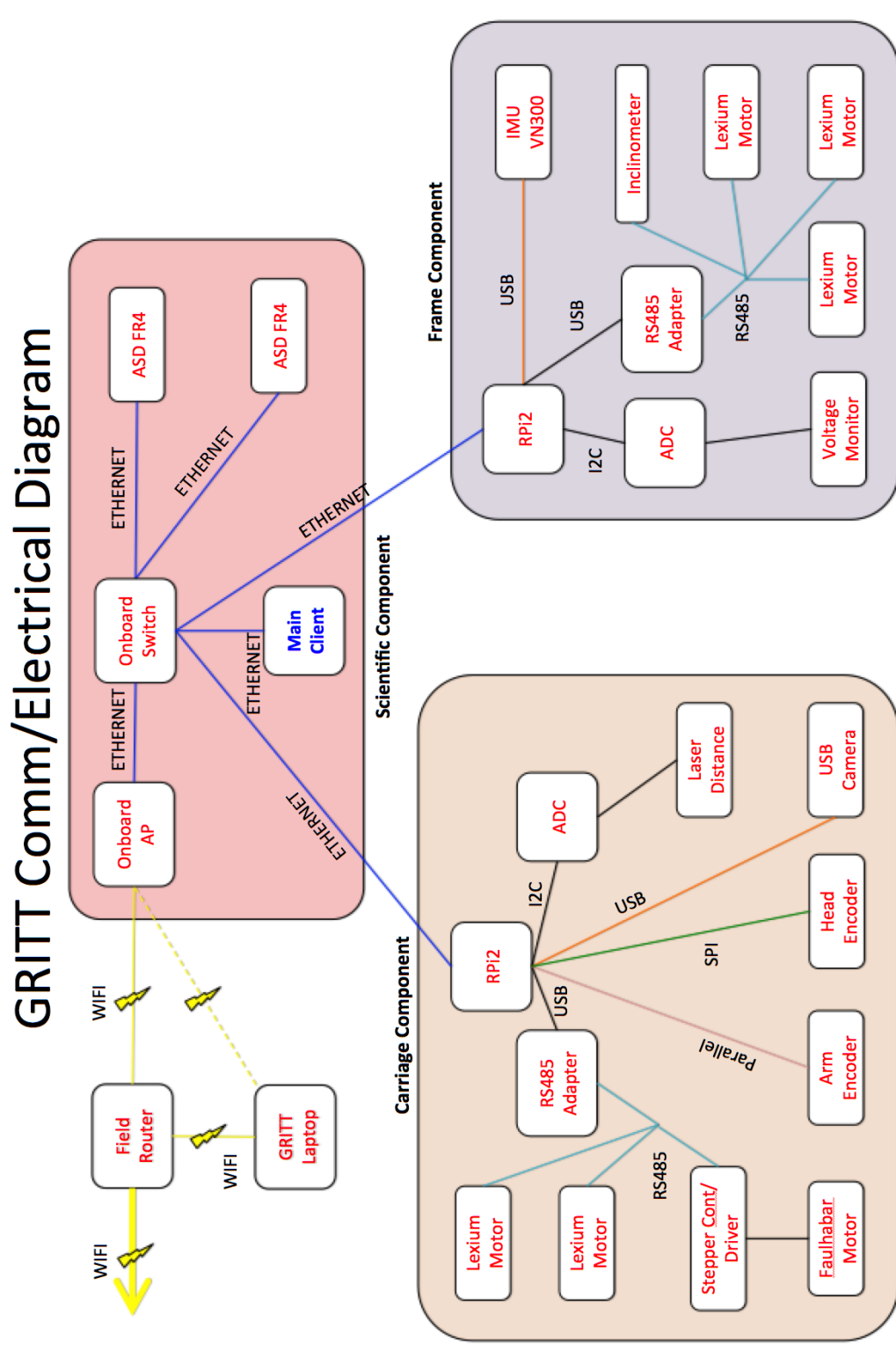


Figure 4.6: Diagram showing the device connections for the three GRIT-T subsystems.

## **Mechanical Design**

As previously mentioned, the mechanical design of the frame subsystem provides the backbone of the pointing accuracy for the entire system, as it includes the frame railing that the carriage rides on. Initially, it was planned to purchase a railing system from an outside vendor that is typically used for high precision optical machinery such as magnetic resonance imaging systems. This ring was a full 360 degree circle that was 1033 mm in diameter, and designed and sold by Hepco Motion in the United Kingdom through Bishop-Wisecarver corporation. The attributes of the Hepco ring fit the requirements of the GRIT-T system from a size and precision perspective. The railing had a double-edged guide that would provide excellent stability to the carriage, and it was geared to allow for precise movement of the carriage around the ring using a custom designed pinion drive. In addition, this ring was created out of stainless steel, and therefore, met the corrosion resistance requirements of a system that would operate near salt spray found in coastal settings. Unfortunately, upon further explanation of the intended use, the manufacturer was not able to guarantee that the ring would hold its tight tolerances for stiffness and concentricity once a 140 degree section was removed to eliminate the issue of self-shading. For a short time, adding a superstructure to improve rigidity and to help ensure that the ring's shape was maintained was investigated, but ultimately scrapped due to the weight requirements that must be met. Due to the lack of a commercially available solution, and the strict requirements for the diameter, rigidity, weight, and concentricity, it was decided that a custom ring would need to be created to fulfill the overall system requirements.

Since the Hepco ring did exhibit certain features that were necessary for the goniometer, the custom design process began by implementing these features into various designs to determine the best course of action. Autodesk Inventor Professional was utilized to model these designs, since it offered options to assemble the system, add appropriate loads, and model the effects of these loads. It was quickly discovered that the most efficient design would be achieved by using a 1033 mm diameter ring crafted out of aluminum. The aluminum design reduced the weight of the ring substantially, and it allowed for an increase in the overall cross-section of the ring. This increase in cross-section was imperative, since the system requirements dictated that the ring must be an open C shape (chosen to be 220 degrees, based on carriage requirements) without any overhead supports. Thus, the ring was very prone to twisting under load. Finite element analysis was implemented with many different cross-sections to determine the exact shape of the ring that would meet the rigidity requirements while minimizing the overall weight. Once this cross-section was determined, the necessary features that allowed for precise motion were added. This included a double edge guiding rail for carriage bearings to ride on, and an external gearing to allow for carriage movement. After a final design had been chosen, it was then split into three layers which allowed for efficient

machining. The top layer included the double edge guide rails as shown in figures 4.8 and 4.9. The middle layer, shown in 4.10 and 4.11, included a MOD 1.5 metric gear machined into the outside edge that would allow for precise carriage movements in the azimuth direction. The bottom layer was designed to add even more structural rigidity and to allow for direct attachment of the leveling support equipment, which can be seen in figures 4.12 and 4.13. These layers were then held together with guide pins and large bolts to create a very rigid three-piece ring that was able to meet all of the requirements spelled out in section 4.2. The final CAD design can be seen in figures 4.14 and 4.15.

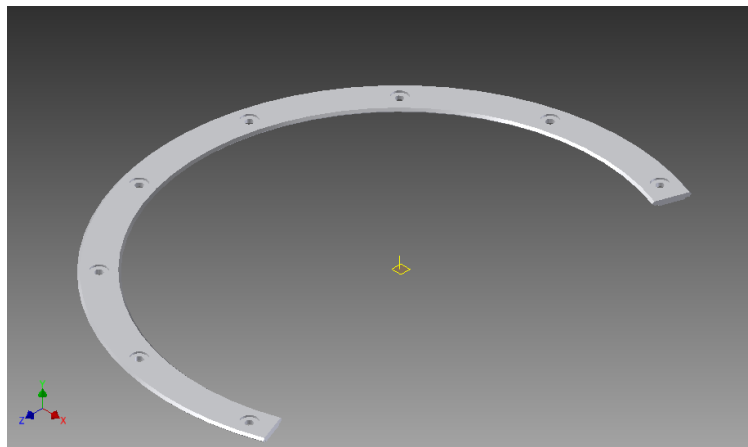


Figure 4.8: The top ring piece.

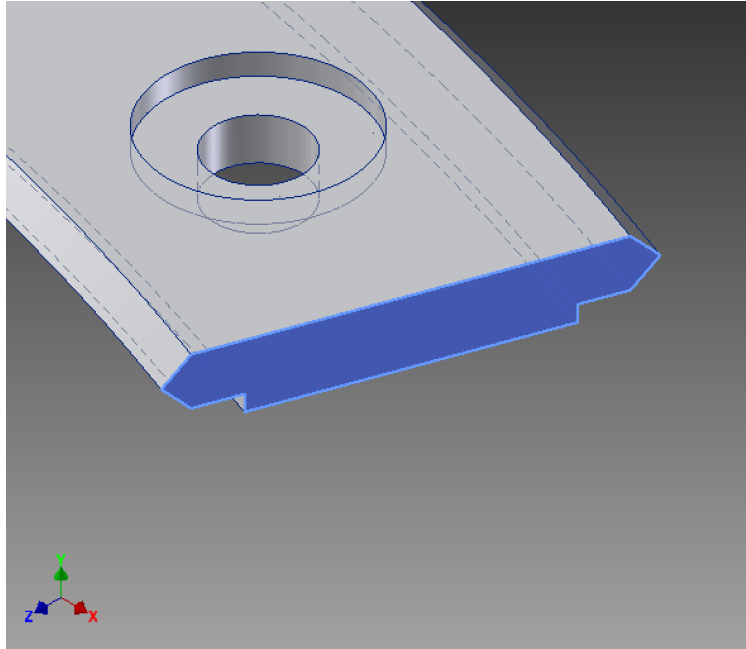


Figure 4.9: The cross-section of the top ring showing the double edge used to guide the carriage.

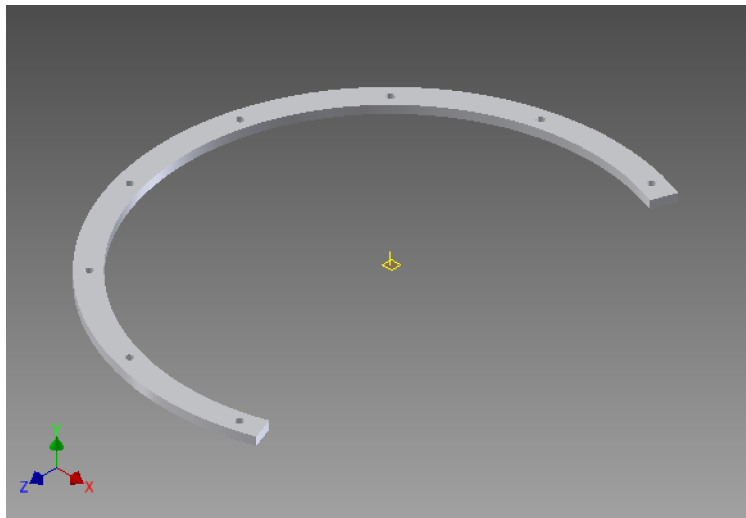


Figure 4.10: The middle ring piece. Note that the external gear is not shown in this rendering.

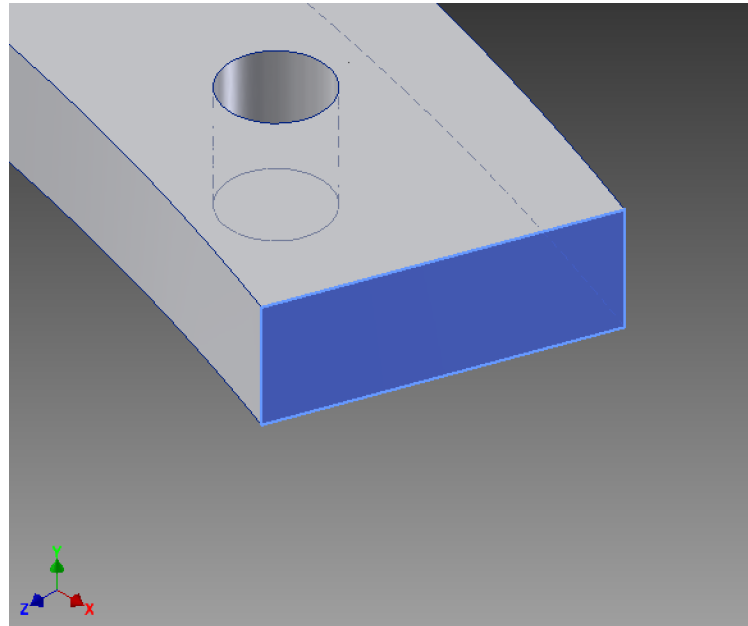


Figure 4.11: The cross-section of the middle ring.

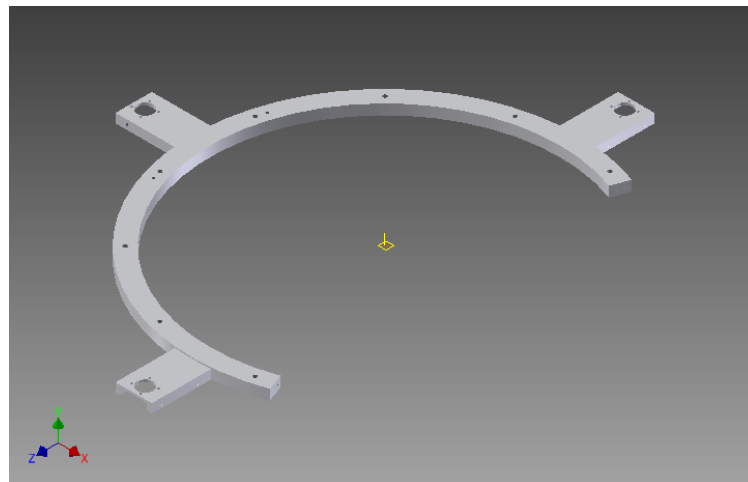


Figure 4.12: The bottom ring piece showing the custom designed tabs that hold the leveling actuators.

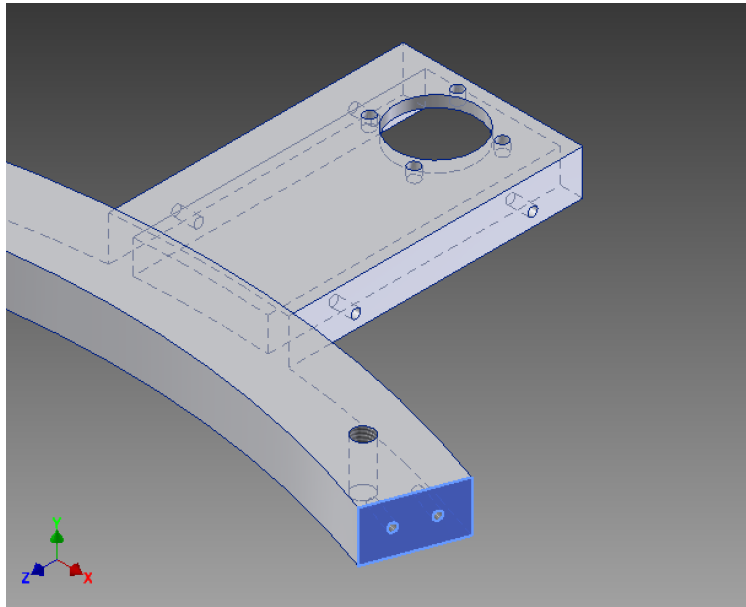


Figure 4.13: The cross-section of the bottom ring. This view also illustrates the actuator mount point in detail.

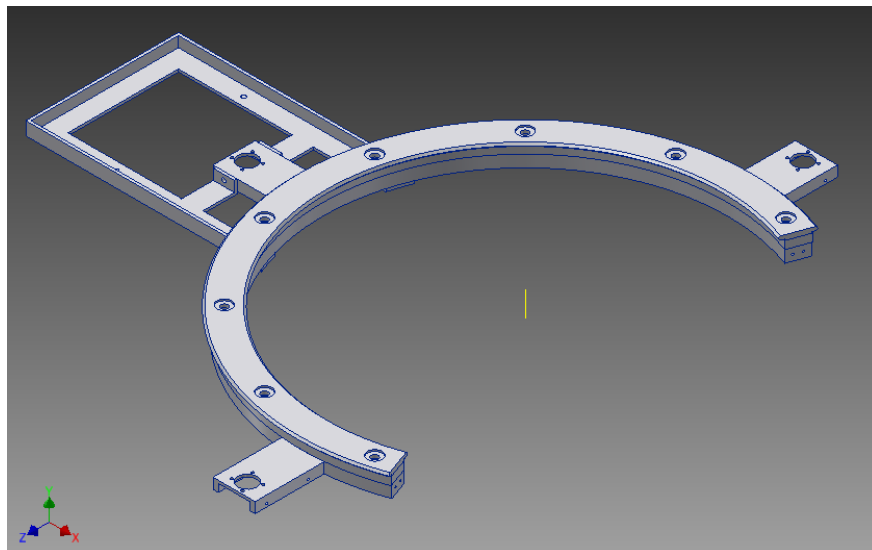


Figure 4.14: The entire frame structure including the mounting bracket for the spectrometers and other support equipment.



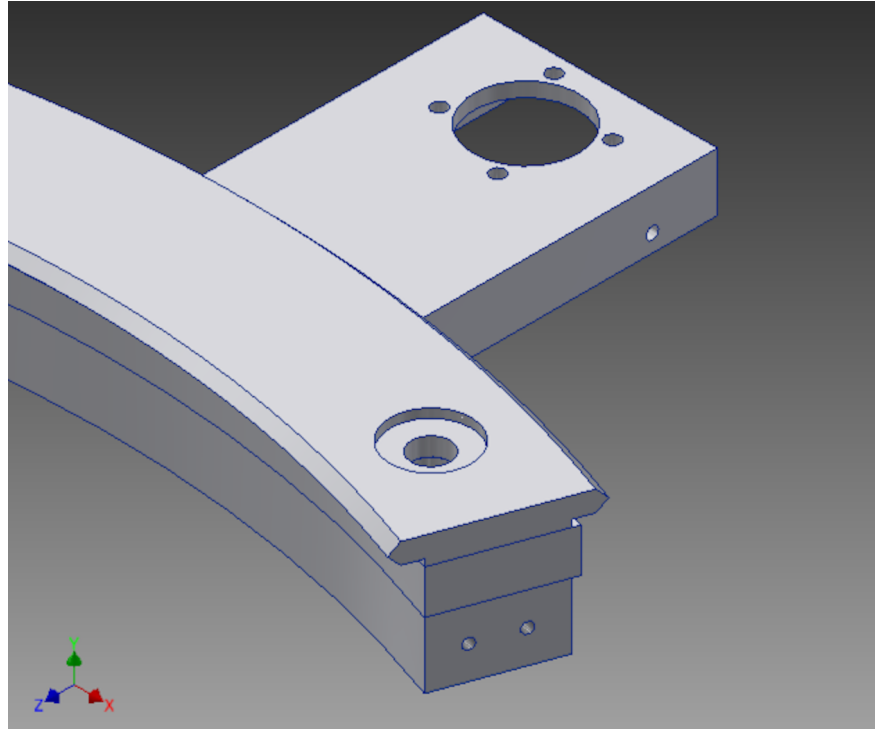


Figure 4.15: The cross-section of entire assembled frame.

This design resulted in the finite element analysis predicting a maximum deflection of the entire ring at approximately 5 mm in the most extreme case. In the analysis, all system weights were applied to their actual locations, and the ring was only attached on one side. While this scenario would never actually be encountered, it provided a very conservative estimate that the frame would exhibit the necessary rigidity. A visualization of this analysis can be found in figure 4.16. Since this ring was custom fabricated specifically for the GRIT-T system, it was also possible to add actuator mounts to which the leveling system could attach. These mounts were designed to be milled into the bottom layer of the ring to avoid any alignment errors or weakness due to welding or bolting. The mounts can be seen in 4.15. To fabricate the large ring pieces, a local precision machining company water-jetted the outside shape from large aluminum slabs, thus, ensuring that an open C design would not warp the material. The blanks were then machined to the appropriate shape, including the gearing, which was completed by a manufacturer in South Carolina. Due to the strict requirements for flatness of the ring, which translated into accuracy for the pointing devices, the surfaces of the layers were ground to ensure that once assembled, the naturally occurring deviations from creating the large aluminum slabs were reduced as much as possible. The concentricity was then tested and measured to approximately 200 microns, which was well within the 1 mm tolerance.

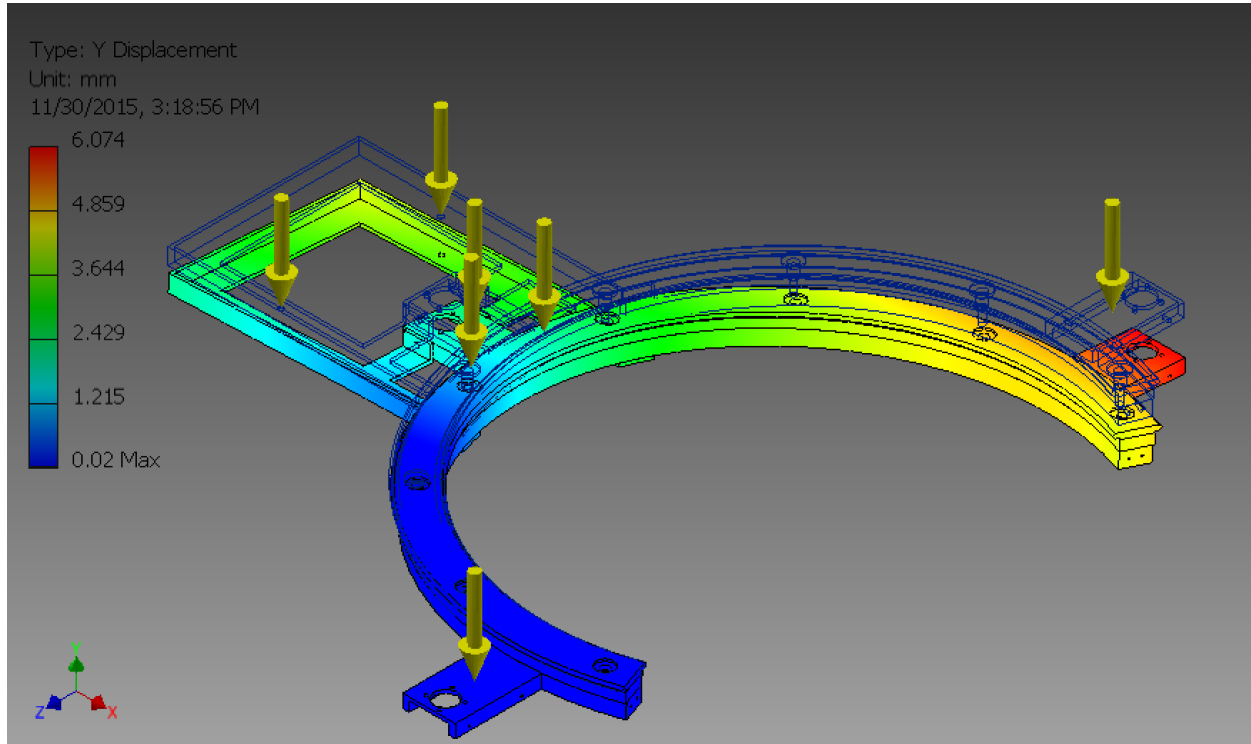


Figure 4.16: A visualization of the modeling results for frame rigidity. Note that the units are in millimeters and the scale of the deformation has been greatly magnified to allow the reader to better understand the deflection that would take place.

Finally, the top and middle layers were sent to be anodized to reduce the impact of wear on the guide railing and gearing.

In order to ensure a compact and easily assembled system, a custom, removable support was created to hold the frame subsystem's electrical components, and to provide a platform to which the main computer and spectrometers would be attached. Placing the spectrometers in a stationary position on this support was pivotal to ensuring the accuracy of the GRIT-T system's pointing over the course of the scan. As seen with other small field-portable goniometers, if the spectrometers move with the system as the scan pattern is performed, then the chance of the entire system settling increases dramatically, thus, changing the reference frame and relative solar position. Since GRIT-T is also expected to measure on sloped terrain, minimizing the amount of moving weight was even more important, since settling in these conditions was more likely. As with the ring, this support was created out of 6061 aluminum, and the design was optimized for rigidity and weight using finite element analysis. The support was designed to be bolted to the ring in six locations to adequately distribute the forces while also ensuring quick attachment. This support can be seen in 4.14.

The frame subsystem also includes the leveling actuators that are used to accomplish many of the goals outlined in 4.2. Due to the importance of a reliable, accurate, and stable leveling solution that is sealed for outdoor use, careful attention was paid to the choice of the actuators. The trade space for these actuators included balancing weight, lifting capacity, lateral loading capacity, ease of removal, precision of movement, environmental rating, and total amount of travel. After investigating multiple brands and models, Exlar K-series actuators were chosen. These actuators were extremely lightweight due to their aluminum housing, but had very desirable lifting capacity and lateral load capacity that would ensure that the system did not experience instability while elevated. Since they were a custom order item, specific parameters were chosen to fulfill the remaining requirements such as a ball screw drive for precision, end mounting bracket for ease of removal, fully sealed piston for an IP65 environmental protection rating blocking dust and splash water, and a custom travel length of 200 mm. This travel length was chosen to ensure that the vast majority of sites could be accommodated without extensions, but also without needlessly increasing skylight obscuration. As shown in figure 4.17, these three actuators were attached to the frame to allow for roll and pitch adjustment. The careful placement of the actuators also ensured that they would never introduce shadow as long as the GRIT-T system was pointed with the open portion of the ring toward the source. These actuators were mated to Schnieder Electric mDrive integrated stepper motors. These motors were chosen to be NEMA23 size for appropriate torque, and were also IP65 sealed using M12 quick disconnecting electrical connectors.

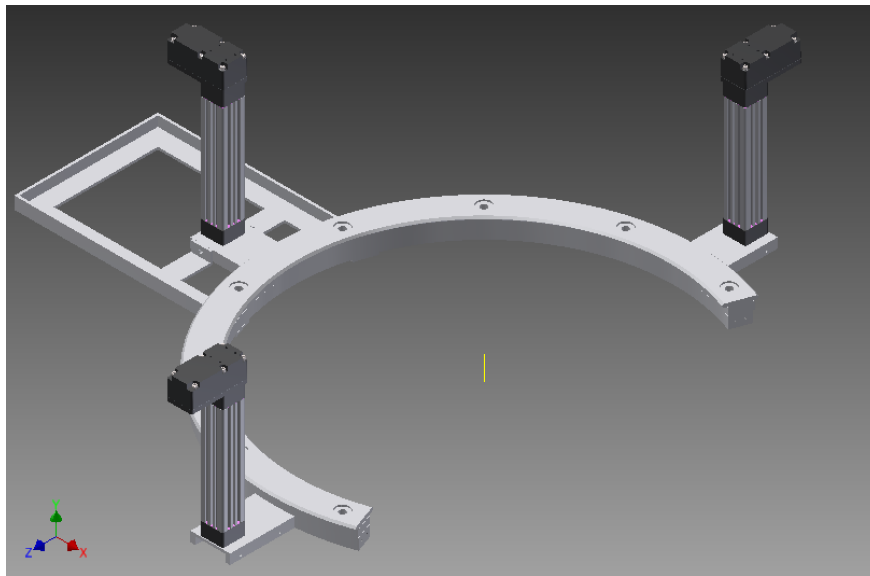


Figure 4.17: Frame design with Exlar actuators attached.

## Electrical Design

The electrical design of the frame subsystem included a variety of components that ensured proper operation of the GRIT-T system as a whole. This subsystem includes the batteries, the DC power supplies for the entire system, the power filters and capacitors for power conditioning, the industrial ethernet switch, the inclinometer and inertial measurement unit (IMU) with differential GPS, and the single board computer (SBC) to control the frame features. To provide power to the GRIT-T system, two lithium ion batteries were chosen to allow for high energy density without unnecessary weight. These batteries are placed at the ends of the open ring to aid in weight distribution as required by section 4.2. Connected to these batteries are three CUI DC to DC power converters which create 200 watts of 24V power, 200 watts of 12V power, and 20 watts of 5V power. The 24V circuit provides power to all of the integrated Schnieder Electric motors onboard, and has a high capacity PI filter and 5500uF capacitor attached to ensure that power spikes and surges are handled without disrupting system operation. The 12V circuit provides power for the main computer, network switch, inclinometer, head motor controller, rotary stage encoder, and laser distance unit. The 5V circuit provides power to the two single board computers and head motor encoder, as well as all devices that are powered through their USB connection. Connecting the large motors to a separate, filtered supply ensures that transient voltage spikes and drops from motions do not affect the more sensitive electronics on the system, and provides for better electronic stability on the system. The B&B Electronics ESW108 industrial ethernet switch provides communication from the main computer, both SBCs, the spectrometers and the WiFi access point. This switch was specifically chosen due to its resistance to vibration and shielding to EMI, which increased the reliability of the onboard communication system even when used in harsh EM environments. The inclinometer utilized for the leveling system was chosen to be a Rieker H6-FLEX series that is designed for industrial applications. This device provides dual axis tilt information via USB and is accurate to 0.1 degrees in both axes, thus meeting the overall system requirements in a relatively compact form factor. The differential GPS solution was chosen to be the VectorNav VN-300 IMU. This IMU is capable of providing GPS-based heading in static situations within 0.3 degree accuracy and provides the GPS timing capability for cuing. While not typically utilized, this IMU can also provide roll and pitch information within 0.5 degree accuracy as a backup to the main inclinometer. The single board computer used for control of all frame operations is the Raspberry Pi 2. This computer features a quad-core 900MHz ARMv7 processor with 1 GB of ram, various GPIO ports and a 10/100 ethernet port, and is running a Linux operating system. This SBC also has a custom designed expansion board that allows for connection to various other system components and provides 5V power to the SBC.

### **4.3.2 Carriage Subsystem**

The carriage subsystem rides on top of the large ring and provides the pointing capability for both azimuth and zenith directions. This subsystem also houses the capability that provides for accurate look angles with respect to the target and reduces the parallax error at the target plane. The mechanical and electrical portions of this subsystem are discussed below.

#### **Mechanical Design**

Since the carriage of GRIT-T would be conducting the pointing of the system, the mechanical specifications for its design were also very strict. This design started with creating a custom engineered plate that would be attached to the ring via four high precision, wash down rated, stainless steel bearings. Since the carriage plate played a pivotal role in ensuring that the dimensions of the system were correct, all mounting holes were precision machined to ensure proper placement. As mentioned, the plate was attached via four Bishop Wisecarver, Inc. bearings that are fully sealed, self cleaning, and never require lubrication. To allow for proper fitting on the ring's guide railing, two concentric and two eccentric bearings were utilized, thus allowing for adjustment of the movement friction. In an effort to reduce weight even further, extra material was removed from the bottom of the plate while carefully ensuring this did not negatively impact rigidity via finite element analysis. Carriage movement around the ring was driven by a custom designed pinion drivetrain shown in 4.18. This drivetrain utilized a Schnieder Electric mDrive motor, a dust-proof and splash water proof Nanotec GPLE60-40 low-backlash planetary gearbox, and a stainless steel MOD 1.5 gear. This drivetrain was attached to the plate via a spring tensioner system to allow for limited debris buildup in the gear path without damage. In order to home this motion and provide emergency limits, two sealed Honeywell 103SR Hall effect sensors were added at each end of the carriage plate. These will be tripped by magnets at the end of motion on the ring to ensure the safety of the equipment. The arm motion of the GRIT-T system was accomplished via a high precision, sealed rotary stage mounted on its side. This custom engineered stage provided virtually no backlash thanks to a preloaded, 72:1 worm gear drive attached to a Schnieder Electric mDrive motor, and it provided ample torque in a relatively small form factor. In order to ensure that movement of the stage is accurately measured, a 13-bit BEI CHM5 absolute encoder is independently attached to the stage. This encoder provides excellent angular feedback on stage position, which is used to home the motion and ensure proper pointing. The BEI encoder was utilized, along with two sealed Misumi MSWF-LD limit/stop switches, to provide emergency stops to this motion. Attached to the stage was an aluminum arm mounting plate which holds the GRIT-T pointing arm shown in 4.19, both of which were custom engineered. This arm provides

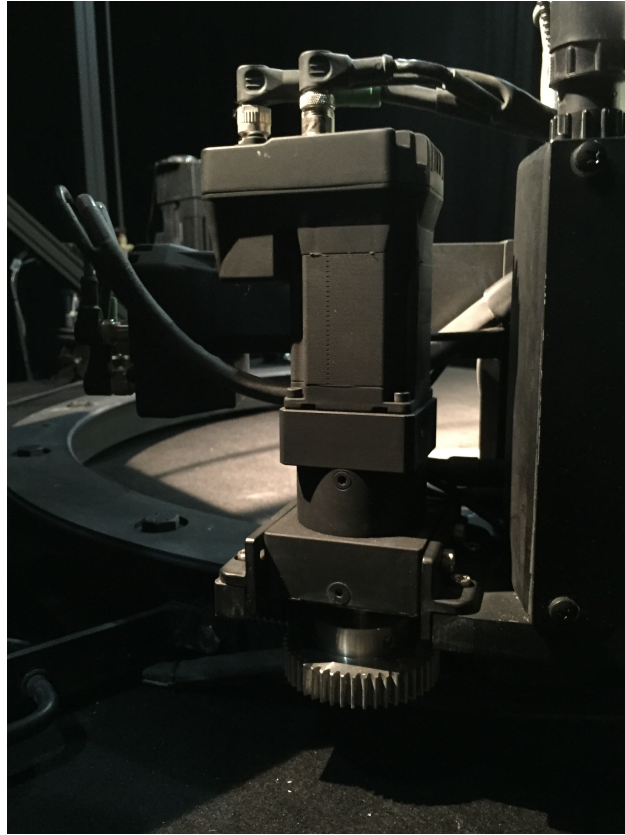


Figure 4.18: The GRIT-T carriage drive motor and gearbox.

the large zenith movements and attaches the head pointing equipment to the rotary stage. This pointing equipment consists of a Faulhaber miniature stepper motor attached to a 246:1, low-backlash planetary gearbox which is used to ensure proper pointing of the sensors. This extremely compact drivetrain resides in a custom designed, sealed aluminum housing as seen in 4.20. This housing also provides a mounting point for a CUI AMT20 compact absolute encoder. This encoder is connected to the output shaft of the gearbox and precisely measures the current position of the head, which points the sensors. To provide homing and emergency stops for this axis of motion, the CUI encoder was used along with two sealed Panasonic ASQM11620 limit switches as emergency stops. The aluminum pointing head, shown in 4.21, attaches the laser distance unit, points the two fiber optic cables from the spectrometers, and attaches the 5 megapixel IDS uEye XS camera used for situational awareness. The fiber optic cables are attached using two custom clamps that position the fiber end with respect to the foreoptics, similar to ASD's pistol grip. For every mechanical component described in this section, dimensions were extremely critical. For that



Figure 4.19: The GRIT-T arm mount attaching the arm to the rotary stage.

reason, each part described was precision engineered out of 6061 aluminum to ensure strength and weight reduction.

### Electrical Design

The electrical design of the carriage subsystem focuses on the sensors used for motion, and obtains power and communication from the frame subsystem via two umbilical cables. Due to this, the carriage's electrical enclosure houses only a motor controller board for the head motor and a single board computer. The motor controller was chosen to be a Trinamic TCM-1140 controller board, which provides a variety of options including limit inputs, current settings, acceleration and deceleration curves, microstepping, and USB communication. This board is powered by 12V and is connected to the Faulhaber motor, the Panasonic limit switches and the single board computer. The SBC is an open source Raspberry Pi 2. This computer features a quad-core 900MHz ARMv7 processor with 1 GB of ram, various GPIO ports and a 10/100 ethernet port, and is running a Linux



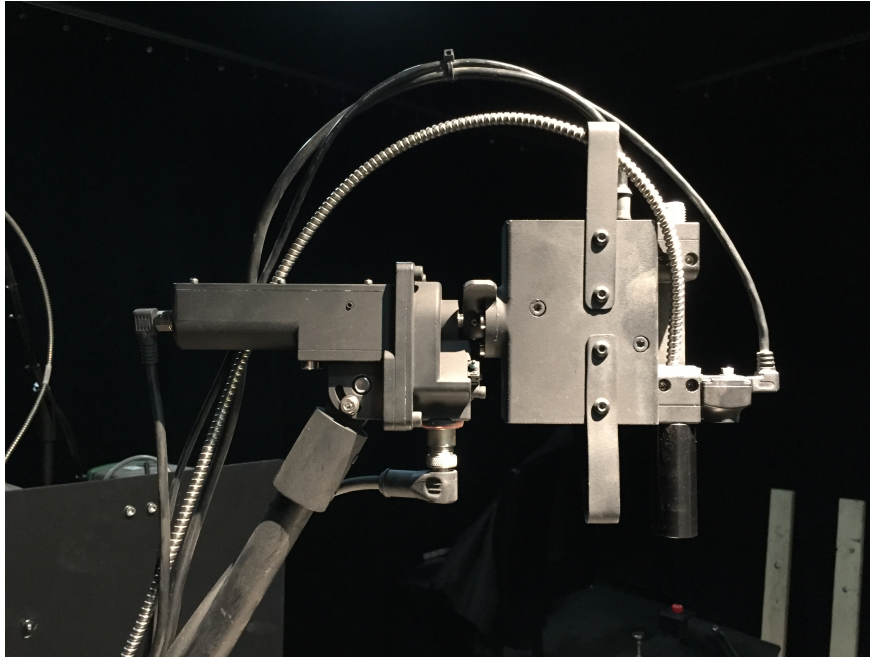


Figure 4.20: A photo of the GRIT-T head motor casing and the attached pointing head.

operating system. This SBC also has a custom designed expansion board that provides connections to the SICK encoder, the CUI encoder, the laser distance unit, and provides power to the SBC. The BEI CHM5 absolute encoder is connected to 12V, and provides 13-bit positioning information over a parallel connection to the SBC. The CUI AMT20 absolute encoder provides 12-bit positioning information for sensor pointing, is connected to 5V, and employs an SPI connection through the expansion board to the SBC. The Banner LE550 laser distance unit is connected via analog voltage to the SBC which provides excellent distance information from the sensor head to the target. This information is used to ensure proper pointing with respect to the target and reduces parallax by allowing for specifically calculated motions. This particular distance unit was chosen based on its excellent characteristics when measuring diffuse targets of varying color and brightness over a wide temperature range. It utilizes a triangulation method with 650 nm active illumination to determine overall distance to the target within 2 mm. In order to ensure that this active illumination does not impact the spectral information collected by the spectrometers, the SBC controls when the laser is enabled. As previously mentioned, this laser unit also provided the possibility of obtaining a DEM of the target area with reasonable accuracy.





Figure 4.21: A photo of the GRIT-T pointing head with both fore optics and fiber optic cables attached.

#### 4.3.3 Scientific Payload Subsystem

The scientific payload subsystem of GRIT-T consists of the two ASD FieldSpec-4 High Res spectrometers, the main GRIT-T computer, and the GRIT-T wireless access point. As previously mentioned in 4.2.1, these spectrometers met the overall scientific objectives of the system. In order to accurately ensure proper timing to fulfill the cuing requirements, these devices are operated without their standard laptops, and instead connected directly to the industrial ethernet switch located in the frame subsystem's electrical enclosure. The spectrometer control and data handling is then completed by the GRIT-T main computer. This computer is a Logic Supply POC-210 industrial computer that is dust proof and fanless. The CPU is a quad-core Intel Atom E3845; it has 8 GB of RAM, and a 256 GB solid state hard drive. This particular computer was chosen due to its fanless design, adequate processing power, adequate storage capacity, extremely compact design, and wide operating temperature range. In addition to controlling the spectrometers, this computer

coordinates all goniometer operations through the SBCs. Communication for this computer is achieved via shielded ethernet to the switch. Since the operator will typically be running GRIT-T via a separate laptop or tablet, the system was outfitted with a sealed, high transmit power wireless access point. This Ubiquiti PicoStation M2 access point is designed for heavy traffic over relatively long distances (100m), and provides a robust method for communicating to the system. The access point is connected to the industrial ethernet switch and is powered via 12V POE adapter.

#### **4.3.4 Software Design**

The software design for the GRIT-T system was architected around the ethernet communication system employed in the frame subsystem. This means that scan patterns, DEM parameters, and system settings are sent from the operator's control laptop to the main GRIT-T computer. In order to provide these details in an easy-to-configure manner that the main computer would accept, a custom designed graphical user interface (GUI) was created to aid the user in programming the instrument. This GUI consists of various modes that allow for ease of use in both a field and a laboratory environment. It provides the user a convenient method for programming scans via a polar plot that illustrates how the scan will be performed. This software was engineered to allow for virtually any pattern that the user can imagine, including imbalanced patterns with high density areas to measure specific phenomenology, such as the opposition effect. This software also allows users to configure the density of the DEM to be captured while indicating the number of total points to be collected. The GUI also provides a convenient status screen that provides users with the current status of every subsystem on the goniometer. For the scientific payload subsystem, this includes current spectra from the ASD spectrometers, current spectrometer battery voltage, time since last optimization, a method for re-optimization, and a generic status indicator that will quickly get the user's attention if an error occurs. This also includes a real-time view of the progress of the current scan showing the points that have been collected and those that still needed to be collected, along with various options for pausing, collecting a white reference, and switching to manual mode. The frame subsystem provides status updates on the current roll and pitch of the entire system, the pertinent GPS information, and the current status of the GRIT-T power systems, including current voltage from each supply. The carriage subsystem provides information about the current distance to target and about the current azimuth and zenith positions. The GUI also provides a manual movement mode. This mode will allow the users to collect spectra of a target manually by moving to user-provided sensor angles and allowing for manual control of the spectrometers. While this may not be as useful in high-tempo field environments, it will provide for an excellent tool in the lab to interrogate interesting targets and to help the user determine the necessary scan density to capture the important features. Another aspect of this manual mode

will allow for movement of the leveling actuators at the operator's discretion. Finally, the GUI provides maintenance screens that can be used to aid in troubleshooting of the goniometer. These include capabilities to move any motor individually to allow for replacement of parts and testing of communications, and will display the current readings from every goniometer sensor including the encoders, the inclinometer, the IMU, and the laser distance unit. These maintenance screens also provide the user with a way to calibrate these instruments for use on GRIT-T after they are replaced.

The various commands from the user's control laptop will then be passed over WiFi to the GRIT-T main computer, which will in turn take action on those commands. The main computer will then issue commands down to the SBCs in the frame and carriage subsystems over ethernet to either perform a coordinated movement, perform a manual motor movement or request a sensor reading. These commands are then interpreted by the SBCs that will, in turn, issue commands out to the motors or sensors and reply back to the main computer when complete. This software architecture provides the user with excellent control of the goniometer while still achieving an elegant solution that does not require every single device be connected to a main computer, or for the main computer to have a large amount of programs/processes running at the same time. This also simplifies the wiring as only one ethernet connection is required to pass information and commands between subsystems, therefore allowing the scientific payload subsystem to control the entire goniometer even though the main computer does not have the required connections to communicate with each device.

## **4.4 Methodology for System Characterization**

In order to perform characterization of GRIT-T, the testing was split into two efforts. The first effort is the mechanical characterization, which investigates GRIT-T's pointing capabilities and will provide an overall pointing error for the scans to provide confidence to those who will use the data product. The second effort relates to the optical characterization of the goniometer. Included in this is an SNR study of the spectrometers and an experiment to determine the improvement achieved by the adjacency compensation approach.

### **4.4.1 Mechanical Testing**

As described by Sandmeier [50], a standard method for measuring mechanical accuracy in a goniometer system is to utilize an alignment laser. In this method, the foreoptic is replaced with a carefully aligned laser that points to the center of the measured target area. The goniometer is then moved through a simulated scan pattern and the movement of the laser is measured with

respect to the center of the intended scan, as determined by pointing the laser straight down from the nadir position. It is then possible to create a plot similar to that in figure 4.22, where the deviation of pointing is visually depicted for each point on a scan. This method provides an absolute understanding of the total combined error present in a system, and gives the user an estimate of how the spot will move over the course of a scan. In a typical goniometer system that does not provide a variable target plane, this characterization only needs to be conducted once, since the motions are always the same. However, on GRIT-T, to adequately characterize the accuracy of the combined mechanical motions, this must be accomplished for at least a few distances to fully understand how well the system is compensating for the changing distance. The outcomes of this experiment will be two fold, i.e. determining the success of reducing spot movement for the purpose of uniformity based on mechanical design, and determining the success of reducing overall parallax when accommodating rugged terrain.

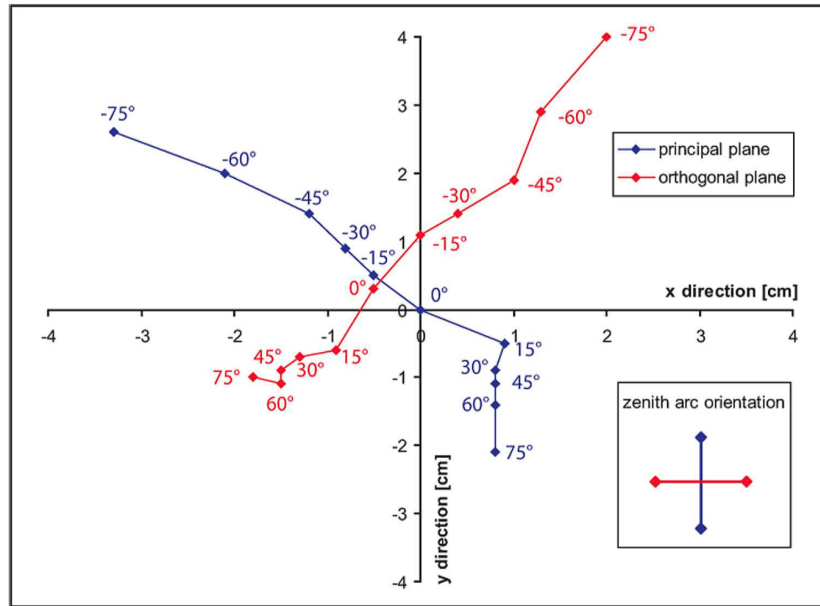


Figure 4.22: An example of a pointing error plot. This plot is for the Dual Field-of-View FIGOS system.[2]

Another necessary test that is related to the mechanical movements is that of the DEM. Since the GRIT-T system's laser distance unit only measures a single point at a time, unlike a standard LIDAR, this point must be positioned by the arm and head to scan over the target area. The motions that occur to point the head ensure that the laser distance unit always keeps a nadir view

of the target area. Any error in these motions will translate to error in the DEM. To characterize the extent of this error, a DEM will be captured of flat surfaces at varying distances and varying colors. In order to isolate the pointing aspects of this experiment from that of the leveling system, it will be ensured that the GRIT-T frame is as level as possible, based on the output from a NIST-traceable 2-axis level accurate to 0.05 degrees. This data will then be compared to the actual surface to determine an overall error in the DEM based on distance and color of the object being measured.

In addition, the automatic leveling system of the goniometer must also be thoroughly tested in a variety of circumstances. To test this, a high precision machinist's level will be used. The system will be placed on various sloped surfaces. A NIST-traceable 2-axis measurement will then be taken of the frame's roll and pitch using a precision level. The system will then be commanded to level, and the 2-axis measurement will be repeated to determine how well the system performed. This will be performed in various orientations on each surface to ensure a full characterization of the system's capabilities. Thus, providing the user with a certain level of confidence that can be applied to the source's zenith position, and the overall plane to which the DEM is referenced.

#### 4.4.2 Optical Testing

The optical testing of the system consists mainly of an SNR examination for the ASD Field Spec 4 spectrometer. While ASD provides noise-equivalent change in radiance,  $NE\Delta L$ , for each of the three sensors inside the FieldSpec-4 spectrometers, the adjustments to fiber optic length from the original 1.5 meters to 2 meters must be considered as this can provide significant attenuation in the SWIR. Also note that the specific light source being utilized for the measurements will introduce a specific amount of shot noise into the measurement. Therefore, the user should capture a measurement of the  $NE\Delta L$  of the ASD system using the specific source that will be used for the spectral measurements. Once the overall  $NE\Delta L$  for the 2 meter fiber lengths is determined by capturing the dark current of the instruments, it would then be possible to determine the correct number of samples and subsamples to achieve adequate SNR based on equation 4.2. Note that in equation 4.1, once the user determines the total noise,  $NE\Delta L$  is then determined by propagating this noise back through the optical system to achieve a radiance value. In ASD spectrometers, since the specifics of the optical system are not entirely known,  $NE\Delta L$  can be found by taking the standard deviation of 30 spectral samples with the specific source to be used, as indicated in the user's guide.[48]

$$N_{total} = \sqrt{N_{electronic}^2 + N_{shot}^2} \left[ \frac{W}{cm^2 \cdot nm \cdot sr} \right] \quad (4.1)$$

$$SNR = \frac{L_{total}}{N_{total}} \quad (4.2)$$

Where shot noise,  $N_{shot}$ , is defined as the square root of the signal and is given in below in 4.3.

$$N_{shot} = \sqrt{L_{total}} \left[ \frac{W}{cm^2 \cdot nm \cdot sr} \right] \quad (4.3)$$

For this system, the goal for SNR for both spectrometers is 400 (over most wavelengths measured by the ASD) or greater. This test should be conducted by determining the standard, single capture SNR for various downwelling radiances under typical testing conditions, and then, by increasing the number of spectral averages, either by adding samples or subsamples through the ASD interface, until the SNR has reached the defined goal for the worst case scenario.

## 4.5 Method for Creating Background-Compensated BRDF

As discussed in section 3.3, there are multiple types of reflectance functions. Typical field goniometers are only able to measure HDRF, since an unknown amount of diffuse skylight is also illuminating the target of interest. For the GRIT-T system, this skylight is being spatially measured to allow for further extraction of the true BRDF or BRF by compensating for the nearby multiple scattering or background effects. The method for performing the compensation was originally proposed by Martonchik [51] and has been used by other similar systems, such as Dual-View FIGOS.[2, 40, 37] This method allows for retrieval of the BRF, and therefore BRDF, by splitting up the sensor reaching radiance into diffuse and direct components in order to solve for each separately using equation 4.4. Note that the notation  $\phi_{i,r} - \phi_0$  refers to the azimuth direction relative to the principal plane.

$$L_r(\theta_i, \theta_r, \phi_r - \phi_0) = \frac{1}{\pi} \cdot \rho_{BRF}(\theta_i, \theta_r, \phi_r - \phi_0) \cdot E_{dir}(\theta_i) + L_{diff}^{refl}(\theta_i, \theta_r, \phi_i - \phi_0) \left[ \frac{W}{cm^2 \cdot nm \cdot sr} \right] \quad (4.4)$$

This process will begin by temporally-compensating the diffuse radiance by creating an illumination factor,  $F_{temporal}(\lambda, t)$ , that describes how the overall downwelled light changed at each scan point. This factor will then be applied to the incoming diffuse radiance data as shown in equation 4.5. The incoming diffuse radiance will be described as  $L_{diff}^{inc}$ ; the purpose of this will become evident further in the processing chain.

$$L_{diff}^{inc}(\theta_i, \phi_i, \lambda, t) = L_{diff}^{inc}(\theta_i, \phi_i, \lambda, t) \cdot F_{temporal}(\lambda, t) \left[ \frac{W}{cm^2 \cdot nm \cdot sr} \right] \quad (4.5)$$

It is then possible to define the diffuse portion of 4.4, as shown in 4.6.

$$L_{diff}^{refl}(\theta_i, \theta_r, \phi_i - \phi_0) = \frac{1}{\pi} \int_0^{\pi/2} \int_0^{2\pi} \rho_{BRF}(\theta_{i0}, \theta_r, \phi_r - \phi_i) \cdot L_{diff}^{inc}(\theta_i, \theta_{r0}, \phi_i - \phi_0) \cdot \sin \theta_i \cos \theta_i d\theta_i d\phi_i \left[ \frac{W}{cm^2 \cdot nm \cdot sr} \right] \quad (4.6)$$

Now that 4.4 has been split into the diffuse and direct portions, it is possible to iteratively solve for the BRF by using 4.4 and the  $(n-1)^{th}$  iteration of 4.6 to refine the BRF estimation with 4.7.

$$\rho_{BRF}^{(n)}(\theta_i, \theta_r, \phi_r - \phi_i) = \frac{L_r(\theta_i, \theta_r, \phi_r - \phi_0) - L_{diff}^{refl}(\theta_i, \theta_r, \phi_i - \phi_0)}{\frac{1}{\pi} E_{dir}(\theta_i)} \quad (4.7)$$

To provide a starting point for the iteration, the diffuse portion of the illumination,  $L_{diff}^{inc}$ , is ignored. This creates the first estimate of BRF, as shown in 4.8.

$$\rho_{BRF}^{(0)}(\theta_i, \theta_r, \phi_r - \phi_i) = \frac{L_r(\theta_i, \theta_r, \phi_r - \phi_0)}{\frac{1}{\pi} E_{dir}(\theta_i)} \quad (4.8)$$

This iteration then calculates the radiance at the sensor,  $L_r$ , using the most current iteration of BRF. When the difference between the calculated sensor radiance and the actual sensor radiance is below a predefined threshold, the iteration is ended and the final iteration of BRF is selected as the actual BRF. [2, 51]

### 4.5.1 Background-Compensation Technique Characterization

While there are various methods to test the accuracy of the background-compensation technique utilized on the GRIT-T system, due to time constraints, only one will be discussed in this paper. The experiment consists of measuring a Lambertian Spectralon plate on a clear day in an open field area, where little background illumination should be present. Once an entire scan is collected, a large colored panel was placed behind the goniometer to introduce dramatic background effects onto the Spectralon surface. The placement of this panel is such that the forward reflection is directed toward the target Spectralon panel. The panel should be approximately 1 meter by 1 meter of colored material and positioned at the rear sides of the instrument approximately 1 meter from the center of the Lambertian panel. The BRF scan should then be repeated with these new illumination effects.

These datasets will then be post-processed using two methods to determine the success of the background-compensation technique. The first post-processing technique that will be used was the standard method utilized by the research group before the GRIT-T system became operational. This technique does not utilize any spatial illumination information but relies on two spectrometers for data collection, one collecting target spectra and the other collecting overall downwelled light, as described by Bachmann, to compensated solely for temporal illumination changes.[9] The other method used was that described in section 4.5, where spatial illumination information was utilized along with temporal illumination information. Applying these two methods to the same dataset provided an opportunity to compare the techniques directly, without the possibility of target, system, or environmental changes that are often evident even when datasets are taken back to back. While taking the necessary data to facilitate this experiment was included as part of this work, the full post-processing and analysis of this method will be part of a future effort to calibrate the system.



## Chapter 5

# Results

### 5.1 System Implementation

As of July 2016, the GRIT-T system has been engineered, fabricated, assembled, and tested as described in this document. The engineering and design effort, as discussed in chapter 4 lasted approximately 9 months from July 2014 to April 2015. While much of the system was designed before the issues were discovered with the Hepco Motion ring solution, designing a new custom ring did have an impact the development of other system components. Therefore, the engineering effort for the other components was placed on hold while the ring was finalized. Upon completion of the ring design and structural modeling effort, fabrication on the 3-piece ring was started at Trident Precision Manufacturing in Webster, New York. Due to the complexity and size of the design, the ring fabrication took 12 weeks to complete. Figures 5.1, 5.2, 5.3, 5.4 show the layers of the ring throughout the fabrication process.



Figure 5.1: A photo of the bottom and middle ring layers after water jet cutting.

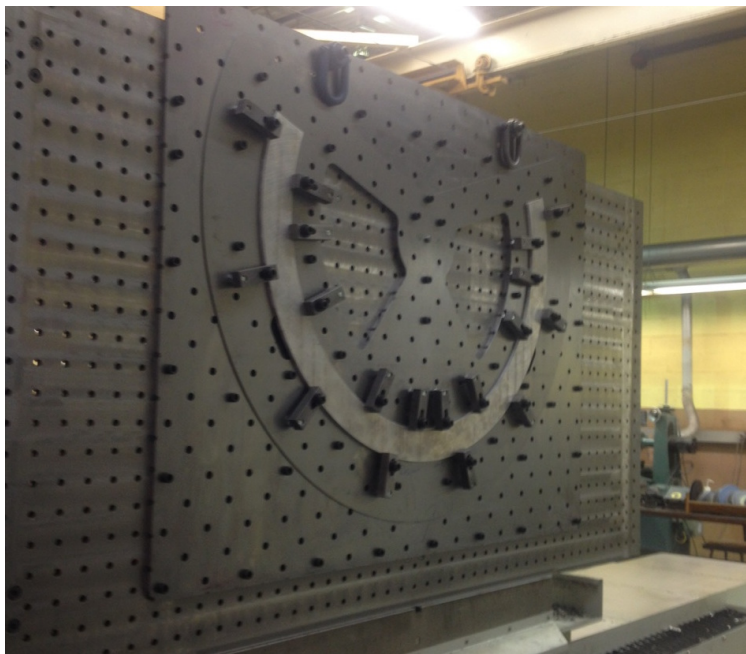


Figure 5.2: A photo of the top layer before the guide rails were machined.

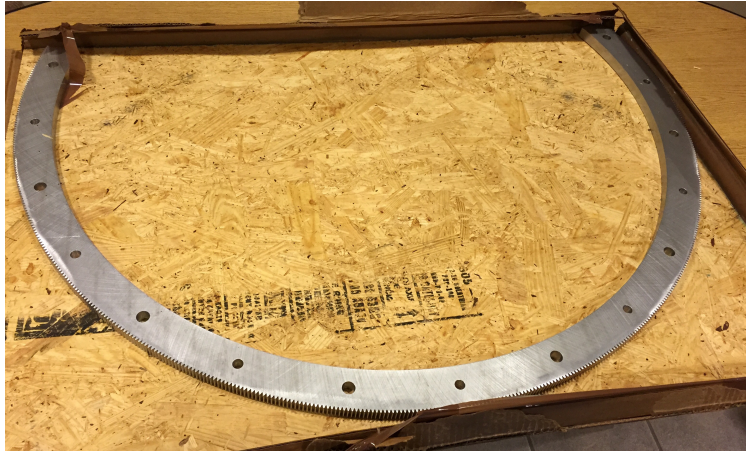


Figure 5.3: A photo of the middle layer after being water jet cut, surface ground, and gear cut.

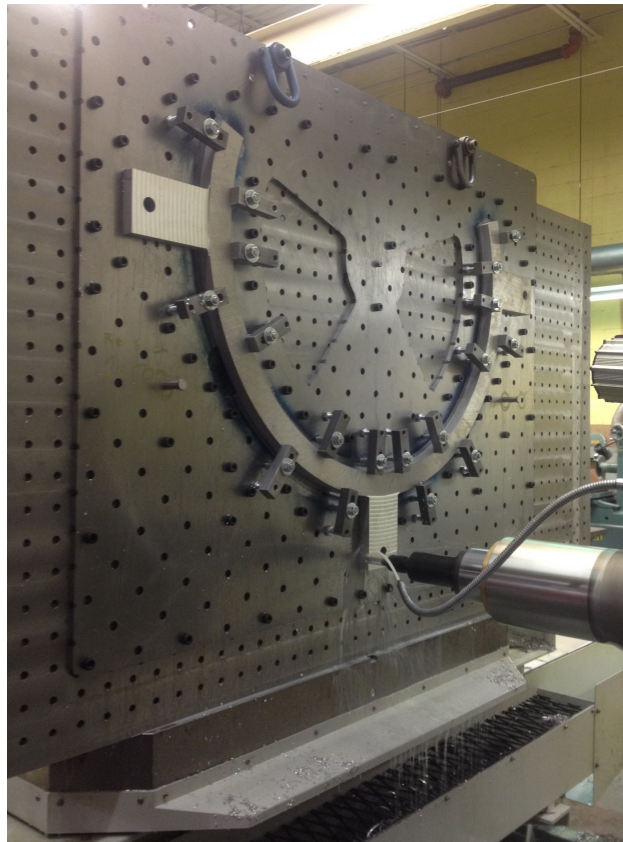


Figure 5.4: A photo of the bottom layer, showing the large computerized numerical control (CNC) mill machining the mounting points for the leveling actuators.

During this time, other components were adjusted and finalized to accommodate the final ring geometry while ensuring that the overall scientific goals of the system were achieved. Procurement for the other system components began around April of 2015 and continued into June, when the integration effort began. During integration, various communication issues were identified between the controlling hardware and the movement hardware. Steps were taken to remedy these problems and ultimately the hardware discussed in section 4.3 was chosen to meet the system requirements while solving the communication difficulties. Due to this, the integration effort continued into the winter of 2015. During the spring of 2016, the final integration effort was completed and much work went into finalizing the GUI control software that is used to control the instrument. During the early summer of 2016, the testing and characterization phases of the project were completed as the software reached maturity. The figure below shows the system in its final configuration, including paint, in the laboratory. More photos of the system in use can be found in section 5.4.

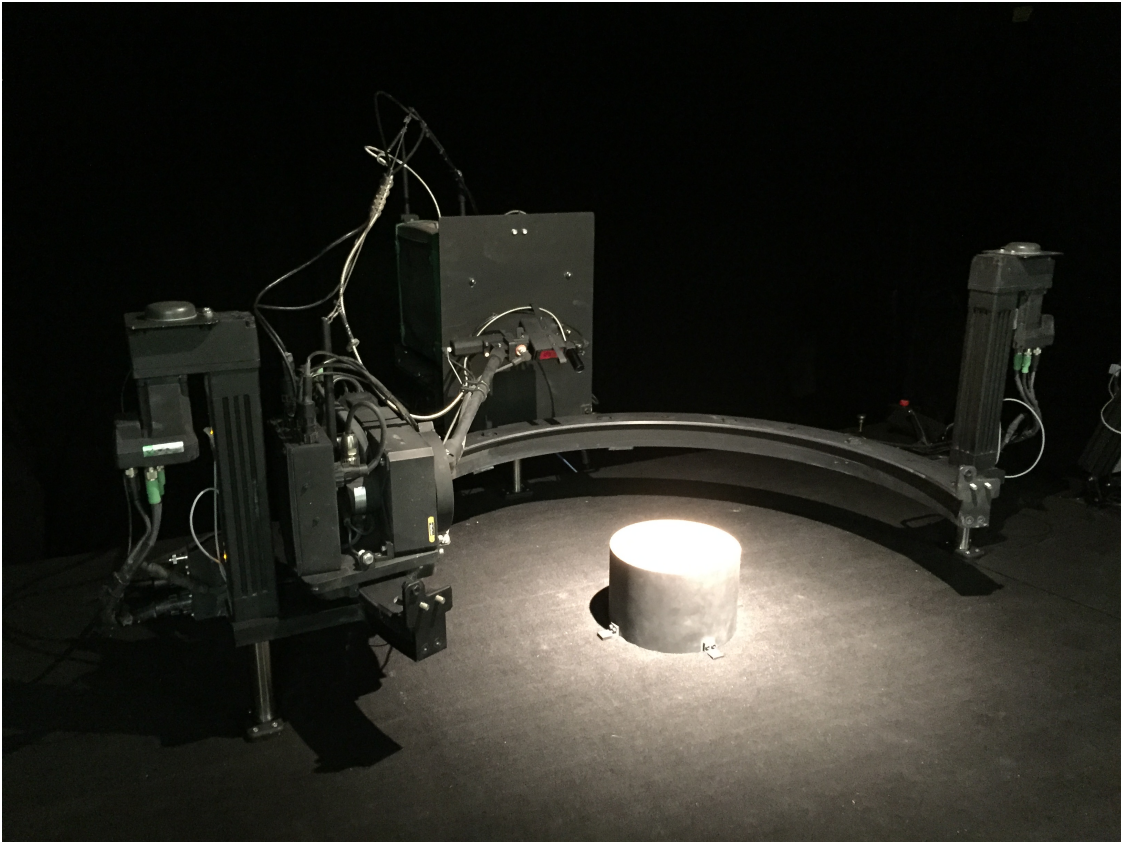


Figure 5.5: GRIT-T after final assembly in the GRIT Lab, note that the spectrometers are not attached in this photo.



## 5.2 System Characterization

### 5.2.1 Mechanical Testing Results

As mentioned in section 4.4.1, three main tests were conducted on the GRIT-T system. These tests consisted of two laser alignment tests, one for target tracking and one for nadir tracking, and a leveling system test. The results for these tests are discussed below.

#### Target/Nadir Tracking Results

The system tracking tests consisted of two phases: (1) target tracking in which the system determined the distance to the target and recalculated movements to ensure that the center of the GIFOV was maintained throughout the scan, and (2) nadir tracking, where the system ensured that the measurement head maintained a nadir view angle throughout the scan. The former was necessary to assess the alignment performance for the collection of reflectance functions, and the latter was necessary to assess the alignment performance for the collection of the DEM. All tests were performed as described in section 4.4.1.

The alignment test was performed and documented in the same manner as that described by Sandmeier.[50] Figure 5.6 indicates the mechanism used to perform this tracking. For these tests, a 632.8 nm laser was placed in the optical axis of the fore optics and the system was then commanded to move through an entire scan. Due to the sheer number of points on each scan, only those that were at the maximum achievable zenith were plotted for each azimuth, since this represented the largest overall error for each azimuth spoke. These tests were completed after the system had been fully calibrated and the arm geometry constants were correctly adjusted to compensate for machining errors. The first test tracked a sheet of white graph paper at a distance of 632 mm, as measured to the bottom of the modular sensor head, in azimuth steps of 45 degrees and recorded for a maximum zenith of 65 degrees. For this test, the maximum error recorded in any direction from the origin was 7.84 mm. The second test tracked a sheet of white graph paper at a distance of 732 mm, in azimuth steps of 45 degrees and recorded for a maximum zenith of 55 degrees. Note that this maximum zenith is less than the first test since the system was artificially raised over the target, and that 55 degrees was the maximum achievable angle with respect to the target. As can be seen in tables 5.7, and 5.8, and figures 5.9 and 5.10, the GRIT-T system was able to track a single point on the ground within  $\pm 8$  mm in the worst case, at a nominal target height and within  $\pm 10.5$  mm in the worst case at the most extreme target height.

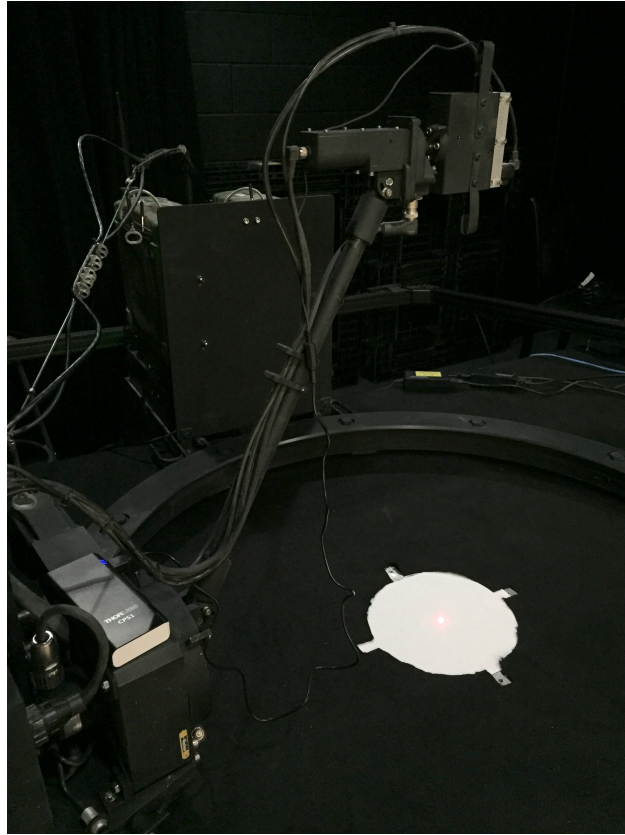


Figure 5.6: Figure showing the alignment test setup, including small optical alignment laser.

Azimuth	Zenith	Y Error	X Error	Distance from Origin
0	0	0	0	0
0	65	-1.94	-4.35	4.76
45	0	0.66	0.75	1.00
45	65	1.99	-4.5	4.92
90	0	0.94	1.05	1.41
90	65	4.9	1.64	5.17
135	0	-0.56	-0.6	0.82
135	65	3.6	5.91	6.92
180	0	0.84	0.64	1.06
180	65	3.92	4.02	5.61
225	65	-2.41	7.46	7.84
270	65	-7.32	2.43	7.71
315	65	-6.11	-3.47	7.03

Figure 5.7: Alignment test results from 632 mm distance. All error measurements and distances are provided in millimeters.

Azimuth	Zenith	Y Error	X Error	Distance from Origin
0	0	0	0	0
0	55	1.24	-8.42	8.510816647
45	0	0.56	0.25	0.613269924
45	55	6.04	-5.75	8.339310523
90	0	0.2	0.93	0.951262319
90	55	8.94	4.7	10.10017822
135	0	-0.56	-0.36	0.665732679
135	55	5.66	8.68	10.36233564
180	0	0.84	0.64	1.056030303
180	55	0.2	9.97	9.972005816
225	55	-4.03	8.99	9.851954121
270	55	-9.59	2.58	9.930986859
315	55	-8.36	-3.12	8.923228115

Figure 5.8: Alignment test results from 732 mm distance. All error measurements and distances are provided in millimeters.

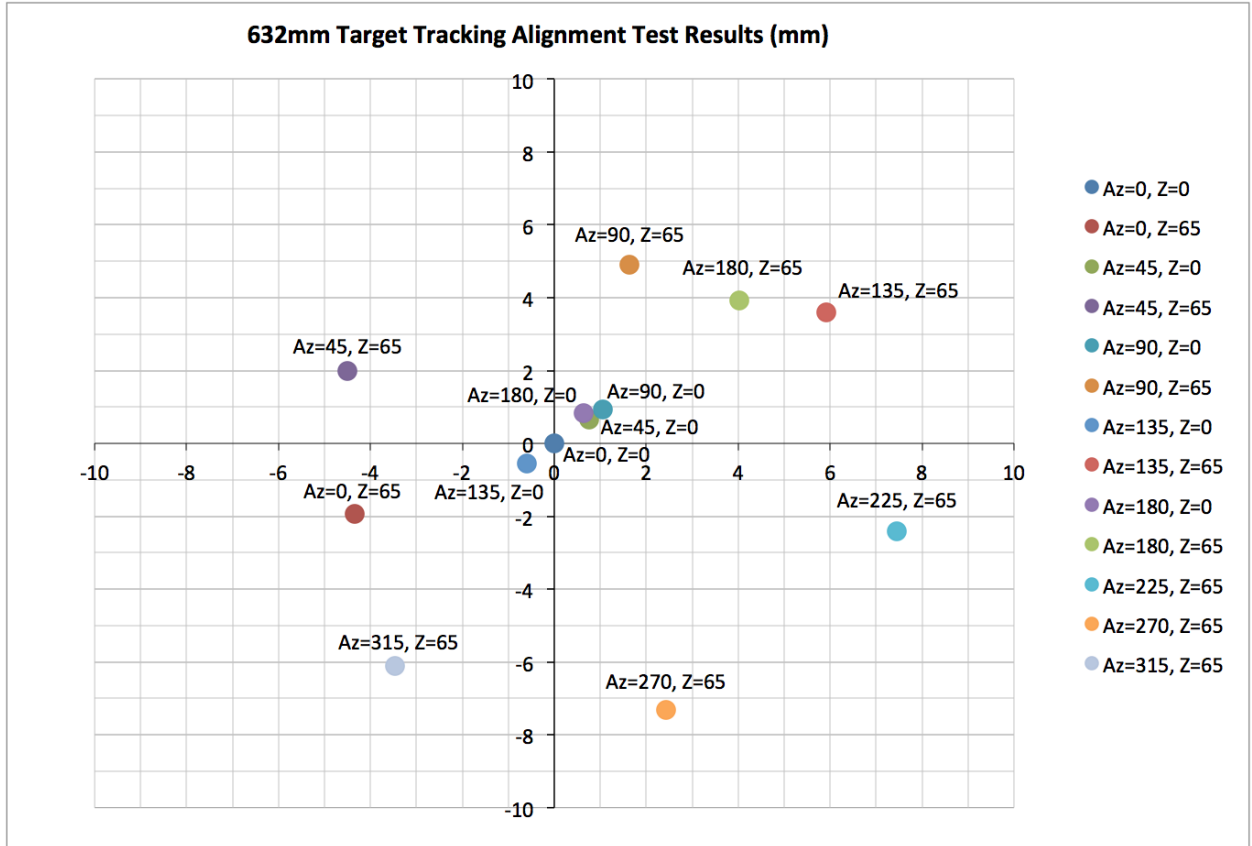


Figure 5.9: Plot indicating the results of the 632 mm distance alignment test.

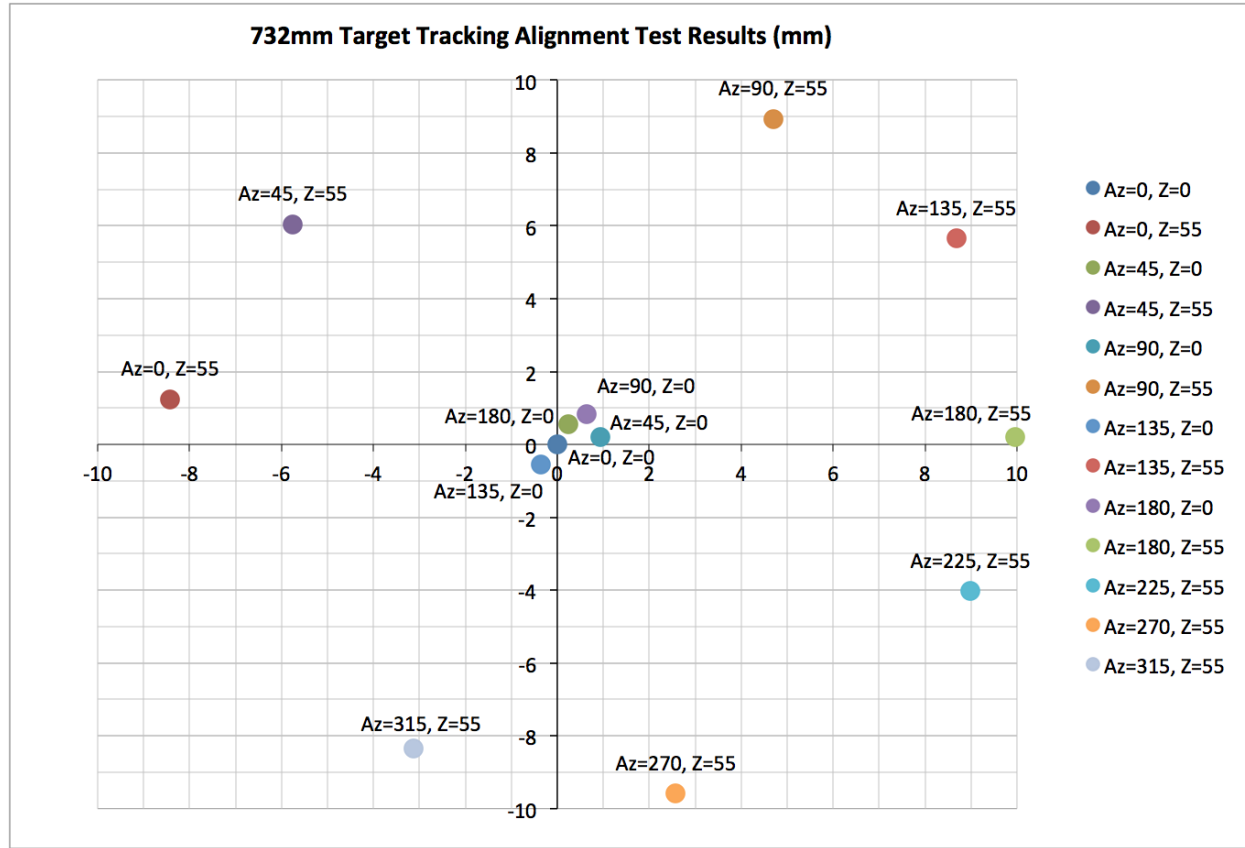


Figure 5.10: Plot indicating the results of the 732 mm distance alignment test.

A nadir view angle tracking test was completed in a similar method to the tracking alignment test. For this test, a nominal DEM scan was utilized with a radius of 20 cm and a density of 27 points. For the DEM positioning test, the deviation from the intended X and Y coordinate was logged based on a target height of 740 mm. The full results of this test are given in table 5.11 and figure 5.12. As can be seen, the average error between the alignment laser and the intended target was 3.6 mm. It is important to note that work on finalizing the DEM capture is on-going by members of the GRIT team and further steps are being taken to reduce the errors shown in the preliminary pointing test. Future nadir pointing tests will likely be conducted once these improvements have been finalized.



## 5.2. SYSTEM CHARACTERIZATION

Point #	Commanded X (mm)	Commanded Y (mm)	Actual X (mm)	Actual Y (mm)	X Diff (mm)	Y Diff (mm)	Overall Diff (mm)
1	-16.41	-86.56	-17.67	-88.24	1.26	1.68	2.10
2	-20.37	-46.73	-21.46	-48.33	1.09	1.6	1.94
3	-40.87	-83.44	-42.49	-84.85	1.62	1.41	2.15
5	-43.04	-41.66	-44.65	-42.39	1.61	0.73	1.77
6	-68.78	-71.03	-71.07	-72.47	2.29	1.44	2.71
7	-0.75	42.42	-2.54	42.35	1.79	0.07	1.79
8	43.55	83.14	43.64	83.53	0.09	0.39	0.40
9	-83.49	-40.76	-86.18	-41.12	2.69	0.36	2.71
10	-42.53	-0.24	-45.73	0.36	3.2	0.6	3.26
11	-14.26	20.42	-16.63	20.61	2.37	0.19	2.38
12	73.64	72.75	72.95	72.48	0.69	0.27	0.74
13	39.02	40.61	37.13	40.44	1.89	0.17	1.90
14	-84.43	-0.09	-86.51	1.24	2.08	1.33	2.47
15	82.35	42.63	81.87	43.18	0.48	0.55	0.73
16	-81.96	43.76	-83.42	45.32	1.46	1.56	2.14
18	84.25	-1.15	84.05	-0.47	0.2	0.68	0.71
19	-43.28	42.94	-44.61	45.28	1.33	2.34	2.69
20	-68.59	71.22	-67.6	74.21	0.99	2.99	3.15
21	42.42	-0.73	42.58	1.88	0.16	2.61	2.61
22	82.8	-41.73	83.05	-40.72	0.25	1.01	1.04
23	-42.57	83.85	-42.61	87.1	0.04	3.25	3.25
24	70.14	-76.13	70.22	-75.48	0.08	0.65	0.65
25	42.44	-42.1	42.96	-38.98	0.52	3.12	3.16
26	-0.77	83.31	1.25	86.32	2.02	3.01	3.62
27	39.73	-83.78	40.64	-80.78	0.91	3	3.13

Figure 5.11: Alignment test results from the DEM alignment test performed at 740 mm distance. All error measurements and distances are provided in millimeters.

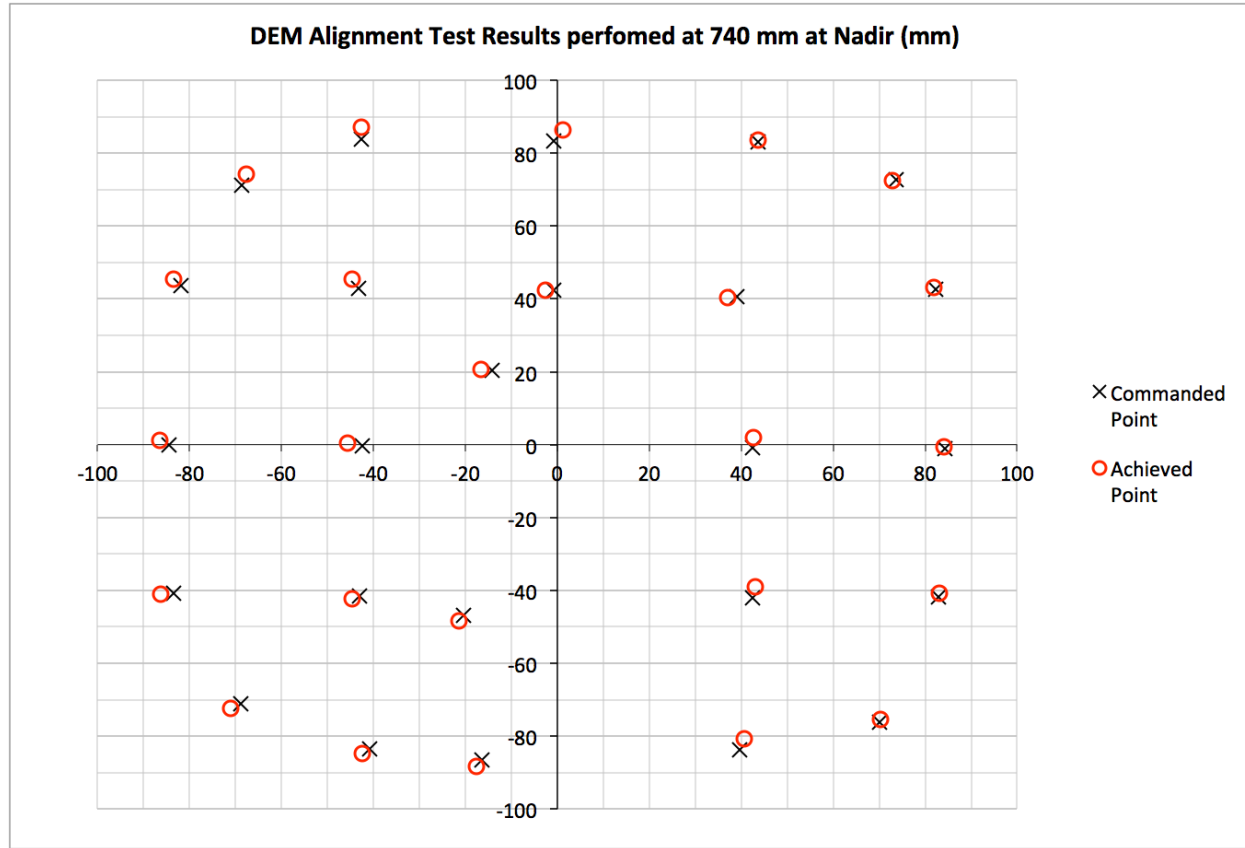


Figure 5.12: Plot indicating the results of the DEM alignment test performed at 740 mm distance.

### Leveling Test Results

The leveling portions of the GRIT-T system were thoroughly tested as discussed in section 4.4.1. This test was conducted while the system was under various levels of artificially-induced roll and pitch. The system was then commanded to level itself using only the Rieker precision inclinometer data. Figure 5.13 indicates the various levels of induced pitch and roll as well as the final inclination of the frame of the system. Based on this testing, it was determined that the system can bring the main frame within 0.1 degrees from level using the three leveling actuators for movement. Note that the leveling algorithm seemed to converge on roughly -0.15 degrees in roll and -0.14 degrees in pitch. This offset was expected for the system and is then used to set the overall offset between the Rieker mounting plate and the frame of the system itself. This adjustable parameter allows for tweaks over time as the system ages, while still ensuring that system can achieve level. Also note that there are both "coarse" and "fine" columns for the leveling test results. These represent two

different mechanisms for leveling the frame. The "coarse" leveling mechanism allows for the system to overcome the large initial discrepancy noticed when beginning the leveling process. This method only drives the actuators outward, and should be used just once. The "fine" leveling mechanism is then used to finish the leveling process and allows for actuator travel both outward and inward, thus allowing the system to settle should the initial "coarse" method overshoot.

Run	Initial roll	Initial Pitch	Coarse Roll	Coarse Pitch	Fine 1 Roll	Fine 1 Pitch	Fine 2 Roll	Fine 2 Pitch	Fine 3 Roll	Fine 3 Pitch	Fine 4 Roll	Fine 4 Pitch
1	0.44	-0.01	-0.15	-0.11	-0.21	-0.11	-0.22	-0.1	-0.22	-0.1	-0.22	-0.1
2	-3.49	0.5	-0.19	-0.29	-0.18	-0.09	-0.17	-0.1	-0.14	-0.14	-0.12	-0.16
3	-1.16	1.5	-0.44	0.22	-0.2	-0.14	-0.19	-0.15	-0.18	-0.15	-0.22	-0.14
4	-2.83	2.34	-0.59	1.12	-0.17	-0.09	-0.15	-0.17	-0.15	-0.14	-0.15	-0.11
5	-4.49	3.1	-0.63	2.07	-0.17	-0.04	-0.17	-0.15	-0.17	-0.13	-0.17	-0.13
6	0.32	-6.7	-0.15	-0.49	-0.13	-0.19	-0.12	-0.16	-0.11	-0.14	-0.09	-0.16
7	0.4	-9.35	-0.24	-1.3	-0.22	-0.19	-0.18	-0.15	-0.18	-0.15	-0.17	-0.16
8	3.81	2.22	0.3	1.22	-0.15	-0.05	-0.19	-0.16	-0.18	-0.16	-0.17	-0.16
9	5.52	2.93	0.41	2.12	-0.12	-0.02	-0.18	-0.15	-0.21	-0.15	-0.19	-0.15
10	2.19	3.56	0.28	1.62	-0.12	-0.06	-0.18	-0.16	-0.18	-0.16	-0.16	-0.16
11	3.8	-0.15	0.05	-0.19	-0.17	-0.15	-0.18	-0.15	-0.17	-0.12	-0.17	-0.11
12	2.02	-4.97	-0.08	-0.41	-0.03	-0.17	0.02	-0.15	0.1	-0.15	0.2	-0.15
13	-1.21	-5.02	-0.23	-0.38	-0.19	-0.15	-0.17	-0.12	-0.15	-0.13	-0.15	-0.14
14	-2.79	0.06	-0.35	-0.14	-0.16	-0.13	-0.16	-0.13	-0.15	-0.13	-0.16	-0.15
15	-1.15	3.64	-0.46	1.47	-0.19	-0.08	-0.15	-0.16	-0.14	-0.16	-0.16	-0.18
Average:									-0.149	-0.141	-0.140	-0.144
Standard Dev.:									0.07424541	0.016676188	0.09957051	0.022614787

Figure 5.13: Leveling Test Results. Note that the test was completed for 15 different roll/pitch scenarios and that the final roll and pitch achieved was then used as an offset for the Rieker inclinometer. Thus allowing the system to achieve true level within 0.1 degrees.

### 5.2.2 Optical Testing Results

The optical testing portion of the results is based on the determination of the SNR in typical illumination scenarios for the on-board spectroradiometers. As this figure of merit is completely illumination dependent, it was determined for a typical laboratory setting with a 70 watt ASD broadband Illuminator. The SNR was determined using the method described in section 4.4.2 for each wavelength of the ASD Field-Spec 4 spectroradiometer. The results of this experiment can be seen below in figure 5.14, which show the typical SNR for the ASD Field Spec 4 spectrometer with 2 meter fiber optic cable, when measured using an actual sediment target in a laboratory setting. As shown, the typical SNR for the VNIR sensor, SWIR 1 sensor, and SWIR 2 sensor were adequately large, based on the requirements, in a laboratory setting. As can be expected, outdoor testing will indicate a much higher SNR due to the increased illumination conditions. However, it is worthwhile to note that the upward-looking spectroradiometer may experience lower SNR depending on the position of the Sun and surrounding objects. Especially in the SWIR, for which the vast majority of the photons are only incoming from the solar direction, SNR for the upward-looking device may dip dramatically. Re-optimization of the spectroradiometer may aid in increasing the SNR in SWIR, based on the internal gain setting chosen for that particular light level. This test also can provide the

user with a general understanding of how many spectral samples should be taken for any particular view angle, since the overall noise decreases by a factor of the square root of the number of samples taken. By default, the ASD spectrometers are programmed to collect 10 spectral samples for each file saved. That is, 10 individual samples are captured, and averaged, before saving one file. In practice, the GRIT team will further increase the SNR by collecting multiple files, typically between 4 and 8, per view angle, with the GRIT-T system, such that between 40 and 80 individual spectral samples are captured and ultimately averaged together. These extra samples serve the purpose of also ensuring that any losses from the longer, 2 meter fiber optic cables required by GRIT-T are also overcome by the increase in overall SNR. Figure 5.15 indicates the signal throughput of the 2 meter fiber optic cable relative to the standard 1.5 meter fiber optic cable typically found on ASD Field-Spec 4 spectroradiometers. However, it is also prudent to ensure that when so many files are being averaged in a field setting, that the overall illumination conditions are not varying quickly enough to have a significant impact during the collection period. It is ultimately up to the user of the system to ensure that the SNR is adequately large, without improperly averaging over rapidly changing illumination conditions.

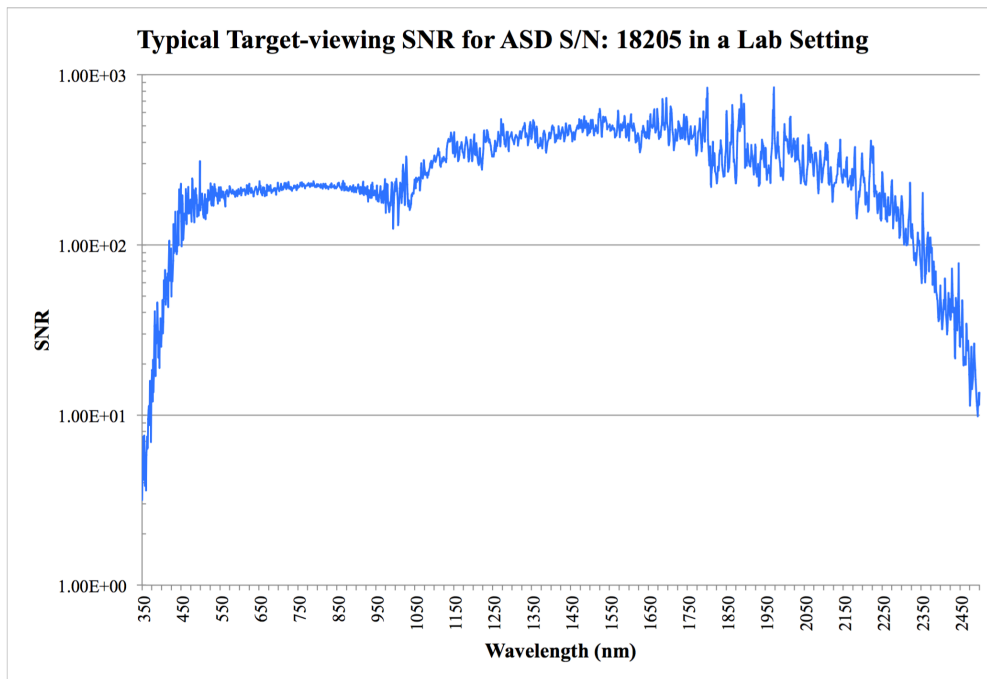


Figure 5.14: Figure showing the signal-to-noise ratio for typical laboratory conditions with ASD S/N: 18205. This SNR was determined for radiance leaving an Algodones Dunes sediment sample collected with a 5 degree fore optic. The broadband source used for laboratory experiments is a 70 watt ASD Illuminator.

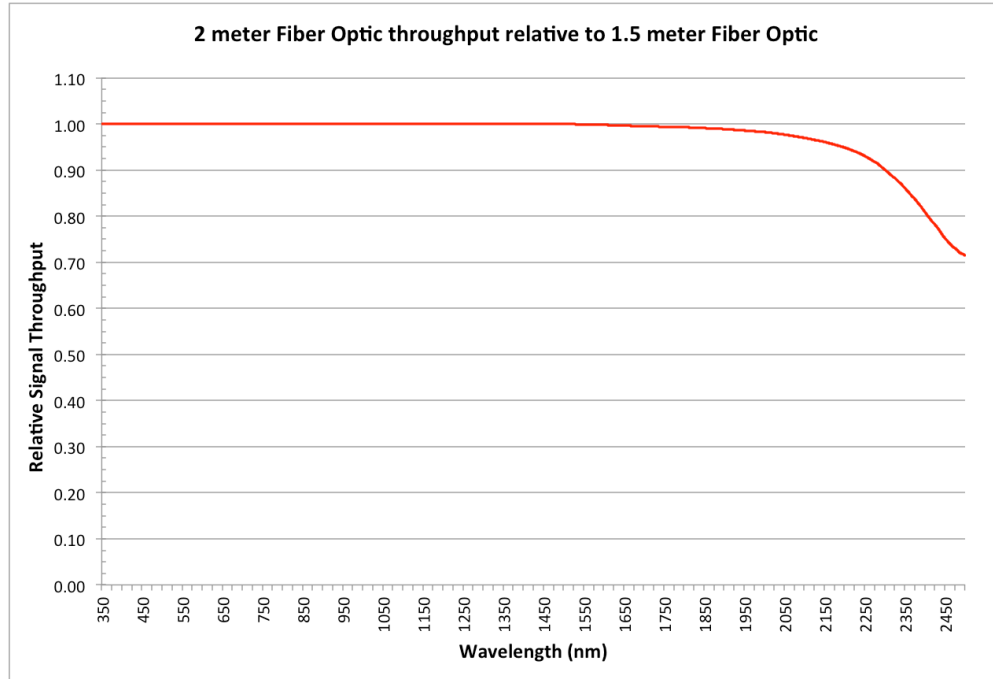


Figure 5.15: Figure showing the relative signal throughput of a 2 meter fiber optic cable versus a 1.5 meter fiber optic cable on an ASD Field-Spec 4 spectroradiometer.

### 5.2.3 Software Implementation and Testing

As mentioned in 4.3.4, The GRIT-T software was separated into two levels: low-level code performing sensor and motor commands at the Raspberry Pi level, and high-level code which the user would interact with and would maintain the system state. While this code was written by two software engineers, Andres Ruiz Torres and Jason Faulring, it was done so with the guidance of the entire GRIT team. Since many of the decisions and initial GUI designs were created by the author, each page of the user interface will be provided here, along with a brief discussion of its purpose.

The first page that the user will interact with when running the GRIT-T control software is the startup page, seen in figure 5.16. This page allows the user to connect to the system, wake the system, and begin the process of creating a scan. It also provides automated buttons to aid in sleeping the system for storage in its portable field case.

The next page that a user will need to view for a field collection is the leveling view. This page provides the user with control of each individual actuator in a manual mode, which may be necessary to accommodate extraordinary terrain, or by using the automated leveling buttons. A view of this page can be found in figure 5.17.

In order to bypass the ASD RS3 control software, the GRIT-T control software included a spectrometer control page, that performs the main functions of setting spectrometer collection settings without leaving the GUI. From this page, users can set site parameters, collection parameters including samples and subsamples, the fore optic being used for each spectrometer, optimize the spectrometer, and perform a fully manual collection, if necessary. This page also shows a live view of the current spectra returned from the spectrometer. See figure 5.18.

It is also necessary for the user to utilize the scan setup page to be able to program the appropriate scan pattern for GRIT-T to collect. From this page, the user can build, preview and save various types of scans. The user provides the scan interval in both azimuth and zenith and the minimum and maximum values for both azimuth and zenith. The software will then create a uniform scan pattern that is immediately viewable and can be set for collection. It is also important to note that the user can choose to perform non-uniform scan patterns if so desired. To input non-uniform scan patterns, it is possible to input desired movement points in a text file. These features can be seen in figure 5.19. Likewise, the user can utilize the DEM scan page to program DEM scans. This can be seen in figure 5.20.

Once the spectrometer parameters and scan have been set, it is then possible to use one of the two progress pages to monitor the scan as it completes. The first of these pages is the field view. This view, found in figure 5.21, contains a wide variety of system status indicators that aid the user in understanding spectrometer performance, scan progress, system performance, leveling status, and IMU/GPS data health. As can be seen, this view offers a real-time view of both spectra from the target viewing and sky viewing spectrometer, the current save progress for each, the time since last optimization, and their respective battery voltages. Also notice the two green indicators near the "Spectrometer #1" and "Spectrometer #2" headings. These indicators notify the user of the health of the spectra by giving real-time feedback of whether either spectrometer is connected and sending data, if a sensor is saturated, if the data is being dark current subtracted, and whether ASD's temperature compensation mechanism is being correctly applied. This information provides the user with a level of confidence about the quality of the data being returned and whether the spectrometer is performing as it should over the course of the scan.

In the upper-right portion of the figure, the current scan that is being executed is shown. This scan includes hollow dots for points yet to be collected, blue dots for points where spectra have already been saved, and a red dot indicating the current system location. This portion also provides the user with the last commanded movement angle, and the current position of the arm based solely on absolute encoder data, which ensures that the system is accurately maintaining its track of the chosen target. In addition, there are also buttons to allow the user to pause a collection, resume a collection, step forward or backward, perform a manual spectral collection, and perform a white

reference sample. The white reference button, once clicked, then guides the user through the process of inserting a white plaque, choosing which spectrometer to view the plaque, and saving the data with a unique filename including the necessary collection parameters.

In the lower-right portion of the view, the user can find various system health information. Under "Controller Status," the user can determine if the Raspberry Pi 2 embedded controllers are performing correctly and returning sensor data at the expected time interval. Again, indicators provide a quick view of this information; and hovering over a yellow or red indicator will provide information about any errors that could be interfering with the measurements or system operation. In this portion, the leveling status and power systems status are also available to provide warning about whether the system has significantly shifted or settled during the course of the scan, and whether the on-board GRIT-T batteries need to be replaced. The user can also clearly see the real-time outputs of the dual-GPS-enabled IMU that captures geolocation information during the scan. This section also provides an estimation of the accuracy of the currently displayed data, as provided by the VectorNav IMU.

While still in progress, the GRIT-T control software does feature a DEM page to control the device while digital elevation maps are collected. The DEM scan page provides the user with a polar plot of the movement angles that will be performed; as well as a scatter plot of the X and Y coordinates that will be captured at the target. Similar to the field view, blue and red dot indicators inform the user of points that have been sampled and the current position, respectively. The DEM view can be found in figure 5.22.

In addition to the pages required to setup and perform scans, three other pages were provided to aid the operator in performing movements outside of a scan and when troubleshooting becomes necessary. The manual movement page provides the user with complete control of each axis of motion available on GRIT-T. This includes head movements, arm movements, carriage movements, and movement of each actuator. This allows the user to home each axis independently and clear any motor faults that may have occurred, without restarting the entire system. Motor faults could be due to reaching the extent of travel despite software limitations, or reaching the set torque limit as programmed to ensure operator safety. This view can be seen in figure 5.23.

The second page used for troubleshooting is the system control view. This view is very simple but allows the user to restart any system control process on the controllers through a supervising process. If any portion of the system fails to respond, the user can first try restarting that individual process before rebooting the entire system. The last page used for troubleshooting is the status view page. This page is only used in extenuating circumstances when the operator must attempt to repair a sensor on the device. In that situation, the status view page allows the operator to see the raw parsed data being returned from the controllers without any interpretation or adjustment,

and can be used to manually test any sensor to ensure its operation. The system control view and status view pages can be found in figures 5.24 and 5.25, respectively.

### **5.3 BRDF Retrieval Results**

To achieve a more ideal BRDF measurement in field settings, the technique originally proposed by Martonchik was proposed for GRIT-T, as described in section 4.5. This technique utilizes an iterative approach that incorporates the effects of non-uniform skylight and the effect of surrounding objects by including spatial illumination information when determining the BRDF of a target. As mentioned in 4.5, the data required to conduct a full characterization of this compensation technique was captured as part of this work. This data consisted of an experiment meant to exaggerate the effect of background illumination by placing a Tyvek-covered board very near the goniometer as it conducted a measurement of a Spectralon plaque. This test was performed twice, once with the board very nearby, and once without the board entirely, to be used as a control. By utilizing this technique, it is possible to test the ability to remove the effects of the board from the reflectance function with the Martonchik method. In a future characterization study, this data will be used to determine how well the iterative approach can remove the very strong spectral features that the Tyvek panel introduced into the scene when combined with the dual-view spectroradiometer design of GRIT-T.

### **5.4 Nevada Field Experiment**

In mid-June of 2016, the system was utilized for a collaborative field experiment with the Naval Research Laboratory (NRL) and the U.S. Army Engineer Research and Development Center (ERDC) that lasted approximately two weeks in the Nevada desert. This experiment served as the first real-world field test for GRIT-T and provided very challenging terrain which fully tested the system's capabilities. As can be seen in figures 5.26, 5.27, and 5.28, a wide variety of sites were tested, from dry, powdery, salt flats to soft silty areas to completely saturated clays.





Figure 5.16: GRIT-T Control Software Startup page.

GRIT-T - Level View

Startup Screen | Level View | Spectrometer Control | Scan Setup | Field View | DEM View | Manual Movement Control | System Control

Frame Actuator A

0

Position

0.00 mm

Move

Home

Stop

Clear Fault

Frame Actuator B

0

Position

0.00 mm

Move

Home

Stop

Clear Fault

Frame Actuator C

0

Position

0.00 mm

Move

Home

Stop

Clear Fault

Position

0.00 mm

Move

Home

Stop

Clear Fault

Move All

Stop All

Head Controls

Head Angle

0

Move Head

Home Head

Stop Head

Level Controls

Fine Level

Level

Min Drive

Level Status

Status:

Roll:

Pitch:

Laser Distance:

Measure Laser

OK

-0.05°

+0.02°

742.19 mm

A

B

C

ERR: Dark Current Correction did not occur!! for Spectrometer 2

Figure 5.17: GRIT-T Control Software Leveling page.

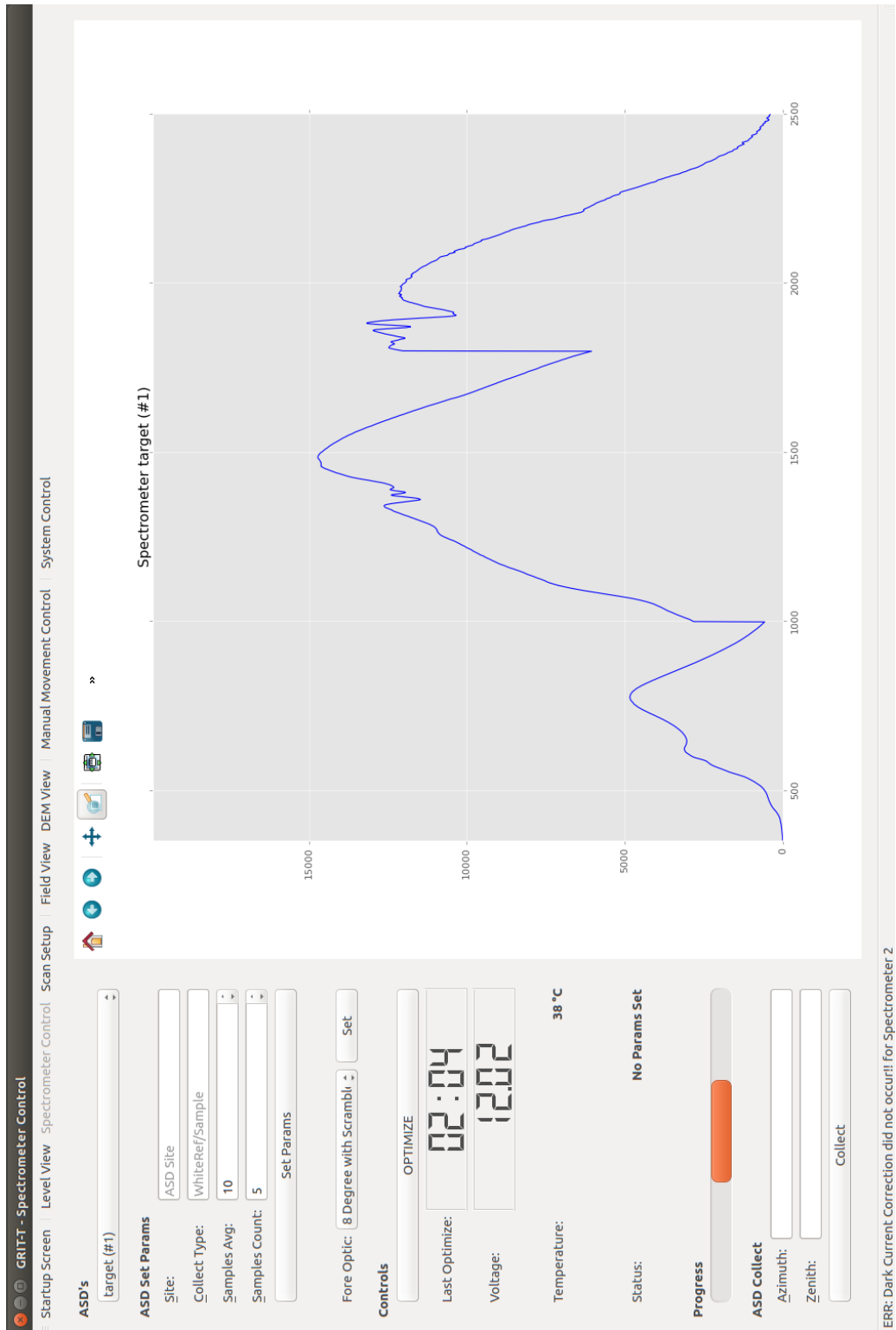


Figure 5.18: GRIT-T Control Software Spectrometer Control page.

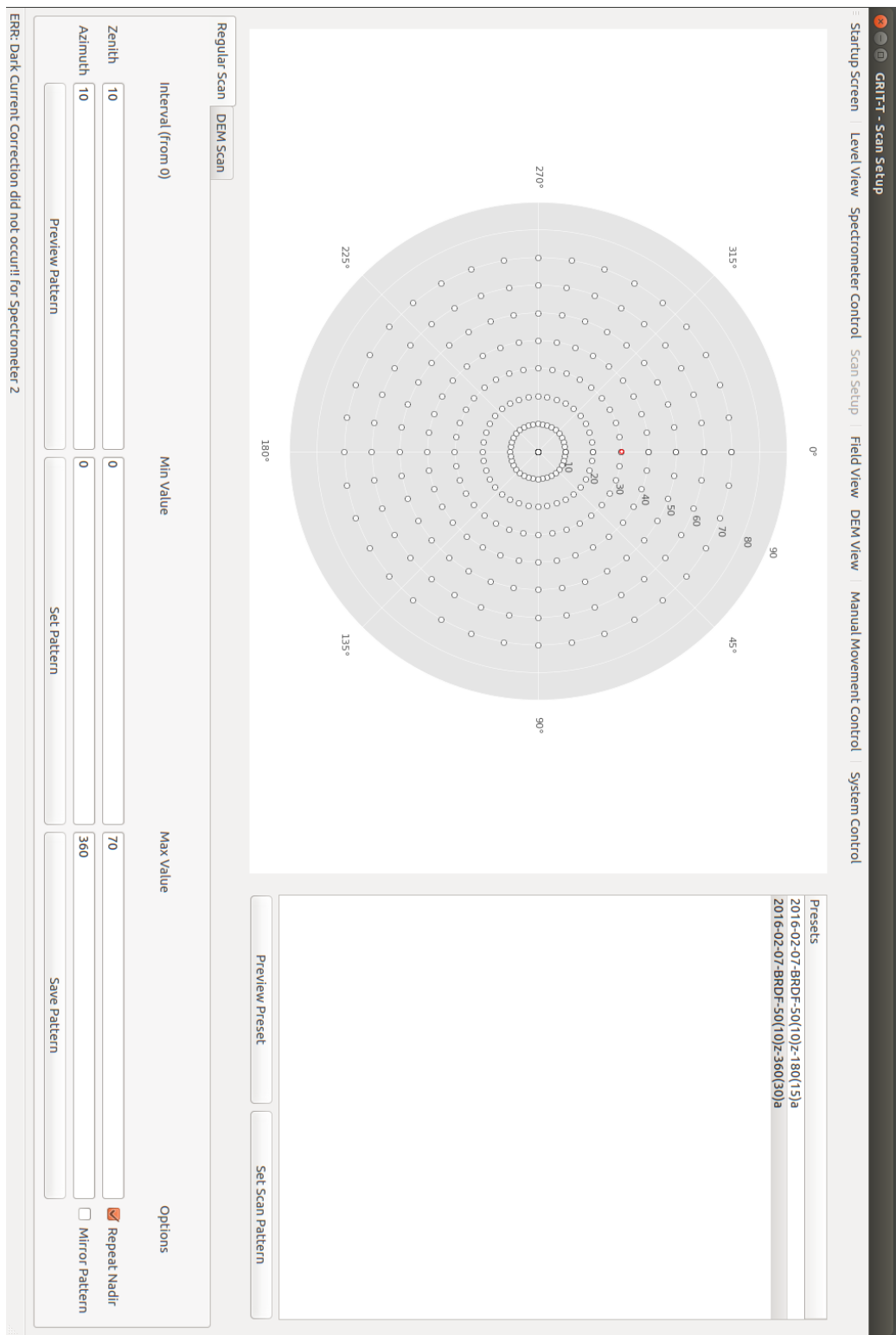


Figure 5.19: GRIT-T Control Software Scan Setup page.

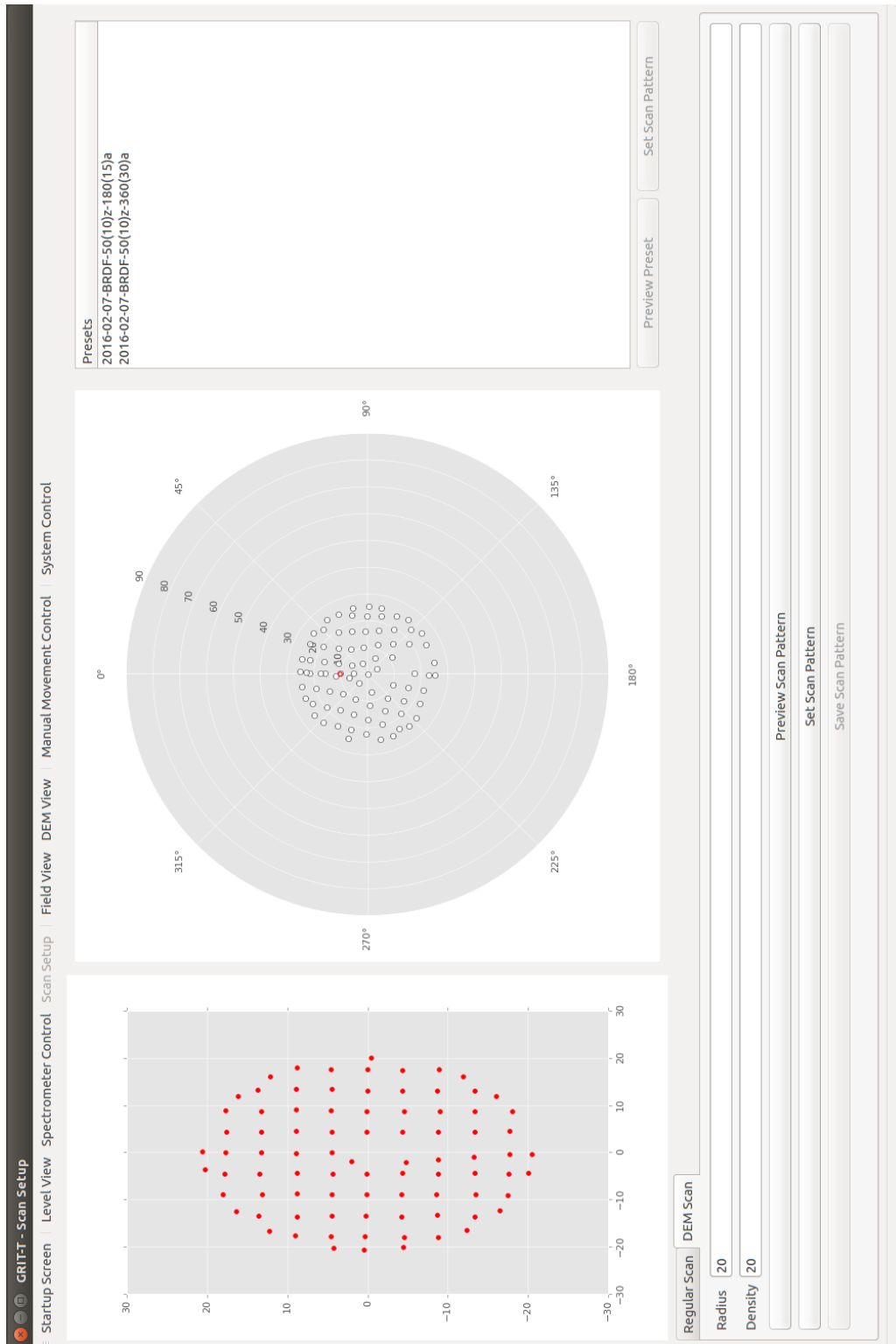


Figure 5.20: GRIT-T Control Software DEM Scan Setup page.

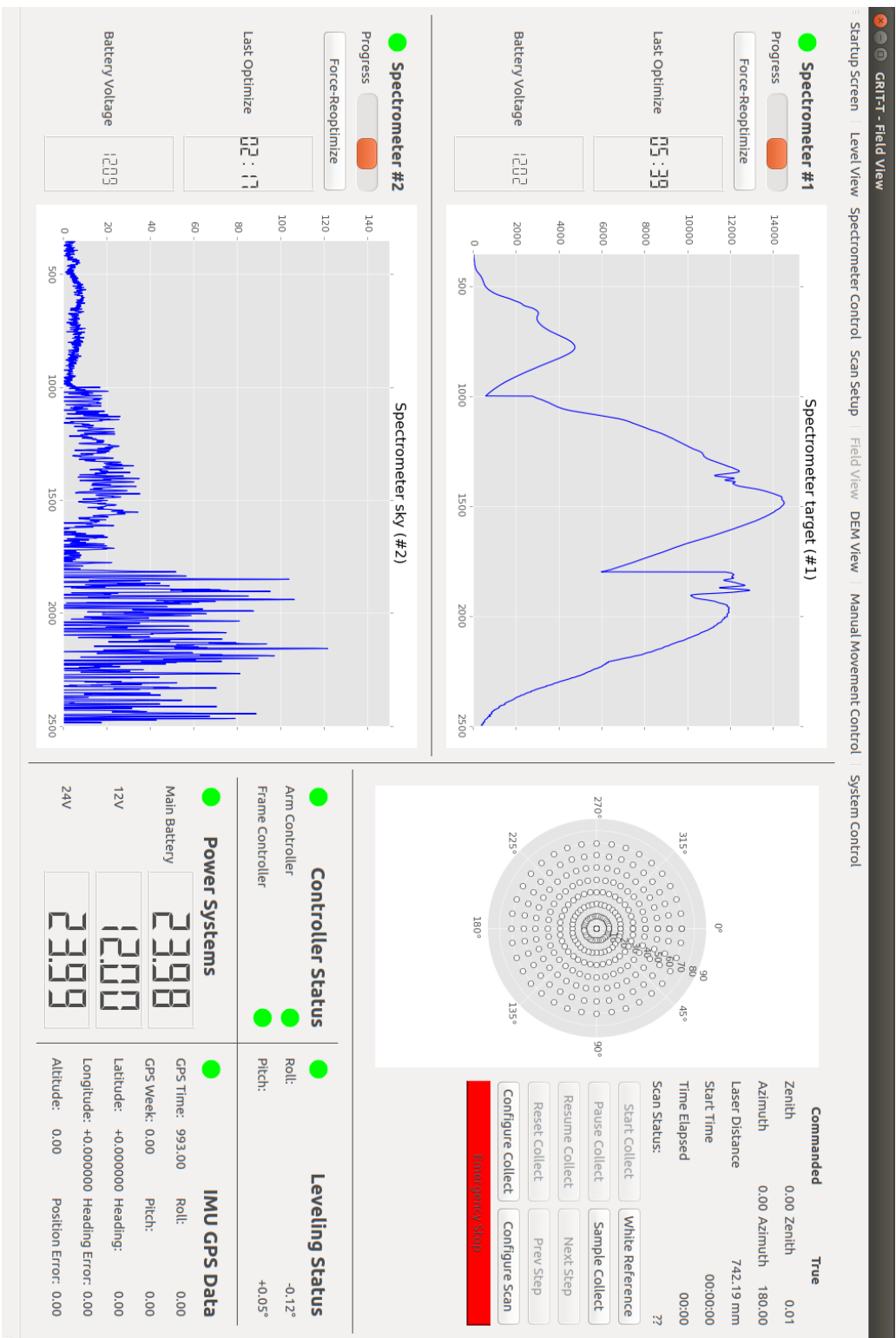


Figure 5.21: GRIT-T Control Software Field View page.

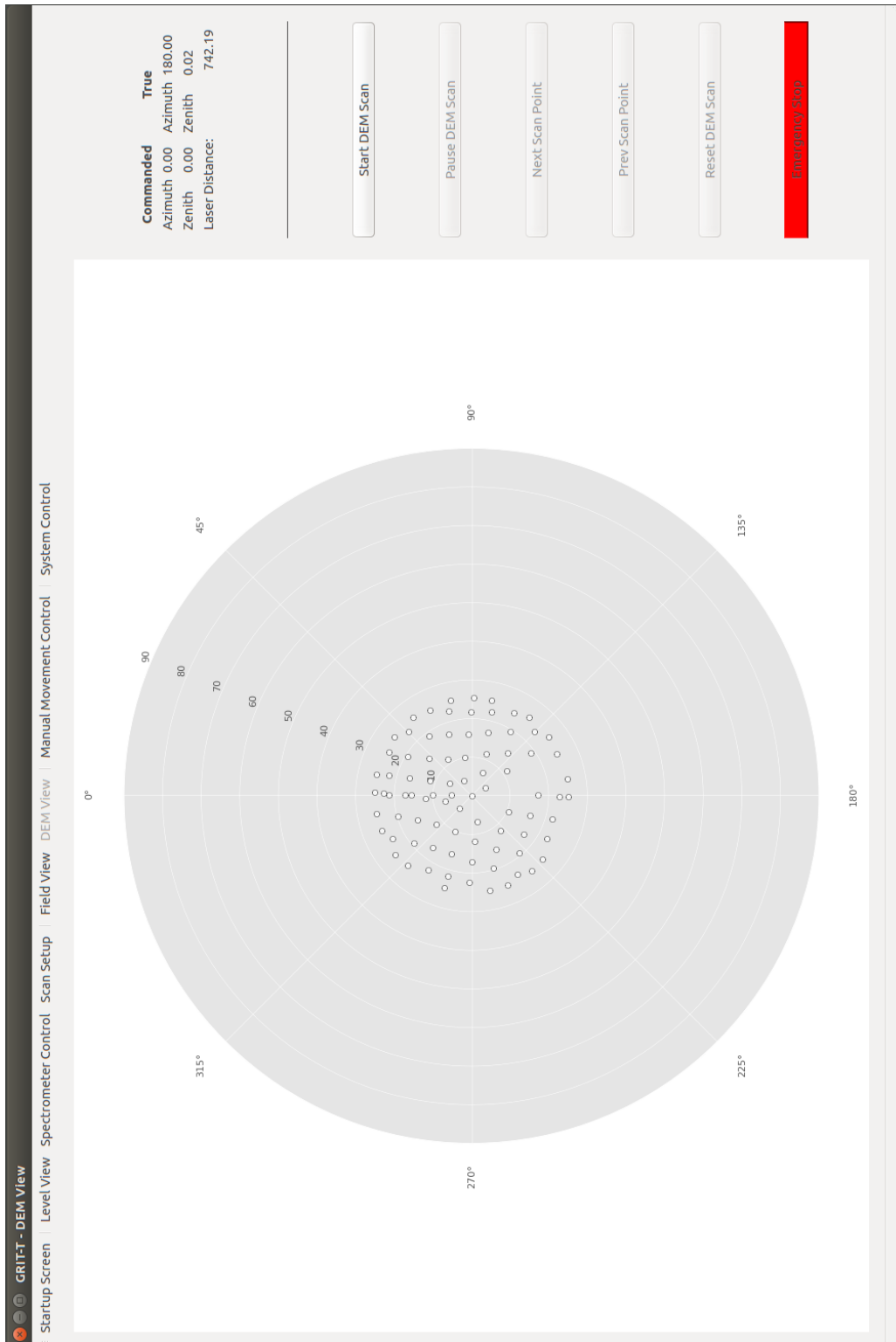


Figure 5.22: GRIT-T Control Software DEM View page.

GRIT-T - Manual Movement Control

Startup Screen | Level View | Spectrometer Control | Scan Setup | Field View | DEM View | Manual Movement Control | System Control

Azimuth

Elevation

Current Azimuth

Current Elevation

0

0.00

0.00

Head Encoder

Arm Encoder

Minimum Elevation

Maximum Elevation

0.01

0.02

0.00

0.00

Home All

Home Arm

Home Carriage

Move Tracking

Move Nadir

Move Manual

Clear Carriage Fault

Stop Move

Distance

742.2 mm

Level

Fine Level

Min Drive

Measure Laser

Head Angle

0

Move Head

Home Head

Stop Head

Frame Actuator A

Position

Move

Home

Stop

Clear Fault

0.00 mm

Frame Actuator B

Position

Move

Home

Stop

Clear Fault

0.00 mm

Frame Actuator C

Position

Move

Home

Stop

Clear Fault

0.00 mm

Home All

Move All

Stop All

Figure 5.23: GRIT-T Control Software Manual Movement page.



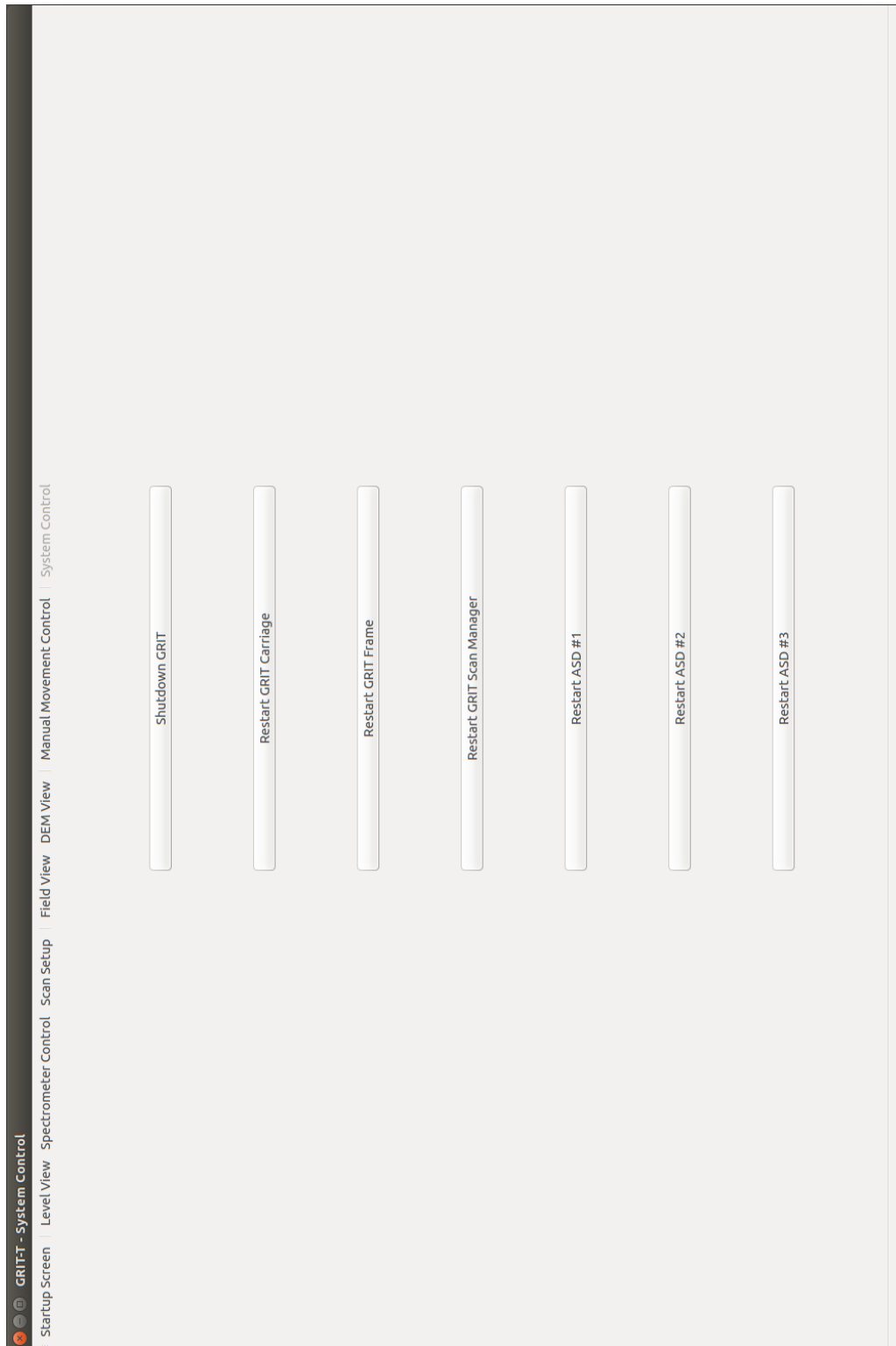


Figure 5.24: GRIT-T Control Software System Control page.

GRT-T - Troubleshooting View

Startup Screen

Level View

Spectrometer Control

Scan Setup

Field View

DEM View

Manual Movement Control

System Control

Carriage Status

Status0

Arm Encoder

0.0229

Status

2

Requested Azimuth

0

Azimuth Angle

0

Head Encoder

0.0098

Target Azimuth

0

Requested Zenith

0

Zenith Angle

0

Azimuth Immotion

False

Target Zenith

0

Min Zenith

0

Head Angle

0

Elevation Immotion

False

In Bounds

True

Max Zenith

0

Laser Distance

742.1875

Head Immotion

True

Vn300 Gpscompass

False

Lega Position

0

Battery Voltage

23.9889

Vn300 Heading Angle

0

Vn300 Vx

0

Legb Position

0

Bus12 Voltage

12.0042

Vn300 Latitude

0

Vn300 Vy

0

Legc Position

0

Bus24 Voltage

23.9882

Vn300 Longitude

0

Vn300 Vz

0

Lega Immotion

False

Reiker X Angle

-0.1009

Vn300 Pitch Angle

0

Vn300 Alt Error

0

Legb Immotion

False

Reiker Y Angle

0.0481

Vn300 Roll Angle

0

Vn300 Pos Error

0

Legc Immotion

False

Vn300 Gps Time

1275

Vn300 Gpsfix

False

Vn300 Vel Error

0

Vn300 Status Bits

1111110010000

Vn300 Gps Week

0

Vn300 Gpsheading

True

Vn300 Status Bits

1111110010000

Switched to Troubleshooting View View

Figure 5.25: GRT-T Control Software Status View page.



Figure 5.26: GRIT-T capturing BRDF in a powdery salt flat area. This surface has a soft, flaky crust that would break away under pressure.



Figure 5.27: GRIT-T capturing BRDF in a very soft, silty area. In areas such as these, multiple people aided in carrying the instrument due to the extremely soft conditions.





Figure 5.28: GRIT-T capturing BRDF in a completely saturated clay environment. Much like the silty areas, approximately 4 people were used to move the system to ensure that the instrument was safe at all times.

During this field experiment, the ability of GRIT-T to adequately capture accurate angles on varying heights of terrain was also thoroughly tested. In many flat areas, the system would easily achieve 70 degree zenith angles as seen in figure 5.29.

In addition to times when the system could achieve very large zenith angles, there were also those where the system reported that it would not be able to accurately reach those angles while still ensuring that the same portion of ground was sampled. Figure 5.30 illustrates a field measure-



Figure 5.29: Photo of GRIT-T capturing a true 70 degree zenith angle with respect to the target. Notice that the head has been counter-rotated to ensure that the same portion of ground is captured at each view angle.

ment where the device could accurately achieve only 60 degree zenith angles while maintaining its tracking.

This experiment was also the first test of the automated leveling system in the field. Despite the challenging variety of terrain and the harsh slope of some targets, GRIT-T was able to achieve level before each scan, due largely to the circular disc-shaped feet created for the ends of the actuator rods. In certain situations, the actuator legs and attached feet would sink into the mud until they achieved solid footing, and then would complete the leveling process. An example of this can be seen in figure 5.31, where the actuator rod and disc-shaped foot near the ASDs was pressed almost 6 inches into the soft ground before slightly lifting the system to level. Figure 5.32 provides a view of the actuator rods extended with attached feet. Note that each foot is a 4-inch diameter, 6 mm thick sheet of aluminum that is attached with a one-inch long stainless steel spike that threads into the bottom of the actuator rod.





Figure 5.30: GRIT-T capturing sediment reflectance while leveled on the side of a large sand dune. Note that the system is still tracking the same spot on the target sediment but that the maximum zenith angle is reduced due to the distance to the target.



Figure 5.31: GRIT-T capturing spectra from a white reference panel at a very muddy target location.



Figure 5.32: GRIT-T artificially lifted with the actuators to show the extension rods and attached feet.



Figure 5.33: GRIT-T capturing BRDF while leveled on a hard clay hillside.

GRIT-T also demonstrated its ability to level on harder surfaces without sinking, as seen in figure 5.33. In this and other situations, the system did slightly settle over the course of the BRDF scan. This settling was captured by the precision inclinometer and ultimately stored in the collection files for incorporation later in the post-processing stage.

Overall, the system captured 27 different targets during the 9 field days of the collect. Of these targets, all were captured with both upward and downward-looking spectroradiometers, however, since the post-processing integration is still on-going, most sites were preliminarily processed using the standard HCRF methods used on previous generation goniometers. Figure 5.34 shows the standard HCRF that was been created from several of the field sites.

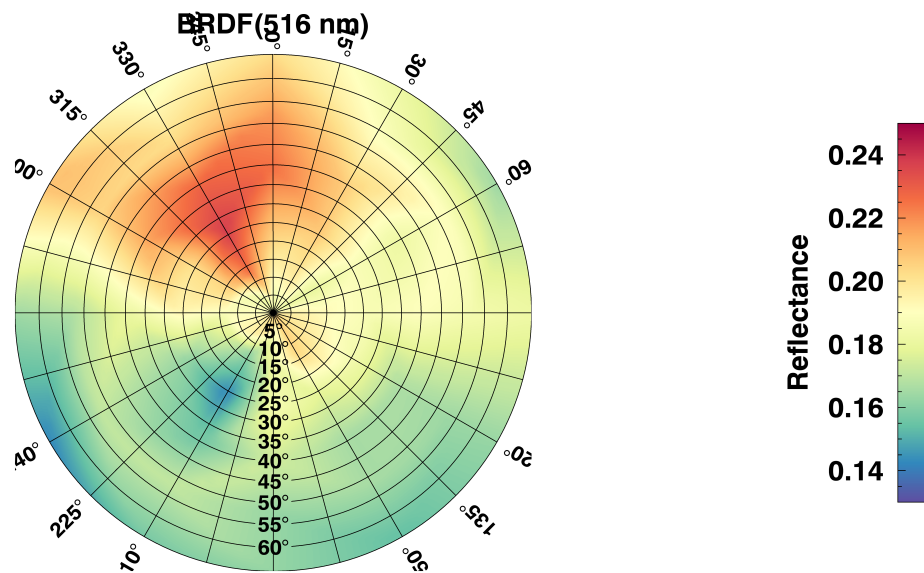


Figure 5.34: A preliminary result of a Nevada test site without the inclusion of background illumination compensation or temporal compensation.



## Chapter 6

# Summary

As seen in this dissertation, capturing accurate reflectance spectra of various targets in-situ can be a challenging endeavor if angular resolution is necessary. In these situations, the use of a field goniometer can dramatically increase the overall accuracy and repeatability of the measurement taken. However, it is important to keep in mind the overall scientific purpose of the device and ensure that each design decision is made with an understanding of how it will affect the quality of the data.

For the GRIT-T device, the key scientific objectives were split into groups related to optical measurement, portability, reduced collection complexity and setup time, increased angular accuracy and flexibility, and interoperability. The optical requirements were broken down into GIFOV size, reduction of parallax, background illumination compensation, temporal compensation, and reduction of self-shading. The portability requirements consisted of system weight, overall rigidity for movement situations from site to site, and compactness. Reducing overall collection complexity required the device to be fully automated with only one operator, quick movements and collections, automatic leveling, and as few components as possible for setup and tear down. In order to increase angular accuracy and flexibility, GRIT-T had to be able to point the sensor with respect to the target itself rather than with respect to the frame. The system also had to exhibit flexibility in order to accommodate measuring various targets, even on sloped terrain. Finally, the system was required to be interoperable with current skylight illumination sensors used by the group, and to allow for future integration with various imaging devices.

Fulfilling all of these difficult scientific objectives, without hampering any of the others, required for each to be broken down into derived system requirements. These new, lower-level requirements further ensured that certain competing objectives were adequately handled through careful navigation of the system tradespace. Ensuring that the optical requirements were properly handled meant adding multiple extra sensors and custom parts to the goniometer. These included a second

upward-looking spectrometer to handle background illumination, a laser range finder to measure actual distance to target, an extra axis of motion to compensate for parallax, and an open concept frame design to reduce self shadow situations. Once these devices were added to the system, it was then possible to further define the mechanical, electrical, and software requirements that would ensure that many of the other, more operational requirements would also be satisfied. It was also at this point that the ability to capture an elevation map became achievable, based on the extra axis of motion and the laser range finder, and this capability was added to the requirements of the system. To meet all of these requirements, they were then further organized into the subsystems that exist on the goniometer, to allow for a better understanding of how they interact with other portions of the system. Ultimately, many pointing, accuracy, and rigidity requirements came down to having a very strong frame that could be a solid backbone for the device. This frame would be where every motion was referenced to, and therefore, had to be custom designed and carefully modeled using finite element methods, especially since it was only a partial ring. This frame, combined with sealed industrial motors, actuators, encoders, and precision engineered movement components, allowed for exceptional accuracy and strength in a rugged, lightweight form factor. Of course, none of this hardware would have been able to achieve any of the overall scientific goals if not paired with good software. For the GRIT-T system, the combination of attention-to-detail on the hardware and software fronts, and how they impacted the overall scientific objectives, ultimately paid the most dividends in ensuring that the system had few weak links and could perform well in rough conditions.

After the system was full realized, it was put through a variety of tests to ensure that it could perform as originally intended. These laboratory tests included pointing accuracy tests, leveling tests, optical tests, and software tests. Based on the derived requirements listed in section 4.2, the GRIT-T was able to meet all pointing requirements and can track a target at any reasonable height within  $\pm 10.5$  mm. This means that at a nominal target height of 600 mm, the system can ensure that the GIFOV is consistent even when measured with the smallest, 1 degree, fore optic. The testing results called out in 5.2 also show that the system was able to achieve a level reference frame within the accuracy of the precision inclinometer chosen, or within  $\pm 0.1$  degrees. This section also noted that the original optical SNR requirements were very easily met since the ASD Field-Spec 4 spectroradiometer has as very low NEdL associated with each band. Therefore, the system can accurately point the fore optics and capture spectra as originally designed, in order to meet the larger scientific objectives of the device.

In addition to the laboratory tests, the system also underwent a brutal, two week field campaign in the Nevada desert where it captured 27 different sites with both upward- and downward-looking spectroradiometers. During this campaign the system was put in a variety of challenging situations

---

including deep mud and large dune structures and performed well in each environment. After a few early software issues, mostly related to network latency, the system became the spectral workhorse of the campaign and was able to collect 120% more spectral information than the original GRIT, in the same amount of time. During this test, GRIT-T was set to capture 66 data points per hemisphere and collect a total of 80 spectral samples per point. This scan and spectrometer parameter combination resulted in 34 minutes scans that would then be bounded by a white reference measurements of both spectroradiometers. Photos of the author operating the instrument can be found in figures 6.1 and 6.2.



Figure 6.1: The author collecting a white reference plaque after a BRDF scan using the GRIT-T.

In addition to the scientific requirements discussed, the methods used for handling them, and the initial outcomes of this design, this document also discussed the proposed methodology for handling the new dual-view output data based on an approach outlined by Martonchik. The data for this approach was captured as part of this work and will lead into future studies about the effectiveness of the approach at removal of background illumination for the purpose of collecting

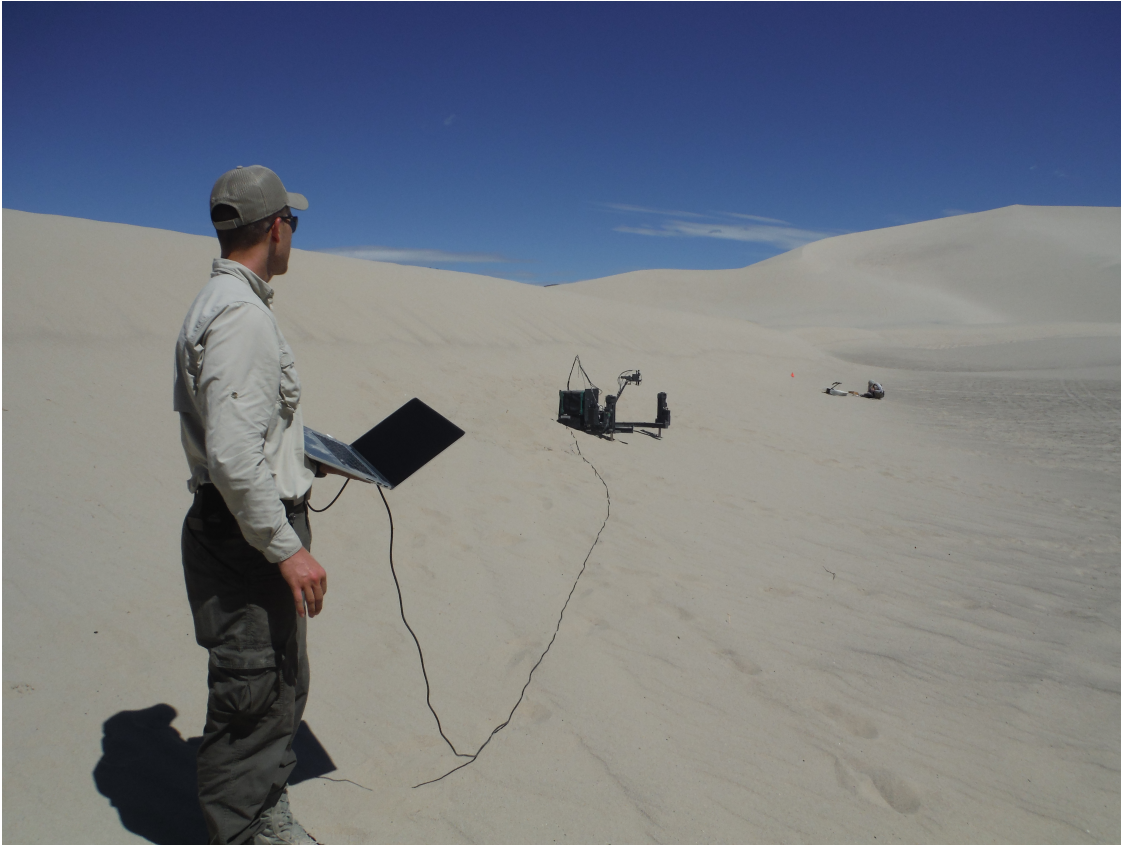


Figure 6.2: GRIT-T measuring reflectance on the side of a sand dune while the author monitors the GRIT-T Control Software.

BRDF in field situations. While this document begins the discussion of how accurate this new goniometer system is, characterization of GRIT-T will continue for some time. In addition, many questions remain about the effect of non-ideal atmospheric conditions when capturing field BRDF with this technique, whether it may be mostly static clouds or rapidly changing conditions, and the most effective way of handling those conditions when they inevitably occur on a field collection day. Much work has been done by Bachmann and others to mitigate these issues[9], but with the inclusion of this new, very portable device, future studies will need to be conducted to ensure that the data collected is as accurate as possible. There also remains a fair amount of work to incorporate the digital elevation map that will be generated by GRIT-T into the post-processing routines. This DEM contains very useful information about roughness and surface inclination and understanding these effects on the overall structure of the reflectance function will require substantial effort from those using this device. It may also be necessary to outfit the goniometer with other sensors that

fulfill future research interests. The system has been designed to be flexible for these future needs in terms of communication and power requirements. One very interesting idea involves the placement of two or more imaging sensors atop the actuator legs that would high resolution views of the target from various angles. This would provide even more detailed information about the surface roughness effects than the current DEM can capture, thus providing greater accuracy should higher fidelity roughness information be required or should the targets ever be recreated in a simulation.

It is important to note that systems such as the FIGOS devices, the GOPHER and ULGS goniometers, and the original GRIT, all played a substantial role in the creation of this new goniometer system. The performance of each of these contributed to the design decisions that the research group felt would represent best practices for the very specific purpose of the RIT field goniometer, in addition to the new features. In the coming years, the GRIT-T system will be put through its paces in a range of environments to test its overall utility for fulfilling the research goals of the group. It is expected that this new device will allow for further analysis of the sediment, and provide for a better understanding of how grain size distribution, density, and moisture content affect the spectral response of in-situ materials and will also be useful for investigation of vegetation biophysical parameters and applications.

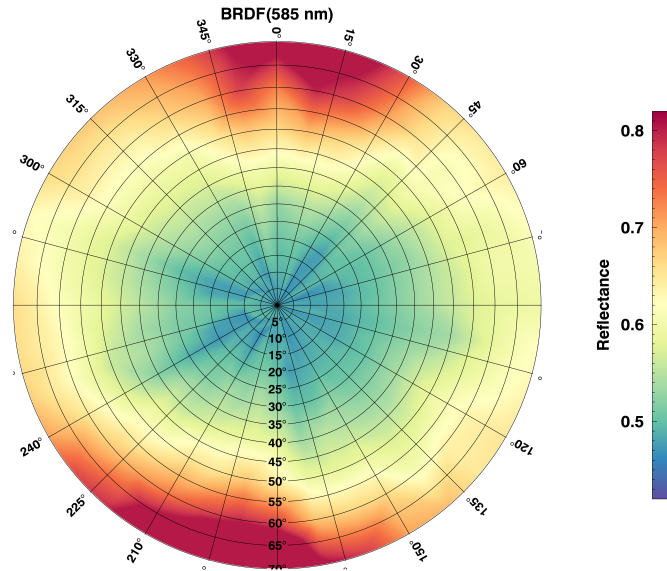


Figure 6.3: BRF of a sediment performed in the laboratory with 10 degree intervals in azimuth and zenith. This BRF was the first performed by the goniometer in the lab.



# Bibliography

- [1] S. Sandmeier and K. Itten, “A field goniometer system (figos) for acquisition of hyperspectral brdf data,” *Geoscience and Remote Sensing, IEEE Transactions on*, vol. 37, pp. 978–986, Mar 1999.
- [2] J. Schopfer, S. Dangel, M. Kneubhler, and K. I. Itten, “The improved dual-view field goniometer system figos,” *Sensors*, vol. 8, no. 8, p. 5120, 2008.
- [3] C. M. Bachmann, D. Gray, A. Abelev, W. Philpot, M. J. Montes, R. Fusina, J. Musser, R.-R. Li, M. Vermillion, G. Smith, D. Korwan, C. Snow, W. D. Miller, J. Gardner, M. Sletten, G. Georgiev, B. Truitt, M. Killmon, J. Sellars, J. Woolard, C. Parrish, and A. Schwarzschild, “Linking goniometer measurements to hyperspectral and multisensor imagery for retrieval of beach properties and coastal characterization,” 2012.
- [4] T. H. Painter, B. Paden, and J. Dozier, “Automated spectro-goniometer: A spherical robot for the field measurement of the directional reflectance of snow,” *Review of Scientific Instruments*, vol. 74, no. 12, 2003.
- [5] D. Biliouris, W. W. Verstraeten, P. Dutré, J. A. van Aardt, B. Muys, and P. Coppin, “A compact laboratory spectro-goniometer (clabspg) to assess the brdf of materials. presentation, calibration and implementation on fagus sylvatica l. leaves,” *Sensors*, vol. 7, pp. 1846–1870, 2007.
- [6] S. Dangel, M. Kneubühler, R. Kohler, M. Schaepman, J. Schopfer, G. Schaepman-Strub, and K. Itten, “Combined field and laboratory goniometer system-figos and lagos,” in *Geoscience and Remote Sensing Symposium, 2003. IGARSS’03. Proceedings. 2003 IEEE International*, vol. 7, pp. 4428–4430, IEEE, 2003.
- [7] P. P. Roosjen, J. G. Clevers, H. M. Bartholomeus, M. E. Schaepman, G. Schaepman-Strub, H. Jalink, R. Van Der Schoor, and A. De Jong, “A laboratory goniometer system for measuring reflectance and emittance anisotropy,” *Sensors*, vol. 12, no. 12, pp. 17358–17371, 2012.
- [8] E. J. Milton, M. E. Schaepman, K. Anderson, M. Kneubühler, and N. Fox, “Progress in field spectroscopy,” *Remote Sensing of Environment*, vol. 113, pp. S92–S109, 2009.
- [9] C. M. Bachmann, M. J. Montes, C. E. Parrish, R. A. Fusina, C. R. Nichols, R.-R. Li, E. Hallenborg, C. A. Jones, K. Lee, J. Sellars, *et al.*, “A dual-spectrometer approach to reflectance



- measurements under sub-optimal sky conditions,” *Optics express*, vol. 20, no. 8, pp. 8959–8973, 2012.
- [10] C. Coburn, “Ulgs: The university of lethbridge goniometer systems.” [http://people.uleth.ca/~craig.coburn/brdf/goni\\_system.htm](http://people.uleth.ca/~craig.coburn/brdf/goni_system.htm), 2015. Accessed: 2015-11-24.
  - [11] S. R. Sandmeier, K. Itten, *et al.*, “A field goniometer system (figos) for acquisition of hyper-spectral brdf data,” *Geoscience and Remote Sensing, IEEE Transactions on*, vol. 37, no. 2, pp. 978–986, 1999.
  - [12] C. M. Bachmann, A. Abelev, M. J. Montes, W. Philpot, D. Gray, K. Z. Doctor, R. A. Fusina, G. Mattis, W. Chen, S. D. Noble, C. Coburn, T. Corl, L. Slomer, C. R. Nichols, E. van Roggen, R. J. Hughes, S. Carr, S. Kharabash, A. Brady, and M. Vermillion, “Flexible field goniometer system: the goniometer for outdoor portable hyperspectral earth reflectance,” *Journal of Applied Remote Sensing*, In press.
  - [13] C. Coburn and D. Peddle, “A low-cost field and laboratory goniometer system for estimating hyperspectral bidirectional reflectance,” *Canadian Journal of Remote Sensing*, vol. 32, no. 3, pp. 244–253, 2006.
  - [14] T. E. Berry, J. C. Morgan, J. S. Furey, T. A. DeMoss, J. R. Kelley, and J. R. McKenna, “Extensive goniometric spectral measurements at desert sites for military engineering,” in *SPIE Optical Engineering+ Applications*, pp. 84950Z–84950Z, International Society for Optics and Photonics, 2012.
  - [15] M. Buchhorn, R. Petereit, and B. Heim, “A manual transportable instrument platform for ground-based spectro-directional observations (mantis) and the resultant hyperspectral field goniometer system,” *Sensors*, vol. 13, no. 12, pp. 16105–16128, 2013.
  - [16] F. Bagenal, “Spectroscopy 101: Spectroscopy of atmospheres.” <http://lasp.colorado.edu/~bagenal/3720/CLASS5/5Spectroscopy.html>, 2015. University of Colorado Boulder: Laboratory for Atmospheric and Space Physics. Accessed: 2015-11-24.
  - [17] M. T. Eismann, *Hyperspectral remote sensing*. SPIE Press Bellingham, 2012.
  - [18] C. M. Bachmann, D. S. Peck, B. Ambeau, J. Harms, and M. Schultz, “Improved modeling of multiple scattering in hyperspectral brdf of coastal sediments observed using the goniometer of the rochester institute of technology (grit),” in *SPIE Optical Engineering+ Applications*, pp. 96110J–96110J, International Society for Optics and Photonics, 2015.
  - [19] C. M. Bachmann, A. Abelev, W. Philpot, K. Z. Doctor, M. J. Montes, R. Fusina, R.-R. Li, and E. van Roggen, “Retrieval of sand density from hyperspectral brdf,” in *SPIE Defense+ Security*, pp. 908807–908807, International Society for Optics and Photonics, 2014.
  - [20] C. Bachmann, C. Nichols, M. Montes, R.-R. Li, P. Woodward, R. Fusina, W. Chen, V. Mishra, W. Kim, J. Monty, K. McIlhany, K. Kessler, D. Korwan, D. Miller, E. Bennert, G. Smith, D. Gillis, J. Sellars, C. Parrish, A. Schwarzschild, and B. Truitt, “Remote sensing retrieval of



- substrate bearing strength from hyperspectral imagery at the virginia coast reserve (vcr'07) multi-sensor campaign," July 2008.
- [21] C. M. Bachmann, W. Philpot, A. Abelev, and D. Korwan, "Phase angle dependence of sand density observable in hyperspectral reflectance," *Remote Sensing of Environment*, vol. 150, pp. 53–65, 2014.
  - [22] B. Hapke, "Bidirectional reflectance spectroscopy: 1. theory," *Journal of Geophysical Research: Solid Earth (1978–2012)*, vol. 86, no. B4, pp. 3039–3054, 1981.
  - [23] B. Hapke and E. Wells, "Bidirectional reflectance spectroscopy: 2. experiments and observations," *Journal of Geophysical Research: Solid Earth (1978–2012)*, vol. 86, no. B4, pp. 3055–3060, 1981.
  - [24] B. Hapke, "Bidirectional reflectance spectroscopy: 3. correction for macroscopic roughness," *Icarus*, vol. 59, no. 1, pp. 41–59, 1984.
  - [25] B. Hapke, "Bidirectional reflectance spectroscopy: 4. the extinction coefficient and the opposition effect," *Icarus*, vol. 67, no. 2, pp. 264–280, 1986.
  - [26] B. Hapke, "Bidirectional reflectance spectroscopy: 5. the coherent backscatter opposition effect and anisotropic scattering," *Icarus*, vol. 157, no. 2, pp. 523–534, 2002.
  - [27] B. Hapke, "Bidirectional reflectance spectroscopy: 6. effects of porosity," *Icarus*, vol. 195, no. 2, pp. 918–926, 2008.
  - [28] B. Hapke, *Theory of reflectance and emittance spectroscopy*. Cambridge University Press, 2012.
  - [29] K. L. Coulson, G. M. Bouricius, and E. L. Gray, "Optical reflection properties of natural surfaces," *Journal of Geophysical Research*, vol. 70, no. 18, pp. 4601–4611, 1965.
  - [30] F. Nicodemus, J. Richmond, J. Hsia, I. Ginsberg, and T. Limperis, "Geometrical considerations and nomenclature for reflectance, natl," *Bur. Stand. Rep., NBS MN-160*, 1977.
  - [31] X. F. Gu, G. Guyot, and M. Verbrugghe, "Evaluation of measurement errors in ground surface reflectance for satellite calibration," *International Journal of Remote Sensing*, vol. 13, pp. 2531–2546, Sept. 1992.
  - [32] B. Hosgood, J. Piironen, G. Andreoli, C. Koechler, and S. Sandmeier, *Goniometers*. John Wiley and Sons, Inc., 2001.
  - [33] K. Serr, T. Windholz, and K. Weber, "Comparing gps receivers: a field study," *URISA Journal*, vol. 18, no. 2, pp. 19–23, 2006.
  - [34] J. R. Schott, *Remote sensing*. Oxford University Press, 2007.
  - [35] S. Dangel, M. M. Verstraete, J. Schopfer, M. Kneubühler, M. Schaepman, K. Itten, *et al.*, "Toward a direct comparison of field and laboratory goniometer measurements," *Geoscience and Remote Sensing, IEEE Transactions on*, vol. 43, no. 11, pp. 2666–2675, 2005.

- [36] J. Suomalainen, T. Hakala, J. Peltoniemi, and E. Puttonen, "Polarised multiangular reflectance measurements using the finnish geodetic institute field goniospectrometer," *Sensors*, vol. 9, no. 5, pp. 3891–3907, 2009.
- [37] A. Hueni, J. Schopfer, D. Schl pfer, M. Kneubuehler, and J. Nieke, "Pre-processing of dual-view figos data: Towards operational brdf retrieval," *Beijing, China, sn*, 2008.
- [38] K. Z. Doctor, C. M. Bachmann, D. J. Gray, M. J. Montes, and R. A. Fusina, "Wavelength dependence of the bidirectional reflectance distribution function (brdf) of beach sands," *Applied optics*, vol. 54, no. 31, pp. F243–F255, 2015.
- [39] M. Turner, "The sandmeier field goniometer: A measurement tool for bi-directional reflectance," in *NASA commercial remote sensing verification and validation symposium*, pp. 1–6, John C. Stennis Space Center MS, 1998.
- [40] J. Schopfer, S. Dangel, M. Kneub hler, and K. Itten, "Dual field-of-view goniometer system figos," *International. Archives of Photogrammetry Remote Sensing and Spatial Information Sciences*, pp. 493–498, 2007.
- [41] C. A. Coburn and S. D. Noble, "UlgS ii: A high-performance field and laboratory spectrogoniometer for measuring hyperspectral bidirectional reflectance characteristics," *IEEE Transactions on Geoscience and Remote Sensing*, vol. 54, pp. 2304–2313, April 2016.
- [42] J. Suomalainen, J. Peltoniemi, T. Hakala, and E. Puttonen, "Finnish geodetic institute field goniospectrometer (figifigo): A device for polarized multiangular reflectance measurements," in *Proc. IEEE IGARSS*, 2008.
- [43] J. Timmermans, "Coupling optical and thermal directional radiative transfer to biophysical processes in vegetated canopies," *Phd, faculty of geo-information science and earth observation, University of Twente, Enchede, the Netherlands*, pp. 1–157, 2011.
- [44] E. Ientilucci and J. Schott, "Radiometry and radiation propagation, draft manuscript," 2011.
- [45] Commission Internationale de L' clairage, *International Lighting Vocabulary*, 1970.
- [46] J. V. Martonchik, C. J. Bruegge, and A. H. Strahler, "A review of reflectance nomenclature used in remote sensing," *Remote Sensing Reviews*, vol. 19, no. 1-4, pp. 9–20, 2000.
- [47] J. Stuckens, B. Somers, W. W. Verstraeten, R. Swennen, and P. Coppin, "Evaluation and normalization of cloud obscuration related brdf effects in field spectroscopy," *Remote Sensing*, vol. 1, no. 3, pp. 496–518, 2009.
- [48] A. S. D. Incorporated, "Fieldspec 4 hi-res: High resolution spectroradiometer technical specs." <http://www.asdi.com/products/fieldspec-spectroradiometers/fieldspec-4-hi-res>, 2015. Accessed: 2015-11-24.
- [49] Department of Defense, *MIL-STD-1472G. Design Criteria Standard: Human Engineering Metric*, 1 2012.

- [50] S. R. Sandmeier, "Acquisition of bidirectional reflectance factor data with field goniometers," *Remote Sensing of Environment*, vol. 73, no. 3, pp. 257–269, 2000.
- [51] J. V. Martonchik, "Retrieval of surface directional reflectance properties using ground level multiangle measurements," *Remote Sensing of Environment*, vol. 50, no. 3, pp. 303 – 316, 1994.
- [52] A. Hueni, S. Rey, D. Schlapfer, J. Schopfer, and M. Kneubuehler, "Visualisation, processing and storage of spectrodirectional data based on the spectral database specchio," in *Geoscience and Remote Sensing Symposium, 2009 IEEE International, IGARSS 2009*, vol. 1, pp. I–84–I–87, July 2009.
- [53] A. Hueni, J. Nieke, J. Schopfer, M. Kneubhler, and K. Itten, "The spectral database {SPECCHIO} for improved long-term usability and data sharing," *Computers and Geosciences*, vol. 35, no. 3, pp. 557 – 565, 2009.
- [54] D. Six, M. Fily, S. Alvain, P. Henry, and J.-P. Benoist, "Surface characterisation of the dome concordia area (antarctica) as a potential satellite calibration site, using spot 4/vegetation instrument," *Remote Sensing of Environment*, vol. 89, no. 1, pp. 83 – 94, 2004.
- [55] C. M. Bachmann, A. Abelev, W. Philpot, K. Z. Doctor, M. J. Montes, R. Fusina, R.-R. Li, and E. van Roggen, "Retrieval of sand density from hyperspectral brdf," 2014.
- [56] E. A. Walter-Shea, C. J. Hays, M. A. Mesarch, and R. D. Jackson, "An improved goniometer system for calibrating field reference-reflectance panels," *Remote Sensing of Environment*, vol. 43, no. 2, pp. 131 – 138, 1993.
- [57] C. J. Bruegge, M. C. Helmlinger, J. E. Conel, B. J. Gaitley, and W. A. Abdou, "Parabola iii: A spherescanning radiometer for field determination of surface anisotropic reflectance functions," *Remote Sensing Reviews*, vol. 19, no. 1-4, pp. 75–94, 2000.